Collected papers dedicated to the 2nd anniversary of establishment of

RESEARCH & DEVELOPMENT CENTRE FOR LOW-COST PLASMA AND NANOTECHNOLOGY SURFACE MODIFICATION – *CEPLANT*

1.12.2010 – 1.12.2012

CEPLANT
Research & development centre for low-cost plasma and nanotechnology surface modifications

EUROPEAN UNION
EUROPEAN REGIONAL DEVELOPMENT FUND
INVESTING IN YOUR FUTURE

2007-13
OP Research and Development for Innovation

s1425

Preface

This volume of Chemical Letters is devoted to current R& D activities of the Regional R&D center for low-cost plasma and nanotechnology surface modifications established as a part of the Institute of Physical Electronics (IPE) at Faculty of Science, Masaryk University in November 2010 in the Operational Programme Research and Development for Innovation. The Centre is a continuation and extension of the more than 50 years lasting tradition of applied plasma physics research at the Department of Physical Electronics, which resulted in several innovations successfully transferred into the industry, the project plan is to launch highly focused applied research of plasma sources and plasma processing development, strategically targeted on industrial end-users.

At IPE the research in applied plasma physics was started more than 50 years ago by prof. Václav Truneček, who was at that time the head of the Institute. His pioneering research of fundamental physics of atmospheric-pressure RF plasma torches launched also fast and systematic developments of the related industrial applications, as well as spectroscopic and microwave diagnostic techniques. Thus already in the early sixties the first research papers were published and the RF plasma torch was successfully tested by company Kavalier Sázava for welding of large diameter glass tubes.

In the mid-sixties the research activities of IPE expanded also to the field of fundamental and applied plasma chemistry. In response to the demands of Czechoslovak industry the team led by prof. Vratislav Kapička and prof. Jan Janča, the former students and successful followers of prof. Truneček, was studying for example the plasma burning and etching, a wide spectrum of methods for plasma depositions including CVD, plasma polymerization, diamond-like thin layers, as well as the deposition of nanocomposite layers and carbon nanostructures. The techniques developed were protected by 12 awarded patents. From the mid-nineties the research activities were extended also to atmospheric-pressure plasma chemistry, first of all to the high-pressure plasma applications for surface activation and cleaning of polymer and metal surfaces, and highly-effective ozone generation. These applications initiated also intense research in the field of high -pressure gas discharge physics aimed at the development of several types of novel atmospheric-pressure plasma sources. The successful research work in the field of atmospheric-pressure plasma chemistry, including several industrial projects, created a base for the establishment of the Center, which covers the major part of the current research activities at INP. The Center is expected to provide practical solutions of technological problems, above all for small and medium-sized enterprises in the Czech Republic. The long-term vision is to create the research team that will be sought after R&D partner also for large international corporations.

The second year of a new institution like the Centre is always likely to be one where consolidation develops alongside innovation and experiment. The short papers collected in this volume present current research lines in the field of applied plasma chemistry at the Centre and collaborating institutions in the Czech Republic.

Prof. Mirko Cernak
director
R&D Center for Low-Cost Plasma and Nanotechnology Surface Modifications
Masaryk University, Brno

IMPORTANCE OF POLYPROPYLENE FIBERS AS A REINFORCEMENT IN CONCRETE

LENKA BODNÁROVÁ[a], MONIKA FIALOVÁ[b], DANIEL KOPKÁNĚ[a], TOMÁŠ MORÁVEK[b], PAVEL SŤAHEL[b], MIRKO ČERNÁK[b,c]

[a] Faculty of Civil Engineering, Brno University of Technology, Veveří 95, 662 37 Brno, Czech Republic, [b] Department of Physical Electronics, Faculty of Science, Masaryk University, Kotlářská 2, 611 37 Brno, Czech Republic, [c] Department of experimental physics, Comenius University, Mlynská Dolina F2, 842 48 Bratislava, Slovakia
bodnarova.l@fce.vutbr.cz

Keywords: fiber-reinforced concrete, polypropylene fibers, wettability

1. Fiber-Reinforced Concrete

Fiber-reinforced concrete[1] is a composite material created by connection of concrete matrix and short reinforcement elements dispersed in matrix, while fibers take up only a small part of total volume. Fibers are added to a concrete mix which contains cement, water and fine and coarse aggregate.

Plain, mass concrete has considerably high compressive strength, stiffness, but high brittleness, low tensile strength and low shearing strength. Dispersed reinforcement compensates mainly tensile stress and prevents formation of micro-cracks caused by shrinking and development of tensile cracks in structures. Adding of fiber reinforcement can reinforce the whole volume of concrete matrix, unlike classic steel bar reinforcement.

Table I
Fibers used as dispersed reinforcement in concrete[2]

Fiber type	Tensile strength [MPa]	Tensile modulus [GPa]	Tensile strain [%] (max-min)	Density [kg m^{-3}]
Asbestos	550–960	82–138	0.3–0.1	3200
Cellulose	400–620	6.9	10–25	1500
Steel	270–2700	200	2–1	7800
Poly ethylene	÷ 690	2–4	400–100	950
Poly propylene	200–750	0.8–9.8	15–10	900
Polyester	800–1300	Up to 15	20–8	1400
AR-Glass	1700	72	2	2680
Carbon	590–4800	28–520	2–1	2000

Table II
Properties of cement matrix

	Flexural Tensile strength [MPa]	Tensile modulus [GPa]	Tensile strain [%]	Density [kg m^{-3}]
Cement matrix	3.7	10–45	0.02	2500

Role of fiber reiforcement

The purpose of dispersed reinforcement is limiting formation of shrinkage cracks, increasing fracture toughness, increasing resistance to dynamic stress, increasing resistance to high temperatures – preventing explosive flaking of concrete, decreasing of wearability and potentially other special properties.

Many different types of fibers can be used as reinforcement for concrete: steel, polypropylene, glass, carbon, cellulose, polyamide, polyvinyl alcohol, aramid or nylon fibers and other fibers.

Type and material of fiber reinforcement is selected in accordance with required properties. Properties of fibers used as dispersed reinforcement for concrete are stated in Tab. I.

Use of fiber reinforcement for preventing of formation of shrinkage cracks

Fine organic and inorganic fibers (polymeric and glass) are used mainly to limit volumetric changes of cement matrix and to limit formation of cracks. In such case, concrete is reinforced with high number of fibers even if proportion of fibers is low (1 kg of polymeric fibers contains around 300 million pieces of fibers). Depending on manufacturing technology, fine polymeric fibers can be fibrillated or monofibril. Monofibril fibers are finer and therefore they are more numerous at the same weight proportion. Monofibril fibers are manufactured individually and then they are cut to required length with smooth, circular cross section. Fibrillated fiber is made from foil and then again cut to required length with rectangular cross section and more coarse surface. Because of different way of manufacture, fibrillated fibers have several times higher section, therefore the number of fibers in a weight unit is lower – several million.

Polypropylene and glass fibers are most frequently used for preventing formation of shrinkage cracks. Compared to glass based fibers, polypropylene fiber have lower values of elasticity modulus, their effect takes place in particular during first hours of setting and hardening of concrete.

Dosage of glass and polymeric fibers to prevent formation of shrinkage cracks is 0.7–1.1 kg m^{-3} of fresh concrete or mortar in accordance with recommendations of manufacturer. If fine fibers are used, it is necessary to bear in mind that workability of concrete is reduced (by ca 30–60 mm of slump).

Increase of resistance to high temperature (to prevent explosive spalling of concrete)

Increasing resistance of concrete to high temperatures is another important role of fine polypropylene fibers or other fine inorganic fibers. Explosive spalling is caused by the build-up of water vapour pressure in concrete during fire. Increased temperature causes melting of PP fibers, which opens space for expanded water vapor, which could otherwise cause cracks in concrete.

Fibers used for such purposes are mostly polypropylene (PP) and natural (cellulose).

Dosage of fine fibers to increase of resistence to high temperature and prevent explosive sparing is 0.6–2 kg m^{-3} of fresh concrete or mortar in accordance with recommendations of manufacturer.

Use of fiber reinforcement for higher strength of concrete (in particular metal fibers or polymeric – macrofibers)

Concrete reinforced with fibers shows higher toughness compared to brittle plain concrete. Fibers (certain dosage – higher volumes) influence working diagram of concrete. Higher tensile strength and slight increase of compressive strength can be observed. Fibers enable deformation of concrete and tensile stress distribution at the point of exceeding strength of concrete, even after formation of cracks. Ultimate tensile strain of fiber reinforced concrete is higher than that of plain concrete. Steel fibers are recommended particularly to increase tensile bending strength, toughness and impact strength.

Depending on recommendation of manufacturers of particular types of fibers, reinforcement fibers can be used for high strength floors, for structures, where increased water tightness and frost resistance are required, to form base layers without cracks for other special layers, for shotcrete to reduce fallout, for renovation mortars and plasters, for production of prefabricated elements, to increase impermeability of concrete or to increase resistance of concrete to fire.

Steel fibers used as dispersed reinforcement can bring following advantages:

higher tensile strength, higher transversal tensile strength and tensile bending strength

higher impact strength

resistance to formation of cracks during setting of concrete.

Most frequently used length of steel fibers is 30–55 mm. Special metal fibers of length about 12 mm are designed for high performance concrete. Section of fibers can be either circular (diameters from 0.6 to 1.4 mm), square or more often rectangular. Fibers with round section are made by means of drawing from a wire. Consequently, they are cut, ends are shaped or pressing of indents to increase bond to concrete. Steel fibers with rectangular sections are manufactured through cutting from sheet metal, often they are shaped by imprints or dents on the surface.

Consistency of steel-fiber reinforced concrete is strongly affected both by the type of steel fibers and by their weight proportion. Dosage rates of steel fibers are between 20 and 50 kg. For this reason, it is necessary to design concrete with workability about 180–200 mm of slump for preliminary tests of pumpable concrete, because addition of steel fibers decreases workability to ca 100–150 mm of slump, which is adequate for pumpable concrete.

Reinforcement with fibers (usually metal, glass or polymeric) can considerably enhance properties of concrete, however, fiber reinforcement is not designed to replace classic steel bars reinforcement.

2. Polypropylene fibers

Polypropylene is a thermoplastic polymer produced by polymerization of monomer units. Propylene, the structural unit, is containing three atoms of carbon and six atoms of hydrogen. Polypropylene, especially in the form of fibers, is widely used in many industrial applications (automotive, textile or food industry)[3].

Nowadays PP fibers are more and more used as a reinforcement in concrete due to their versatile properties such as a resistance to many chemical solvents, high melting point and low cost. The main technological problem of using PP fibers as a reinforcement is a weak adhesion between PP fibers and cement matrix, related to the hydrophobic surface of fibers. There were tested several methods of PP surface treatment that lead to the stronger bonding such as chemical, mechanical or plasma treatment[4–6].

The plasma technique is relatively new, simple and effective method of polymer surface modification. It was confirmed that the plasma treatment of polymers results in the increase of the surface energy[7–9]. In this contribution the plasma treatment by a Diffuse Coplanar Surface Barrier Discharge (DCSBD)[9] was studied.

Wetting properties of PP fibers after plasma treatment

The wetting properties of PP fibers were investigated by two methods of measuring the weight of absorbed water in bunches of PP fibers. In a first case there was measured a weight of a bunch of PP fibers before and after soaking in water. The difference between these weights gave the absorption capacity of the bunches as shown Fig. 1.

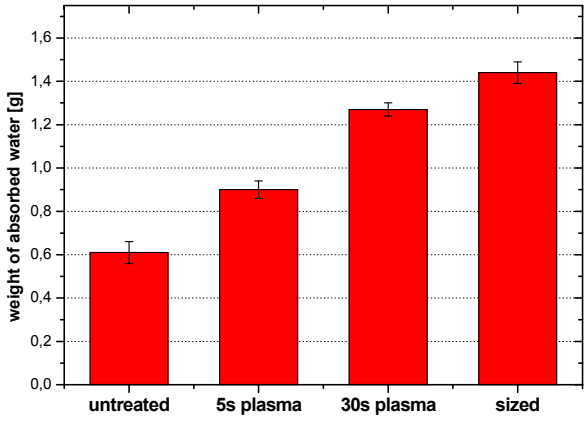

Fig. 1. **The comparison of weights of absorbed water in bunches of untreated, chemically treated and plasma treated PP fibers**

The other method is based on the measuring the weight of absorbed water as well, but the principal effect is the capillarity. The bunch of PP fibers was touching a surface of water and absorbed it. The weight of absorbed water as a function of time was measured (Fig. 2).

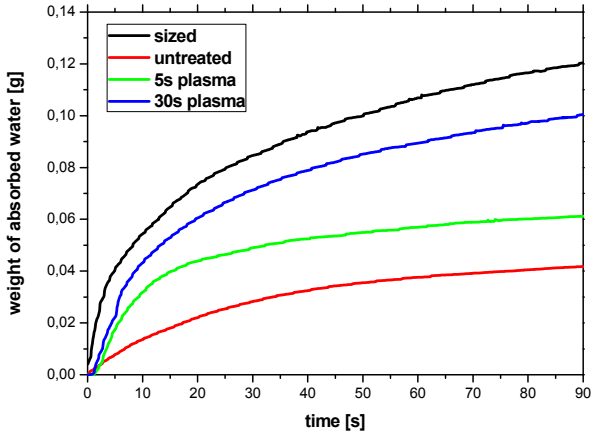

Fig. 2. **The weight of absorbed water in a bunch of untreated and treated PP fibers as a function of time**

The plasma treatment of PP fibers led to an increase of wetting properties, accordingly the water absorption of PP fibers was improved. The 30s plasma treated PP fibers absorbed twice as much water as untreated fibers and about 12% less water than sized fibers as shown Fig. 1 and Fig. 2.

3. Plasma treated PP fibers as a reinforcement for concrete

The performed test was based on testing of flexural strength in early age, mainly 12 hours after mixing. The experiment set up is based on three point test of bending flexural strength, where the test continued after the rupture of specimen until 4mm of total deflection was reached (in one minute). In this way the behavior of fibers and its effect on immature concrete can be evaluated. The Fig. 3 shows results obtained on specimens 4*4*16 cm in size. The results indicate that mixes with fibers had better performance at every level.

Table III
Composition of cement paste

Component	Mass [kg m^{-3}]	Volume [%]
Cement 32,5R	535,3	17,3
Aggregate 0-4	1472,3	55,6
Water	269,1	26,9
PP fibers	2,4	0,26

If comparing sized and plasma treated fibers the maximal strength was about the same level, while results for obtained for continuing deflection were definitely better for the plasma treated fibers. This could be explained as direct effect of change in wettability as has been discussed above.

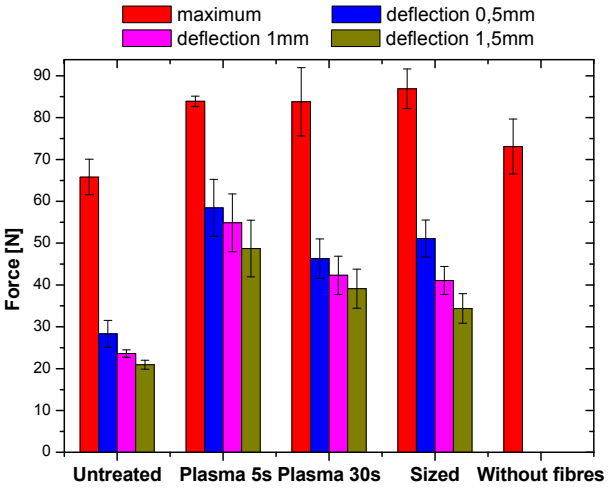

Fig. 3. **The comparison of weights of absorbed water in bunches of untreated, chemically treated and plasma treated PP fibers**

This research has been supported by the project CZ.1.05/2.1.00/03.0086 funded by European Regional Development Fund and project TA01010948 funded by Technology Agency of Czech Republic. The authors also would like to thank to KrampeHarex Company for providing PP fibers.

REFERENCES

1. Brandt A. M.: *Fibre reinforced cement-based (FRC) composites after over 40 years of development in building and civil engineering*. COMPOSITE STRUCTURES. 86 (2008).
2. 544.3R-08: *Guide for Specifying, Proportioning, and Production of Fiber-Reinforced Concrete*. ACI Committee 544.
3. William J. K., James H. H., Jefferey A. M.: *Polypropylene: Structure, Properties, Manufacturing Processes and Applications in Handbook of Polypropylene and Polypropylene Composites* (Haruhun G. K., ed.). Mercel Dekker Inc., New York 1999.
4. Pei M., Wang D., Zhao Y., Hu X., Xu Y., Wu J., Xu D.: J. Appl. Polym. Sci. 92 (2004).
5. Tu L., Kruger D., Wagener J. B., Carstens P. A. B.: Mag. Concr. Res. 50 (1998).
6. Zheng Z., Feldman D.: Prog. Polym. Sci. 20 (1995).
7. Carrino L., Moroni G., Polini W.: J. Mater. Process. Technol. 121 (2002).
8. Cui N.-Y., Brown N. M. D.: Appl. Surf. Sci. 189 (2002).
9. Šimor M., Ráheľ J., Vojtek P., Černák M.: Appl. Phys. Lett. 81 (2002).

L. Bodnárová[a], M. Fialová[b], D. Kopkáně[a], T. Morávek[b], P. Sťahel[b], and M. Černák[b,c] *([a] Faculty of Civil Engineering, Brno University of Technology, Brno, Czech Republic, [b] Department of Physical Electronics, Faculty of Science, Masaryk University, Brno, Czech Republic, [c] Department of experimental physics, Comenius University, Bratislava, Slovakia):* **Importance of Polypropylene Fibers as a Reinforcement in Concrete**

The main role of dispersed short discrete fibers as a reinforcement for concrete is to prevent formation of shrinkage cracks, their spreading in the structures and increasing resistance of concrete to high temperatures. The plasma treatment of polypropylene (PP) fibers was discussed as a method that leads to the increasing of surface freee energy of polypropylene, accordingly better adhesion between the fibers and cement matrix.

The plasma treatment improved the surface wetting properties of PP fibers. The three point bending test confirmed the improving of the mechanical performances of concrete with plasma treated fibers as a reinforcement.

Chem. Listy *106*, s1431−s1434 (2012) CEPLANT

DEPOSITION OF POLYMER FILMS ON ALUMINIUM SURFACE USING ATMOSPHERIC-PRESSURE PLASMA

LUCIA BÓNOVÁ[a]*, ANNA ZAHORANOVÁ[a], DUŠAN KOVÁČIK[a,b], MIRKO ČERNÁK[a,b]

[a] *Department of Experimental Physics, Faculty of Mathematics, Physics and Informatics, Comenius University, Mlynská dolina, 842 48 Bratislava, Slovak Republic,*
[b] *R&D Center for Low-Cost Plasma and Nanotechnology Surface Modifications, Faculty of Natural Science, Masaryk University, Kotlářská 2, 611 37 Brno, Czech Republic*
bonova@fmph.uniba.sk

Keywords: atmospheric-pressure plasma, aluminium alloy, hexamethyldisiloxane, hydrophobic film

1. Introduction

Aluminium alloys are getting renewed attention due to their light weight and high strength to weight ratios that could be transferred into higher efficiency for various technological application including aerospace, automotive, architecture and packaging. However, the corrosion of aluminium surface is a real problem. Painting and adhesive bonding of aluminium alloy are commonly used methods to prevent the aluminium surface from the corrosion. Unfortunately these methods include chemicals such as solvents and chromates. The first one is used to clean the surface from grease and dust, while chromates are used for the corrosion protection. However, plasma treatments offer an ecologically friendly alternative for cleaning and functionalizing metal surfaces.

The deposition of plasma polymerized thin-film coatings on aluminium for corrosion inhibition could provide an alternative to the conventional chromate conversion and to the wet chemistry.

Plasma polymerization is a universal method for the deposition of layers with properties useable for a wide range of applications[1]. This is caused by the high degree of control of their properties, which may be varied widely by plasma parameters. Plasma polymerized films have special advantages such as a thin film, a highly cross-linked, pinhole-free structure and in general good adhesion on substrates.

Widely used thin film material is silicon dioxide (SiO_2), which is the most common dielectric in semiconductor technology, serves as corrosion protection or permeation barrier in the packaging industry. Preparation of SiOx films by plasma enhanced chemical vapour deposition (PECVD) at low pressures has been extensively studied in the past[2,3]. Plasma polymerization of hexamethyldisiloxane (HMDSO) as monomer admixture to carrier gas seems to be very suitable for preparing thin-film coating on the surface.

In the recent years many works has been published using the radio-frequency (RF) low-pressure discharge for plasma polymerized coatings on different materials. Vasallo et al.[4] demonstrated in their work that hexamethyldisiloxane (HMDSO) layers deposited on steel exhibited good anti-corrosion properties when RF plasma discharge is fed with oxygen in addition to HMDSO. The anti-corrosion effect of organosilicon-based coatings deposited on aluminium alloy by means of a low-pressure plasma process was studied by Fernandes et al.[5] where different gases were used for HMDSO deposition process. Pre-treatment of the aluminium surface like cleaning is the important part of the polymerization process. Azioune et al.[6] investigated that the most effective way to clean the aluminium surface is pure argon plasma fed by RF discharge. Also oxygen and argon/oxygen mixtures were tested. The effectiveness of plasma cleaning was checked by means of X-ray photoelectron spectroscopy (XPS) and contact angle measurements.

Recently the attractive alternative to these low-pressure processes is the SiO_x deposition at atmospheric pressure, where no expensive vacuum pumping systems and batch processing would be necessary in a production line. Dielectric barrier discharges (DBDs) are nowadays widely used for many plasma processes such as modification of surface properties (improving wettability of polymers, adhesion properties, etc.) and also for functionalization of surfaces and plasma polymerization processes by DBDs are studied.

Plasma discharges working at atmospheric pressure like DBDs and plasma jets are suitable to treat flat surfaces. Bour et al.[7] deposited HMDSO layer on galvanized steel to give a protective coating against corrosion using DBD discharge. Plasma polymerization was carried out in different ways. To protect the aluminium from corrosion Lommatzsch et al.[8] apply an atmospheric pressure plasma jet. Also Trunec et al.[9] used a DBD discharge for HMDSO layer deposition on different materials.

2. Experimental setup

The organosilicon monomer used in this work was HMDSO (for synthesis, Merck Schuchardt OHG, Germany). As the aluminium substrates the aluminium alloy (99.5% Al) was used. To establish well defined initial conditions, before the experiment all samples were chemically pre-cleaned.

The plasma polymerization process was carried out in the plasma reactor based on the new type of surface DBD

– so called Diffuse Coplanar Surface Barrier Discharge (DCSBD)[10] – a planar source of the low-temperature plasma (Fig. 1). DCSBD plasma source generates thin (~ 0.3 mm) layer of diffuse non-equilibrium plasma of an extremely high plasma power density about 100 W cm^{-3}, which results in plasma processing times in order of one second.

The discharge was generated in the mixture of nitrogen and HMDSO. The N_2/HMDSO mixture was prepared by mixing the pure nitrogen with the nitrogen gas bubbled through liquid HMDSO monomer at 20 °C. To find suitable conditions for polymeric thin layer deposition, the ratios of nitrogen and HMDSO were experimentally tested.

The DCSBD electrodes consisting of 19 pairs of silver strip electrodes embedded 0.5 mm below the surface of 96% Al_2O_3 ceramics was energized by 14 kHz sinusoidal voltage, supplied by HV generator LIFETECH VF 700. The power supplied to the discharge was 195 W and the gap between the ceramics and sample was 0.3 mm.

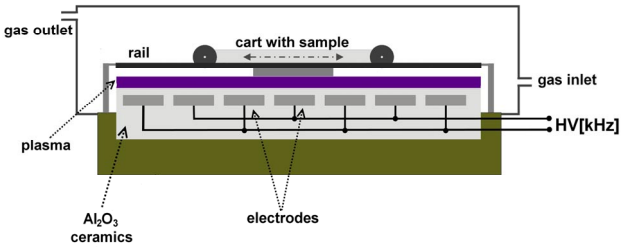

Fig. 1. **Scheme of the experimental atmospheric DCSBD plasma deposition reactor**

Contact angle measurements were carried out with Surface Energy Evaluation System (SEE System, Advex Instruments s.r.o., Czech Republic). Water drops of 2 μl were used to determine the contact angles. Each contact angle is an average of 10 measurements.

Chemical structure of the coatings was evaluated by Fourier Transform Infrared (FTIR) spectroscopy in attenuated total reflectance (ATR) using Bruker Optics Vector 22, MIRacle^{TM} spectrometer (PIKE Technologies). As the ATR crystal diamond/ZnSe was used (45° incidence angle). Data were collected from 600–4000 cm^{-1} wavelength range with 20 scans for each sample. The resolution was 4 cm^{-1}.

TOF SIMS IV (ION-TOF, Münster, Germany) spectrometer was used to measure the evidence of HMDSO layer. Measurements were carried out with a bismuth ion gun, operated at 25 keV ion energy and current 1 pA.

Measurements for the polymer layer thickness was carried out by FIB-SEM LYRA 3 GM nanotechnology workstation (TESCAN, Czech Rebublic).

Corrosion protection of HMDSO layer was tested by the immersion of aluminium samples into the 5% NaCl solution with the temperature of 35 °C and immersing time 120 h.

3. Results and discussion

To investigate the optimal deposition parameters for plasma polymerized HMDSO (pp-HMDSO) layer deposited on aluminium surface, different nitrogen and HMDSO ratios were used. The plasma polymerization process time was set to 60 sec. Table I shows results of Water Contact Angle (WCA) measurements for different HMDSO relative concentrations used in polymerization process.

Table I
Results of WCA measurements for different HMDSO relative concentrations in gas mixture of (N_2+HMDSO) measured immediately after polymerization and after 24 hours ageing

(HMDSO+N_2)/ N_2 concentration [%]	WCA immediately [°]	WCA after 24 hrs [°]
8.3	87.60 ± 3.25	100.64 ± 1.67
12.5	93.62 ± 1.29	103.25 ± 4.57
16.6	66.84 ± 1.90	81.2 ± 2.61
20.8	86.24 ± 4.22	95.97 ± 1.68
25	66.72 ± 14.94	80.94 ± 2.47

The contact angles were measured directly from the image of the solid-liquid meniscus of a liquid drop set taken with CCD camera. First measurements of WCA were taken immediately after the plasma-polymerization. Samples with deposited layer were stored on air and measured again after 24 hours ageing. These measurements indicate that the hydrophobicity still increase after the polymerization process and the most hydrophobic deposited layer is achieved at 12.5 % relative concentration of HMDSO in gas mixture.

The chemical composition analysis of the polymer film deposited on aluminium surface from mixture N_2/HMDSO was done by means ATR-FTIR. In the Fig. 2 the ATR-FTIR spectra of pp-HMDSO layer deposited on the sample for 60 sec (a), for 30 sec (b) as well as the reference sample spectrum (c) are shown. ATR-FTIR spectroscopy of the deposited pp-HMDSO layer confirms the presence of vibrational state primary amino functional groups (NH, NH_2), vibrational states of hydrogen (C-H, O-H) and also methyl groups (CH_n), generated by fragmentation of the monomer in the plasma and bounded to the surface of the aluminium substrate[11]. The IR spectrum exibits intensive absorption band at 2960 cm^{-1} and 2925 cm^{-1} which indicates the presence of CH_3 and CH_2 groups respectively. The deposited film exhibited strong absorption at 1270 cm^{-1} associated with the Si-CH_3 group. The most intensive absorption band is at 1070 cm^{-1} and peaks in this region can be interpreted as Si-O-Si, Si-CH_2-Si, Si-O-C or Si-NH-Si groups. It is clear from the Fig. 2 that longer

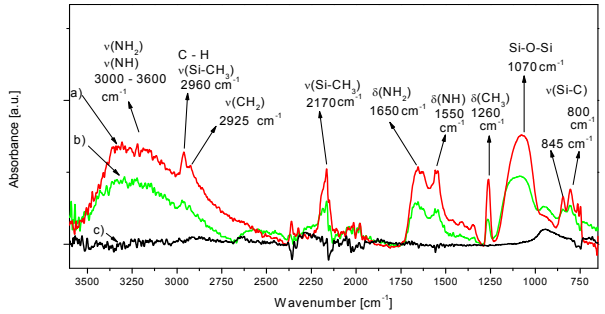

Fig. 2. **ATR-FTIR absorption spectra of: (a) pp-HMDSO – 60 s polymerized, (b) pp-HMDSO – 30 s polymerized, (c) aluminium surface – reference sample**

polymerization time brings more intensive absorption in regions denoted of HMDSO fragments bounded on aluminium surface.

The changes of the polymer film deposited on aluminium surface after the salt water test of corrosion protection were analysed by the means of FTIR also. The results are presented in Fig. 3, where chemically cleaned Al sample (d), chemically cleaned Al sample after salt water test (a), sample with HMDSO layer (c) and sample with HMDSO layer after the salt water test (b) are shown.

From analyses of the most intensive peaks in Fig. 3 is clear, that the polymer layer deposited on the aluminium surface is the same after salt test, and there is evidence of the changes on the aluminium surface. The are the most intesive peak in the region of 3000–3600 cm^{-1} , which may be assigned to –OH groups and the intensive peak at 1067 cm^{-1} which may indicate the presence of Al-O or Al-Cl group.

SIMS measurement was used to study the existence of monomer fragments in deposited film. The SIMS spectrum of pp-HMDSO coated aluminium sample is

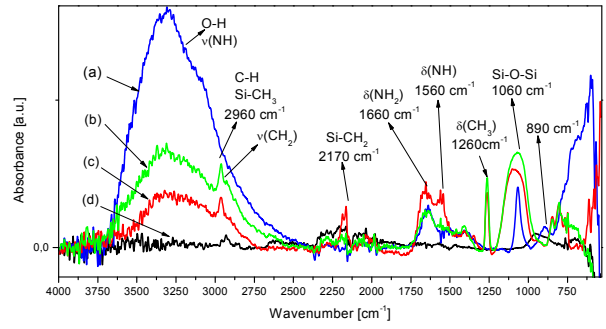

Fig. 3. **ATR-FTIR absorption spectra of: (a) chemically cleaned Al sample after salt test, (b) pp-HMDSO sample after salt test, (c) pp-HMDSO sample, (d) chemically cleaned Al sample**

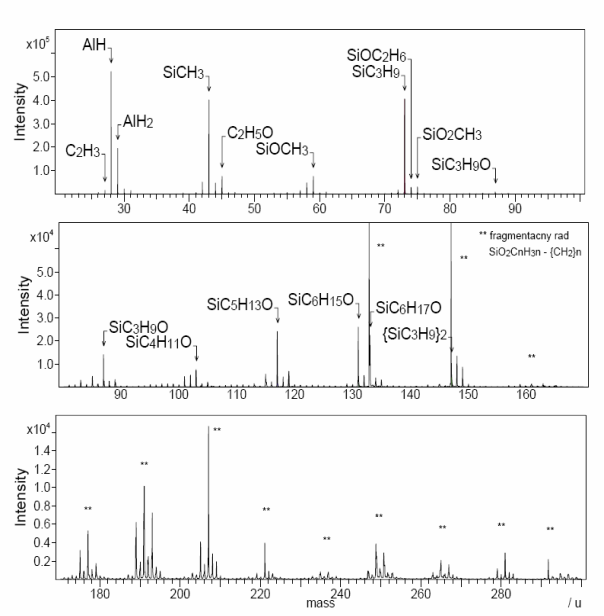

Fig. 4. **SIMS spectrum of pp-HMDSO coated Al sample**

shown in Fig. 4. As can be seen the evidence of pp-HMDSO layer was confirmed by measuring the fragmentation row of $Si\text{-}O_2\text{-}C_n\text{-}H_{3n}\text{-}\{CH_2\}_n$ and also by detection of the methyl groups bonded to Si or SiO.

To confirm the corrosion protection of pp-HMDSO layer on aluminium surface, samples were immersed in the NaCl solution for 120 h. For comparison uncoated aluminium samples were also tested. The results can be seen in Fig. 5 where the aluminium surface without protection coating and pp-HMDSO layer coated aluminium samples are shown before and after the salt test. Salt water test showed the protective effect of the pp-HMDSO layer on

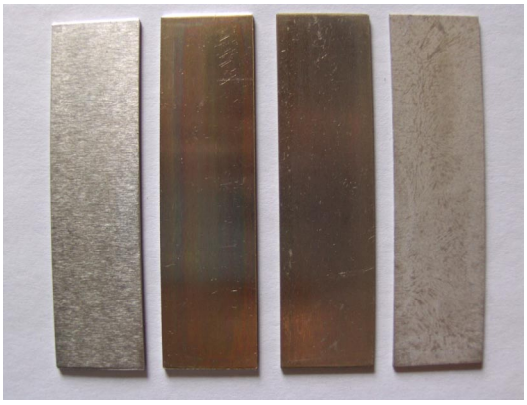

Fig. 5. **Photographs of Al samples: (a) chemically cleaned Al sample, (b) pp-HMDSO sample, (c) pp-HMDSO sample after salt test, (d) chemically cleaned Al sample after salt test**

the aluminium surface. On the aluminium surface without deposited layer there were spots of typical aluminium corrosion after immersion in the salt water.

To measure the thickness of pp-HMDSO layer the FIB-SEM was used. The surface of the sample was sputtered using gallium ion gun with accelerating voltage 30 kV. The measured pp-HMDSO layer was 250 nm.

4. Conclusion

In this paper the preliminary results of the polymer hydrophobic layer deposition on the aluminium surface were presented. The layer was deposited from the mixture of organosilicon monomer HMDSO with nitrogen using the DCSBD plasma source at atmospheric pressure. The optimal deposition time was 60 second at energy power to plasma 195 W. The polymer layer was hydrophobic with the water contact angle about 100 degrees. The FTIR spectra showed the chemical structure of the polymer layer – the presence of Si-CH_3, Si-CH_2, Si-O-Si, C-N, and O-H groups. The SIMS analyses confirmed also the fragmentation of monomer and presence of methyl groups bounded on Si or SiO. Salt water corrosion test confirmed the protection properties of polymer layer on the aluminium surface. By this manner it can be deposited on the aluminium surface the thin hydrophobic polymer layer with good adhesion to the surface and anticorrosive properties, as was demonstrated by the results of surface analyses (WCA, FTIR, SIMS, salt test).

This work is the result of the project implementation: 26240220002 and 2622020004 supported by the Research & Development Operational Programme funded by the ERDF. This work has been supported also by the project R&D center for low-cost plasma and nanotechnology surface modifications CZ.1.05/2.1.00/03.0086 funding by the ERDF.

REFERENCES

1. Cho S. H., Park Z. T., Kim J. G., Boo J. H.: Surf. Coat. Technol. *174-175*, 1111 (2003).
2. Aumaille G., Vallée K., Granier A., Goullet A., Turban F.: Thin Solid Films *359*, 188 (2000).
3. Hegemann D., Vohrer U., Oehr C., Riedel R.: Surf. Coat. Technol. *116-119*, 1033 (1999).
4. Vassallo E., Cremona A., Laguardia L., Mesto E.: Surf. Coat. Technol. *200*, 3035 (2006).
5. Fernandes J. C. S., Ferreira M. G. S., Haddow D. B., Goruppa A., Short R., Dixon D. G.: Surf. Coat. Technol. *154*, 8 (2002).
6. Azioune A., Marcozzi M., Revello V., Pireaux J. J.: Surf. Interface Anal. *39*, 615 (2007).
7. Bour J., Bardon J., Hugues A., Del Frari D., Verheyde B., Dams R., Vangeneugden D., Ruch D.: Plasma Process. Polym. *5*, 788 (2008).
8. Lommatzsch U., Ihde J.: Plasma Process. Polym. *6*, 642 (2009).
9. Trunec D., Zajíčková L., Buršíková V., Studnička F., Sťahel P., Prysiazhnyi V., Peřina V., Houdková J., Navrátil Z. and Franta D.: J. Phys. D, Appl. Phys. *43*, 225403 (8pp) (2010).
10. Šimor M., Ráheľ J., Vojtek P., Brablec A., Černák M.: Appl. Phys. Lett. *81*, 2716 (2002).
11. Milata V. et al.: *Applied Molecular Spectroscopy*, STU Bratislava, Bratislava 2008.

L. Bónová[a], A. Zahoranová[a], D. Kováčik[a,b], and M. Černák[a,b], *([a] Dep. of Experimental Physics, Comenius University, Bratislava, Slovak Republic, [b] R&D Center for Low-Cost Plasma and Nanotechnology Surface Modifications, Masaryk University, Brno, Czech Republic):*
Deposition of Polymer Films on Aluminium Surface Using Atmospheric-Pressure Plasma

The paper presents results of plasma polymerised coating deposited from the mixtures of HMDSO monomer with nitrogen on aluminium substrate using plasma reactor based on Diffuse Coplanar Surface Barrier Discharge (DCSBD). Contact angle measurement was used to investigate the optimal deposition parameters. The deposited films were characterized by FTIR and SIMS methods. The corrosion protection of the HMDSO layer was proved by salt water test.

DIAGNOSTICS OF DIFFUSE COPLANAR SURFACE BARRIER DISCHARGE OPERATED IN ARTIFICIAL AIR WORKING GAS: BASIC RESULTS

JAN ČECH*, JANA HANUSOVÁ, PAVEL SŤAHEL

R&D center for low-cost plasma and nanotechnology surface modifications, Faculty of Science, Masaryk university, Kotlářská 2, 611 37 Brno, Czech republic
cech@physics.muni.cz

Keywords: DCSBD, diffuse coplanar surface barrier discharge, time resolved, discharge pattern, spatially resolved, optical emission spectroscopy, OES, iCCD, plasma diagnostics

1. Introduction

In past decades the importance of barrier dicharges[1] as the sources of non-equilibrium plasmas for material processing has raised. With increasing demand on so called "green technologies" and low environmental footprint, low-cost plasma treatment technologies have become requested alternatives to classical chemical treatment.

The Diffuse Coplanar Surface Barrier Discharge (DCSBD) belongs to group of barrier discharges. Plasma of DCSBD is generated in thin layer[2] above dielectric at relatively high power densities of the order of 100 W cm^{-3}. The discharge consists of thin channels (filaments or microdischarges[3]) crossing the electrode gap between electrodes and visually diffuse-like layer above electrodes. These properties make DCSBD a promising candidate for high-speed plasma processing[4].

DCSBD has been successfully tested as the low-cost atmospheric pressure plasma source. DCSBD operated in ambient air at industrial production lines in continuous regime (in-line) seems to be suitable plasma source for plasma treatment of low-value-added materials[5].

To better understand the DCSBD behavior in artificial air at atmospheric pressure the spatially resolved optical emission spectroscopy (OES) and time-resolved optical imaging of DCSBD were performed. The basic results are given in presented paper.

2. Experimental setup – simplified DCSBD cell

For the study of DCSBD properties over wide range of physical conditions and discharge configurations the simplified DCSBD cell or system was developed. This setup (discharge cell) is given in Fig. 1. In Fig. 1 (left) the cross-section of discharge cell is given. The discharge cell is made of polymer capsule in which the system of semi-movable electrodes is placed. Both electrodes are pressed against dielectric plate and dipped in insulating oil bath. The arbitrary rectangular electrode gap between electrodes can be set with width up to 5 mm. The minimum distance between electrodes is governed by the insulating properties of oil bath and in present study the electrode distance was set to 0.55±0.05 mm. The maximum electrode distance is governed by power supply unit, resp. by the maximum allowable high voltage applicable to the powered electrode. In practice the limit of maximum electrode distance of described system is about 2.5 mm.

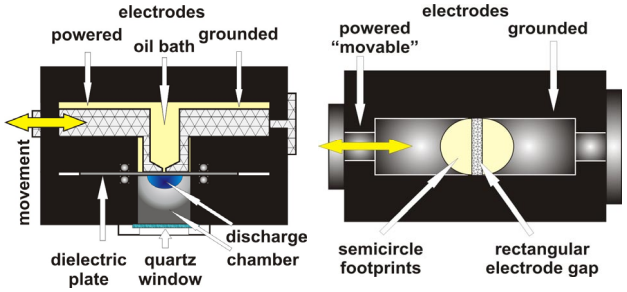

Fig. 1. **Simplified DCSBD discharge cell. Cross-section of simplified developmental DCSBD cell (left) and electrode system ground plan, with electrode gap (right) are depicted. The dimensions are not proportional**

Great advantage of the simplified DCSBD setup is the ability of easy of change of dielectric plate and electrode gap width. The dielectric plate is pressed directly to the surface of electrodes, which form two semicircle footprints on the dielectric plate, forming rectangular electrode gap in between. The schematic view of the electrodes is given in Fig. 1 (right). The view plane of the picture is the same as if the paper would be the dielectric plate. The diameter of semicircle electrodes is approx. 20 mm.

Discharge chamber is placed from the opposite side of dielectric plate; see Fig. 1 (left). The dielectric plate is made of 96% alumina (Al_2O_3) with dimensions of 10×10 cm and thickness of approx. 0.6 mm. Discharge chamber enables us to operate the discharge in controlled working gas environment. Quartz window on the opposite side of discharge chamber enables us to perform optical diagnostics of the discharge.

3. Experimental setup of time resolved iCCD imaging and spatially resolved OES, resp.

Experimental setup for time resolved iCCD measurements is given in Fig. 2. The discharge cell described in section 2 is used.

Two gas flow controllers Voghtlin Instruments red-y GCR were used to set requested working gas mixture. As primary gasses nitrogen of the purity better than 99.996 % and oxygen of the purity better than 99.996 % were used. The gas mixture ratio of nitrogen to oxygen of 80:20 was used in described experiments. The total gas flow rate was kept at 3 slpm.

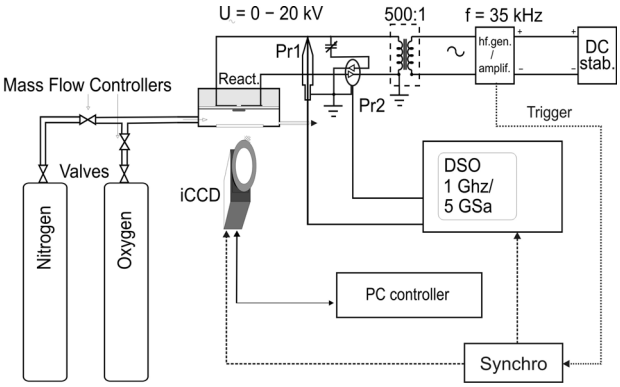

Fig. 2. **Experimental setup of time resolved iCCD imaging**

High voltage (HV) power supply was used to ignite and maintain the discharge. The HV power supply consists of high frequency tunable generator LIFETECH HF Power Source powered by stabilized DC power source STATRON 3262 and LIFETECH HV transformer. The HV power supply was operated at 30 kHz and 30 $kV_{peak\text{-}to\text{-}peak}$ for OES measurements, resp. 28 $kV_{peak\text{-}to\text{-}peak}$ for iCCD measurements, sine-wave.

The current-voltage characteristics were recorded using LeCroy WaveRunner 6100A 1 GHz/5 GSa digital storage oscilloscope coupled with HV probe Tectronix P6015A 1000:1 (in Fig. 2. Denoted as Pr1) and Pearson Current Monitor 2877 (in Fig. 2. Denoted as Pr2).

Variable high voltage capacitor was used as the displacement current compensator. The HV capacitor was connected antiparallel through current probe. Tuning the HV capacitor to the capacity close to discharge cell capacity effectively reduces measured displacement current of discharge cell which is of the same order as the discharge current. This increases effectively the signal-to-noise ratio of discharge current measurements.

For the high speed synchronized discharge imaging, the Princeton Instruments PI-MAX 1024RB-25-FG-43 iCCD camera equipped with 50 mm, f/2.8 UV lens was used. The iCCD camera was placed along axis of symmetry perpendicular to DCSBD plasma layer.

To synchronize and semi-automate the measurements, the Agilent 33220A function generator was used. As the source signal the reference signal of HF generator was used. The generator fires triggering signals for synchronous iCCD image capture together with current-voltage measurement of the same event.

This setup enables us to take series of synchronized images of the discharge together with its current-voltage characteristics with the resolution of single half-period of high voltage waveform. In presented work the 100 images series of first, second and both half-periods were taken with gate times of 17, resp. 34 μs. The iCCD delays were set in the way to guarantee that images represent all discharge events of half-periods that can be identified in current-voltage waveforms.

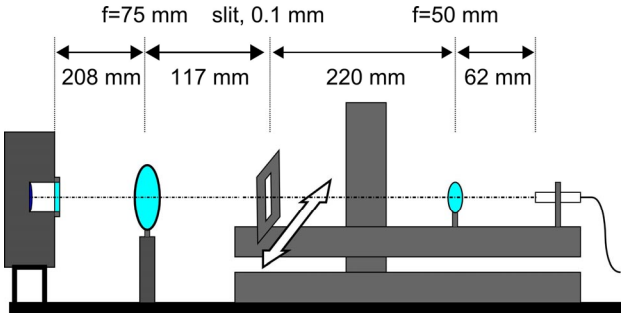

Fig. 3. **Schematic view of the optical bench system, optical parameters are marked and also the scanning direction**

Experimental setup for spatially resolved optical emission spectroscopy (OES) measurements is similar to previous one. The discharge cell and electrical parameters setups were the same as described for iCCD measurements. The experimental setup given in Fig. 2 was kept with the exception of the iCCD/optical bench system substitution.

For spatially resolved OES the computer programmed 3D stage carrying optical bench coupled to spectrometer was used instead of iCCD camera. We used 3 precision motorized linear stages Zaber T-LSQ 150 B coupled to develop XYZ-3D motion stage. The schematic view of the optical bench system is given in Fig. 3. From the left to the right the optical pathway is as follows: The image of discharge in discharge chamber is focused using fixed positioned f = 75 mm quartz lens to the entrance slit of the 0.1 mm width placed on movable bench. The spatially resolved light is then collected using f = 50 mm quartz lens and optical fiber holder. As the detector, the quartz fiber coupled spectrometer Avantes AvaSpec-2048TEC-2 with thermoelectrically cooled CCD was used. The optical resolution of spectrometer was 1.4 nm FWHM.

4. Results and discussion

In Fig. 4 the typical optical emission spectrum of DCSBD burning in the mixture of nitrogen and oxygen is given. To emphasize signal from atomic oxygen lines the spectrum with higher oxygen ratio was selected. The correction to spectrometer sensitivity was not performed in Fig. 4 to enhance readability and suppress noise and background shift in the spectrum. Dominant part of the spectra consists of molecular bands of second positive system of

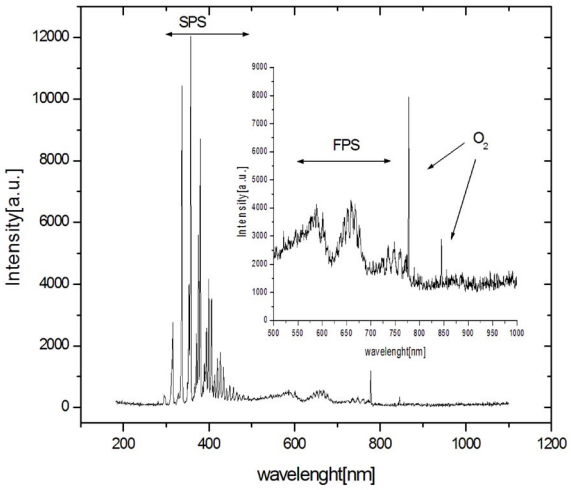

Fig. 4. **Optical emission spectrum of DCSBD near the nitrogen emission intensity maximum. The nitrogen:oxygen ratio was 20:80**

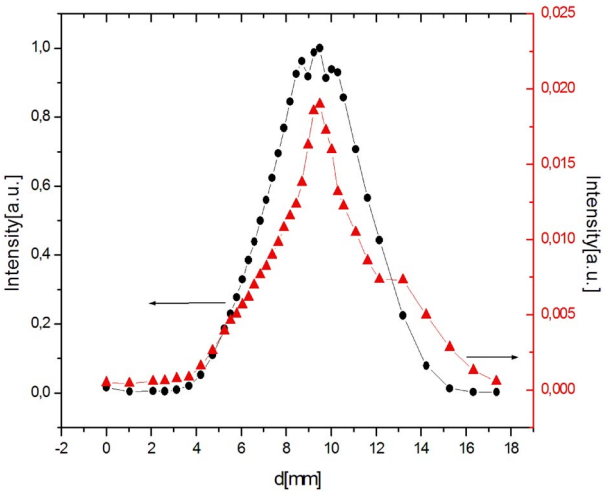

Fig. 5. **Spatial intensity profiles of nitrogen molecular band at 337.13 nm (circle symbols) and atomic oxygen triplets at 777.45 nm (triangle symbols). The distance across discharge pattern is given on the horizontal axis and it is denoted by *d***

nitrogen (SPS, $C\,^3\Pi_u \rightarrow B\,^3\Pi_g$) with maxima at 337.13 nm. At higher wavelengths the weak bands of first positive system (FPS, $B\,^3\Pi_g \rightarrow A\,^3\Sigma_u^+$) can be also identified. At wavelengths of 777.45 nm and 845.64 nm the spectrally unresolved triplets of atomic oxygen are identified. Due to limited sensitivity and spectral resolution of spectrometer other spectral systems as first negative system of nitrogen or NO-γ system (in UV range) cannot be observed.

Using the semi-automated stage with optical bench system, the spatially resolved spectral intensities can be obtained. The spatially resolved spectra were taken from approx. 1–2 mm wide zone along the horizontal diameter of the discharge pattern, distance *d* in figures, see also Fig. 7. The estimated spatial resolution is about 0.3 mm. The spatial profiles of intensities of 0-0 vibration transition of SPS of nitrogen (337.13 nm) and corresponding profile of atomic oxygen triplet intensity (777.45 nm) is given in Fig. 5. The SPS of nitrogen intensity profile has symmetrical structure with fine three-peak behavior in the middle of the discharge gap and above electrodes near gap edges. In order to confirm that this fine structure is not caused by measurement error, the comparison with independent technique (iCCD) was performed, see Fig. 8. In the profile of oxygen line emission intensity such fine structure was not observed and only one broad peak symmetrical to electrode gap position was observed.

From the SPS (vibration transitions 0-2, 1-3, 2-4 and 3-5, stopped at 380.5 nm) the vibration temperature can be estimated using the Spectrum Analyzer[6]. The spatial profile of estimated vibrational temperature is shown in Fig. 6. The estimated error is about 100 and 200 K. For comparison the nitrogen intensity profile is plotted. It can be seen, that the spatial behavior of SPS emission intensity and SPS vibration temperature is in close correlation under presented conditions. The most intensive area of the discharge is also the area of the highest vibration temperature.

The iCCD imaging was used to characterize discharge patterns of DCSBD under given conditions. In Fig. 7 the iCCD images of the discharge spatial evolution is shown. Fig. 7 contains two groups of images. In first row the images of single-shot captures of discharge patterns is given for positive (left), negative (middle) and both half-periods (right) of input HV waveform. The second row shows software accumulated images of 100 of single-shot events to emphasize the discharge pattern structures. Polarity and expected electrode/gap positions are depicted as

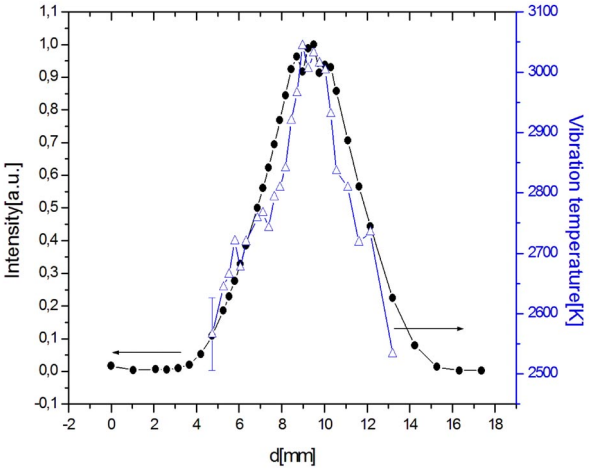

Fig. 6. **Spatial behavior of SPS intensity (circle symbols) and vibration temperature (triangle symbols) shows high spatial correlation. The distance across discharge pattern is given on the horizontal axis and it is denoted by *d***

dotted curves. Polarity is taken as polarity of HV signal on the left electrode, see Fig. 1 and 2. The discharge burns in numerous micro-discharges[3] spread along discharge gap.

To be able to compare the iCCD imaging results with the results obtained using spatially resolved OES, the image intensity calculations from similar discharge area were performed. The results are given in Fig. 8. For both half-period curve one can see the same spatial structures as in curve representing nitrogen emission intensity. This is in agreement with the spectral intensities of the discharge and spectral response of iCCD camera intensifier stated by the manufacturer.

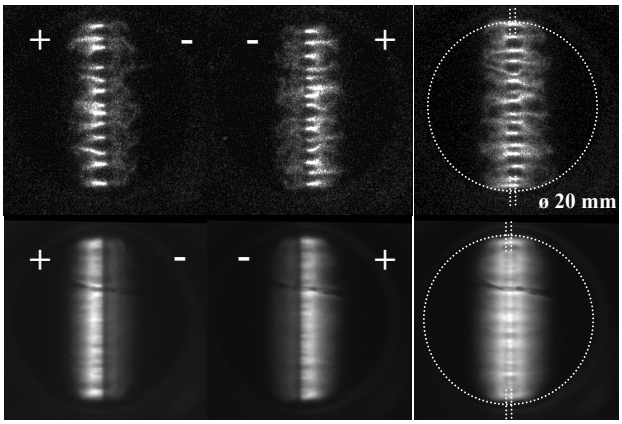

Fig. 7. **iCCD images of DCSBD. From the left to right: positive, negative and both half-periods are given. First row shows selected single-shot images, second row represents sum of 100 of single images. The dark artifact in upper third of images was related to dielectric plate artifact. The input voltage of 28 kV_{pp} was used**

5. Conclusion

In this paper we have presented optical measurements of DCSBD in artificial air. The close correlation of spatial profiles of vibration temperature estimated from SPS of nitrogen with spatial profile of SPS intensity was presented. It was shown that the SPS intensity has a fine spatial structure above electrode gap, while the oxygen triplet profile has a single peak behavior. The fine structure of SPS intensity profile was confirmed using time resolved optical imaging (iCCD). This fine structure can be reconstructed using accumulated intensity profiles of positive and negative half-period that have double-peak intensity behavior.

This research has been supported by the project R&D center for low-cost plasma and nanotechnology surface modifications CZ.1.05/2.1.00/03.0086 funded by European Regional Development Fund and projects No. TA01011356/2011 and TA01010948/2011 of the Technology Agency of the Czech Republic.

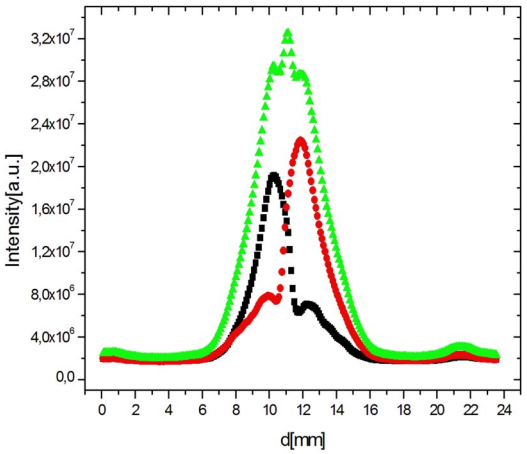

Fig. 8. **Integrated intensity profiles along horizontal diameter of discharge pattern. Curves are calculated from the sum of 100 of discharge pattern images (see Fig. 7). Positive, negative and both half-periods are depicted using square, circle, resp. triangle symbols. The distance across discharge pattern is given on the horizontal axis and it is denoted by *d*. The input voltage of 28 kV_{pp} was used**

REFERENCES

1. Kogelschatz U.: Plasma Chem. Plasma Process. *23*, 1 (2003).
2. Čech J., Hoder T., Buček A., Ráheľ J. Černák M.: *17th Symposium on Application of Plasma Processes*, 145–146 (2009).
3. Hoder T., Brandenburg R., Basner R., Weltmann K.-D., Kozlov K.V. and Wagner H.-E.: J. Phys. D, Appl. Phys. *43*, 124009 (8pp) (2010).
4. Černák M., Kováčik D., Ráheľ J. Sťahel P., Zahoranová A., Kubincová J., Tóth A., Černáková Ľ.: Plasma Phys. Control. Fusion *53*, 124031 (8pp) (2011).
5. Černák M., Černáková L'., Hudec I., Kováčik D., Zahoranová A.: Eur. Phys. J.: Appl. Phys. *47*, 22806 (2009).
6. Navrátil Z., Trunec D., Šmíd R. and Lazar L.: Czech. J. Phys. *56*, Suppl. B, B944-951 (2006).

J. Čech, J. Hanusová, and P. Sťahel, *(Masaryk University, Brno, Czech Republic):* **Diagnostics of Diffuse Coplanar Surface Barrier Discharge Operated in Artificial Air Working Gas: Basic Results**

In this paper we present measurements of DCSBD in artificial air. Simplified DCSBD cell with one electrode pair with electrode gap width 0.55±0.05 mm was used. Discharge was driven using high voltage sine-wave generator at 30 kHz and 28, resp. 30 kV_{pp}. Spatially resolved optical emission spectroscopy and time-resolved optical imaging was performed. Close correlation of spatial profiles of vibration temperature of SPS of nitrogen with spatial profile of SPS intensity was presented. SPS intensity shows fine spatial structure above electrode gap, while oxygen triplet profile has only single peak behavior. The fine structure was confirmed using time-resolved optical imaging.

IMPROVEMENT OF SURFACE PROPERTIES OF REINFORCING POLYPROPYLENE FIBRES BY ATMOSPHERIC PRESSURE PLASMA TREATMENT

MONIKA FIALOVÁ[a]*, DANA SKÁCELOVÁ[a], PAVEL SŤAHEL[a], MIRKO ČERNÁK[a,b]

[a] Department of Physical Electronics, Faculty of Science, Masaryk University, Kotlářská 2, 611 37 Brno, Czech Republic, [b] Department of experimental physics, Comenius University, Mlynská Dolina F2, 842 48 Bratislava, Slovakia
mfialova@mail.muni.cz

Keywords: DCSBD, polypropylene fibre, wettability, fibre-reinforced concrete, contact angle measurement

1. Introduction

Mechanical properties as toughness, tensile strength and flexural ductility[1] of concrete can be significantly improved with addition of polypropylene fibres. For this purpose low density polypropylene is typically used. The advantage of PP fibres is their low cost and chemical stability. However, their surface energy is low. Because of hydrophobic properties of PP fibres the adhesion to cement matrix is very low and it is difficult to distribute fibres uniformly in matrix. The modification of the PP fibre surface can achieve higher wettability. There are several ways of increasing the surface energy of PP fibres: mechanical, chemical or plasma treatment[2,3]. In the first case the surface of PP is mechanically roughened, however, this modification negatively affects the mechanical properties. The chemical modification is widely used in the industry[4]. This technology is based on the surfactants which are deposited on the surface of PP and make the surface wettable. The disadvantage of this method is its instability in contact with water (the surfactants are washed away) and also it is necessary to use chemicals which are restricted by the EU legislative REACH. The method based on cold plasma treatment creates reactive hydrophilic group on the surface of PP fibres whereas bulk properties of fibre remain unchanged. Various low pressure plasma sources for treatment of PP fibres have been widely studied[3,5], however, using the low pressure plasma technologies is limited because of the necessity of expensive vacuum systems and high energy consummation. Plasma technologies operating at atmospheric pressure provide a simple low-cost technique compared with the low pressure plasmas. The dielectric barrier discharge (DBD) technology is one of the most used methods to generate cold atmospheric pressure plasma[6].

In this paper the plasma treatment of polypropylene fibres in Diffuse Coplanar Surface Barrier Discharge (DSCBD) operated at atmospheric pressure was investigated. DCSBD was developed at the Masaryk University in Brno and Comenius University in Bratislava[7–9].

This type of discharge is featured by high electron temperature, however, rotational temperature is close to room temperature. Due to high non-isothermicity of discharge it has a great potential for industry plasma treatment of thermal sensitive material such as polymers, paper, wood or felt[10,11].

2. Experimental setup

DCSBD operated at atmospheric pressure was used for plasma treatment of polymer fibres. Fig. 1 shows the electrode configuration of DCSBD. The electrodes are created by 32 parallel metallic strips embedded in Al_2O_3 ceramic. Thin film of macroscopically diffuse atmospheric pressure non-equilibrium plasma is created on the surface of the electrode. An image of the DCSBD plasma is shown in Fig. 2.

Plasma treatment of polypropylene fibres was carried out in ambient air. We tested the effect of plasma treat-

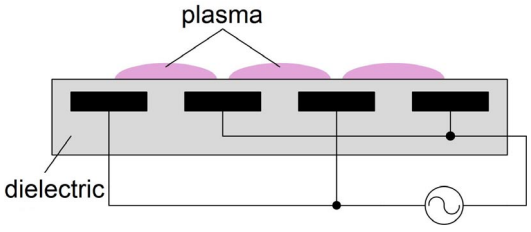

Fig. 1. **Cross-section of the discharge electrode system**

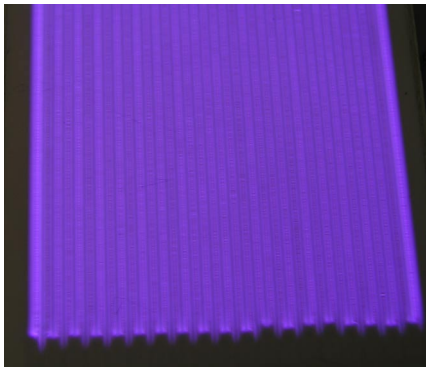

Fig. 2. **Image of thin film of DCSBD plasma**

ment on fibres for discharge power in range 250–400 W and treatment time in range 5–30 s. A high frequency voltage (14 kHz, 13 kV peak to peak) was applied between the electrodes.

Polypropylene fibres commercially produced by KrampeHarex company were used as samples[12]. The diameter of fibres with round cross section was 32 μm (±10 %), the density of fibres was 910 kg m^{-3} and tensile strength was 300 N mm^{-2} (±15 %) .

The effect of the plasma treatment on surface properties of the fibres was studied by contact angle measurement using Surface Energy Evaluation System (SEE System) made by Advex Instruments[13]. Distilled water was used as a testing liquid.

Wetting properties of treated and untreated fibres were investigated by water absorption measurement method. For this purpose 20 cm long bunch of PP fibres was used. The bunch of fibres was weighed before and after the soaking with water for 10 s. The difference of the weight of fibres after and before soaking with water gave absorption capacity of the bunch of fibres. This simple experiment shows how water absorption capacity and wetting properties of PP fibre changes after the plasma treatment.

The surface morphology was studied by stereo microscope LEICA S6 D with maximum resolution 432 lp/mm and magnification 80×.

3. Results

An image of the water drop on PP fibre before and after plasma treatment is shown in Fig. 3. The water contact angle of untreated fibre (110°) decreased to about 50° after the 30 s of the plasma treatment. This effect can be related to the formation of functional polar groups and radicals on the PP surface after plasma treatment.

Fig. 4 shows, the wettability of PP fibres increased with treatment time for four discharge power (250, 300, 350, 400 W). Water absorption of fibre increased during the first 15 s of plasma treatment, above 15 s remained constant. Moreover maximum water absorption capacity was depending on plasma power density and it increased with increasing power density.

The washing out resistance of plasma treated fibres was also investigated. Plasma treated fibres were soaked with water for 10 s, than samples were dried and consequently characterised by water contact angle measurement. The change of wettability and contact angle was measured.

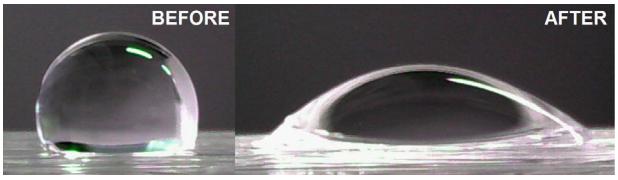

Fig. 3. **The water contact angle before and after 30 s plasma treatment at 300 W discharge power**

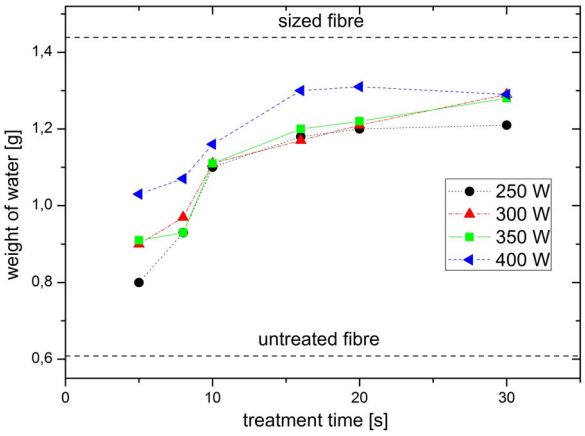

Fig. 4. **Weight of absorbed water in bunch of PP fibres as a function of plasma treatment time for different discharge power. There are marked also the values of weight for sized and untreated fibres**

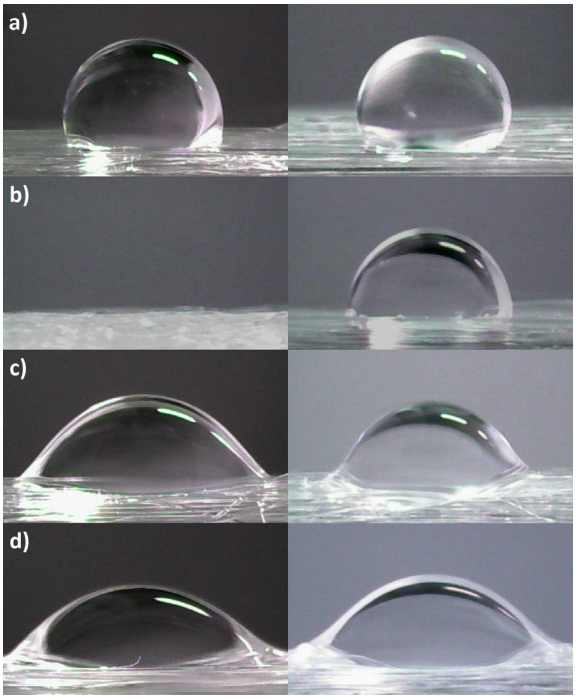

Fig. 5. **Comparison of wettability of a) untreated, b) sized and c) 5 s and d) 30 s plasma treated fibres in a left column and effect of washing out in right column. The discharge power was 300 W**

It was proven that the effect of plasma treatment was resistant to washing out in contrast to the commercial size. Soaking with water did not influence the wettability of plasma treated fibres. Commercially produced sized fibres

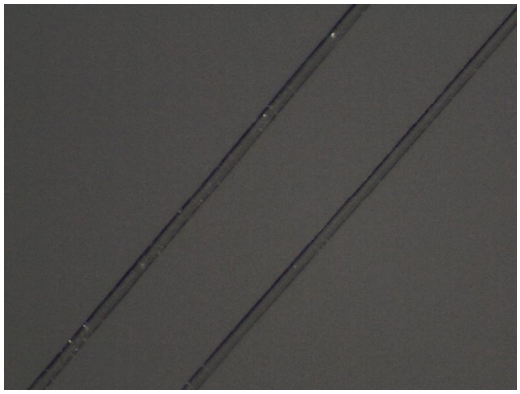

Fig. 6. **Stereo microscope image of as-received untreated fibres**

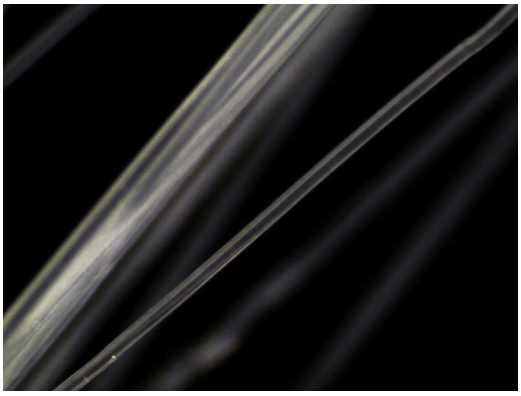

Fig. 8. **Stereo microscope image of 30 s plasma treated fibres. Discharge power was 300 W and treatment time 30 s**

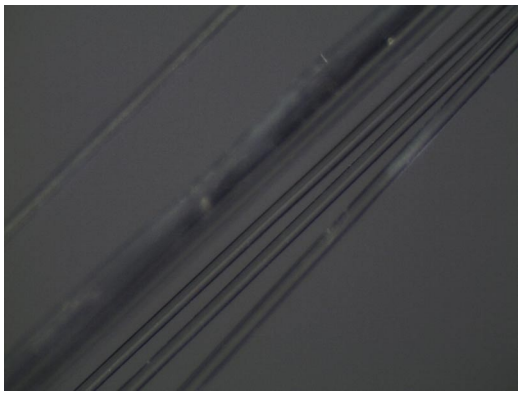

Fig. 7. **Stereo microscope image of plasma treated fibres. Discharge power was 300 W and treatment time 5 s**

were totally wetted, but after soaking with water the fibre became hydrophobic almost as untreated fibres (see Fig. 5).

The influence of plasma treatment on the surface appearance of PP fibres was studied by stereo microscope. In Fig. 6 two untreated PP fibres are shown. Plasma treatment did not affect the surface structure of PP fibre (see Fig. 7 and Fig. 8). During plasma treatment no macroscopic mechanical damage was observed.

4. Conclusion

The influence of plasma treatment on the wetting and surface properties of polypropylene fibres was investigated.

The plasma treatment of PP fibres by DCSBD led to an increase of the wettability, accordingly the water absorption of fibres improved. The surface morphology remained unchanged.

Commercially produced sized PP fibres were totally wetted, but after soaking with water the surfactants were washed out and PP fibre became hydrophobic. Plasma treated fibres exhibited washing out resistance in contrast with the sized PP fibres.

This research has been supported by the project CZ.1.05/2.1.00/03.0086 'R&D center for low-cost plasma and nanotechnology surface modifications' funded by European Regional Development Fund and by the project TA01010948 funded by Technology Agency of Czech Republic. The authors also would like to thank to KrampeHarex Company for providing polypropylene fibres.

REFERENCES

1. Shi C., Mo Y. L.: *High-Performance Construction Materials – Science and Applications*, p. 91–154, World Scientific Publishing Co. Pte. Ltd., Singapore 2008.
2. Wei Q. F.: Mater. Charact. *52*, 231 (2004).
3. Felekoglu B., Tosun K., Baradan B.: J. Mater. Process. Technol. *209*, 5133 (2009).
4. Garbassi F., Morra M., Occhiello E.: *Polymer surface: from physics to technology*, J. Wiley, Chichester 1998.
5. Wu H.-Ch., Li V. C.: Cem. Concr. Compos. *21*, 205 (1999).
6. Ma Z., Qi H.: Surf. Coat. Technol. *201*, 4935 (2007).
7. Šimor M., Ráheľ J., Vojtek P., Brablec A., Černák M.: Appl. Phys. Lett. *81*, No. 15 (2002).
8. Černák M., Černáková L., Hudec I., Kováčik D., Zahoranová A.: Eur. Phys. J.: Appl. Phys. *47*, 2 (2009).
9. http://gimmel.ip.fmph.uniba.sk/treaters/
10. Černák M.: Method and apparatus for treatment of textile materials. US Patent Appl. No. 2004/0194223, 07 October 2004.
11. Černák M.: An apparatus and method for improving felting properties of animal fibres by plasma treat-

ment. CZ Patent Appl. No. 2009/000123.
12. http://www.en.krampeharex.com/
13. http://www.advex-instruments.cz/

M. Fialová[a], D. Skácelová[a], P. Sťahel[a], and M. Černák[a,b] *([a] Department of Physical Electronics, Faculty of Science, Masaryk University, Brno, Czech Republic, [b] Department of experimental physics, Comenius University, Bratislava, Slovakia):* **Improvement of Surface Properties of Reinforcing Polypropylene Fibres by Atmospheric Pressure Plasma Treatment**

Activation polypropylene (PP) fibres used for reinforcement of concrete was tested in atmospheric pressure Diffuse Coplanar Surface Barrier Discharge generated in ambient air. The surface properties and wettability were studied by contact angle measurement and amount of absorbed water measurement. Surface morphology was investigated by optical stereo microscope.

The plasma treatment changed totally hydrophobic surface of untreated PP fibres with water contact angle about 110° to hydrophilic surface with contact angle of about 50°. In comparison with sized fibres plasma modification was resistant to washing out. The plasma treatment improved surface wettability without any macroscopically observable mechanical damage of PP fibres.

Chem. Listy *106*, s1443−s1446 (2012) CEPLANT

SOME ASPECTS OF UNDERWATER DISCHARGE GENERATED BY HV PULSES AT ATMOSPHERIC PRESSURE

OLEKSANDR GALMIZ*, ANTONÍN BRABLEC, ZDENĚK NAVRÁTIL

Dep. of Physical Electronics, Faculty of Science, Masaryk University, Kotlářská 2, 61137 Brno, Czech Republic
oleksandr.galmiz@gmail.com

Keywords: underwater discharge, OES, HV pulses

1. Introduction

Underwater electrical discharge systems attract attention of many research groups mainly for their proven efficiency in the wastewater remediation[1]. A recently emerged application for underwater discharge offering substantial economical and environmental benefits compared with conventional wet chemical methods is the surface functionalization of textile materials[2]. So far, only a small number of works has been published about diagnostics of the discharge itself due to the main concern for material treatment[3,4] and also due to the complicated nature of filamentary underwater plasma.

Surface modification of textile materials extends over a wide range of alterations to provide the desired single or multi-features for various applications. It is a highly focused area of research in which alterations to physical and/or chemical properties lead to new textile products that provide new applications or satisfy specific needs. These processes can involve numerous chemicals, some of which are toxic to humans and hazardous to the environment. In an effort to eliminate these harmful chemicals and waste products, surface modification and finishing via plasma treatment has become an attractive alternative.

As discussed in (ref.[5]), polypropylene (PP) is being increasingly used for industrial applications thanks to its beneficial properties and ability to be recycled. However, PP has a very low surface free energy, resulting in poor wettability and bonding strengths. To overcome this shortcoming, various techniques have been employed to modify the surface of polypropylene materials[6–8]. Plasma treatment is one of the most important surface modification techniques and has proven to be an environmentally friendly technique in the textile industry.

Investigation of underwater discharges generated in water solutions at atmospheric pressure has shown effective production of OH radicals, solvated electrons and a number of others active species[9,10]. This primary source of radicals is often localised in a small region related to the size of the plasma discharge. Those radicals are highly reactive. Their oxidation potentials are one order of magnitude higher than usual chemical substances used to sterilise or to remove pollutants from the liquid phase.

Electrical breakdown in liquids is generally preceded by events called streamers. The two possible mechanisms for streamer initiation need to be considered: the first is due to electron avalanche which cause electrons to be injected in the liquid and drift to the cathode, and the other is due to the formation of micro-bubbles which cause gaseous cavities to be formed that give rise to electrical breakdown in the gas bubbles. The electric field around the electrode, or the streamer channel, is highly increased, which causes an intense field emission current that eventually vaporizes the water. Streamer discharge phenomena in water are known to be influenced by various factors, such as gap geometry, water conductivity, pulse duration and amplitude of the applied voltage[11].

While in other contributions published in this issue we deal with surface treatments of PP textile as well as with binding of various atoms on the surface, in this article we studied an application of optical emission spectroscopy (OES) which has been usually used as a standard method making it possible to estimate basic parameters of plasma discharges. However, it is also a well known fact, unfortunately, that an accuracy of this method is not too high. This is also the case of the underwater discharge generated by HV pulses at atmospheric pressure when low intensity of emitted light and simultaneously high electrical interferences from the discharge reduce the chance to estimate these plasma parameters with reasonable accuracy. On the other hand OES remains the only one method due to small volume of generated plasma.

2. Experimental setup

The underwater plasma treatment was performed using two versions of experimental arrangement: single diaphragm (SD) discharge and double diaphragm (DD) discharge as illustrated in Fig. 1. The discharge was generated between two metallic electrodes at 2 cm mutual distance, the electrodes were connected to a pulsed HV power supply based on the double rotating spark gap. The maximum peak voltage was 30 kV DC and the maximum repetitive rate of pulses was 60 Hz. The propagation of discharge filaments could be influenced by parameters such as voltage, water conductivity, etc. In this case distilled water was used as a working medium. The electrodes and the slit (diaphragm) were positioned under the water level. The water conductivity range was from 0.5 to 3.7 mS cm^{-1}. A more detailed description of the experimental set-up can be found in (ref.[5]).

The discharge was studied with optical emission spectroscopy of the light coming from a narrow discharge region between the electrodes. The spectra were measured

by means of HR640 spectrometer, Jobin – Yvon (grating 1200 grooves, focal length 640 mm, CCD detector cooled by nitrogen). Molecular spectra bands of CN violet system ($B\ ^2\Sigma^+ \rightarrow X\ ^2\Sigma^+$, $\Delta v = 0$) were used for determination of vibrational temperature. H_α line profile was used to determine electron temperature and density based on tables calculated by (ref.[13]).

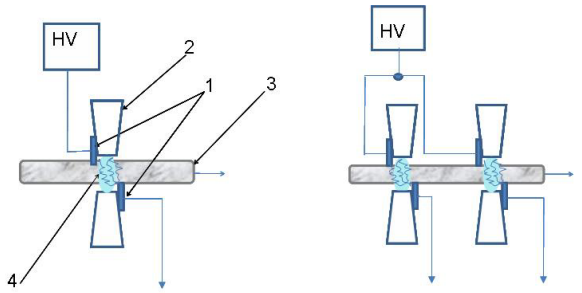

Fig. 1. **SD discharge (left) and DD discharge (right):** 1 – electrodes; 2 – diaphragm; 3 – polypropylene nonwoven fabric; 4 – discharge

The discharge was generated using a diaphragm electrode, where a narrow slit of 0.1×1×40 mm was positioned between two metallic electrodes at 2 cm mutual distance. The arrangement for double diaphragm is similar with the single diaphragm, but in this case we have two diaphragms in the same basin, the material undergoing two successive treatments. The distance between the diaphragms is 13 cm. Polypropylene nonwoven fabric of 50 gsm (grams per square meter) and 30 mm width was used for this experiment.

To keep optimal characteristics of the discharge the current and voltage measurements were done using the LeCroy WaveRunner 6100A Oscilloscope.

We performed standard Optical Emission Spectroscopy (OES) to check the plasma discharge by means of the plasma parameters[12]. The spectra profiles were measured by means of the Triax HR550 spectrometer, Jobin – Yvon (grating 1200 grooves, focal length 550 mm, CCD detector cooled by Peltier). The procedure presented in (ref.[3]), which takes into account the impact broadening by electron and quasi-static broadening by ions, in combination with new data for H_α line profile[13] was used to determine electron temperature and density. The typical profile of H_α is shown in Fig. 3.

3. Results and discussion

The typical spectrum is shown in Fig. 2 while the isolated hydrogen (H_α) and CN ($B\ ^2\Sigma^+ \rightarrow X\ ^2\Sigma^+$, 0-0) are displayed in Fig. 3 and 4, respectively.

The intensity of CN ($B\ ^2\Sigma^+ \rightarrow X\ ^2\Sigma^+$, 0-0) vibrational band and hydrogen (H_α) line vs. discharge voltage are displayed in Fig. 5. The intensity of CN band is decreasing with increasing applied voltage, in contrast with H_α. This

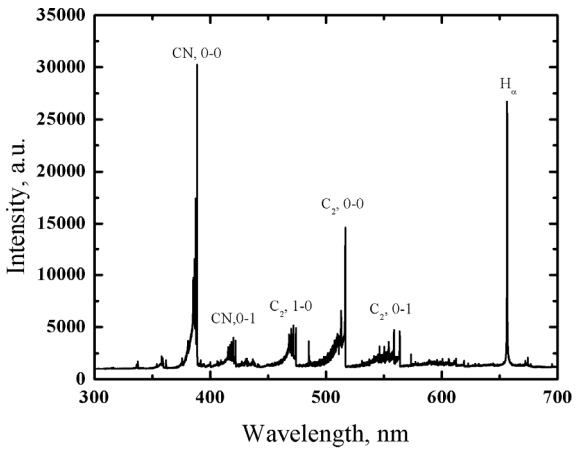

Fig. 2. **Typical spectrum of the discharge recorded in the visible range**

can be attributed to the observation, that the filaments became brighter and longer with increasing voltage in the interelectrode region. It was also found that the temperature depends significantly on conductivity as shown in Fig. 6.

The vibrational temperature estimated from CN bands remains approximately the same with increasing voltage, whereas increasing the water conductivity causes substantial rise of vibrational temperature.

The electron density changes from $1{\cdot}10^{22}$ m^{-3} to $2{\cdot}10^{24}$ m^{-3} while the electron temperature was practically constant $4{\cdot}10^4$ K in all experimental conditions studied. The error of the measured electron density was less than 5 %. The error of electron temperature was much higher, which is due to the weak dependence of the line profile on the electron temperature.

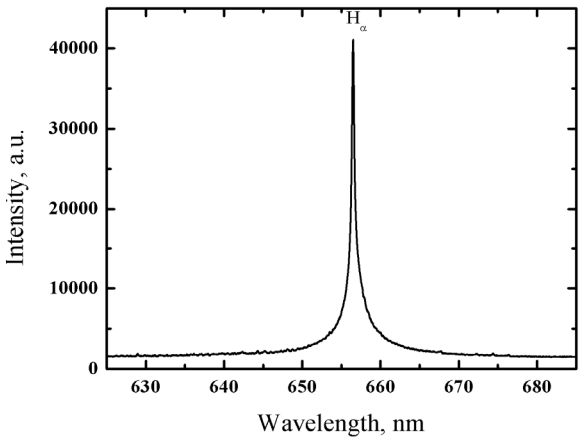

Fig. 3. **An example of hydrogen line used for the estimation of electron number density**

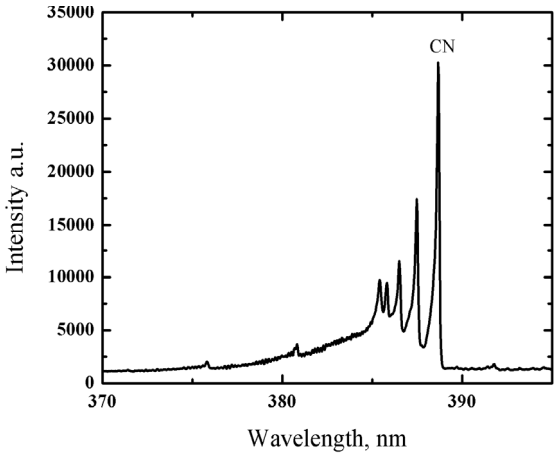

Fig. 4. **A typical example of CN (B $^2\sum^+ \rightarrow$ X $^2\sum^+$, 0-0) molecular band in case of double diaphragm discharge**

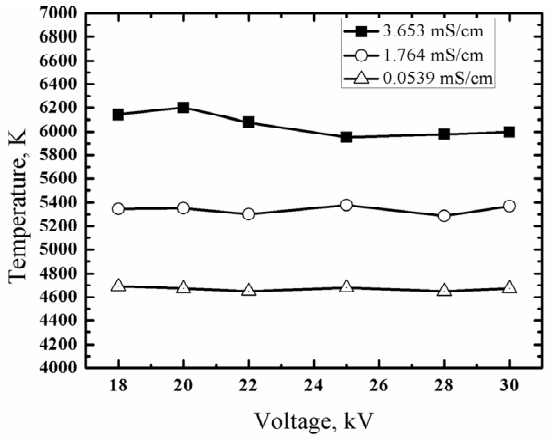

Fig. 6. **Temperature vs voltage and conductivity for double rotating spark gap and different conductivity**

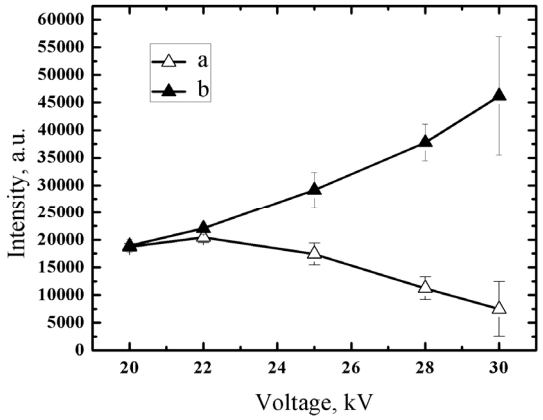

Fig. 5. **Intensity of selected components in OES spectra versus applied voltage for HV power supply based on double rotating spark gap:** a) selected CN vibrational band, b) H_α line profile

Note that presented results must be taken for preliminary ones although a characteristic data set was at disposal and individual data were obtained with reasonable precision (see above). However, individual graphs presented in Fig. 5 appear surprising and it is evident that the suggested relationship to the structure of filaments does not explain completely the origin of this phenomenon. On the other hand, the intensity of the hydrogen line is proportional to the concentration of excited atoms while the intensity of the molecular band reflects the concentration of CN molecules in concrete vibrational state and both intensities depend nonlinearly on voltage. Therefore, it could reflect nonisothermic behaviour of the discharge.

4. Conclusion

In this contribution, OES is used in order to characterize the underwater plasma discharge generated by HV pulses at atmospheric pressure. Although the knowledge of these plasma parameters does not play a dominant role in comparison with those characterizing qualities of an surface treatment by plasmas the study is very important for finding main processes running in the plasma and for determination of appropriate quantity (or quantities) making it possible, in this way, to keep the discharge in an optimal regime.

This research has been supported by OP RDI CZ.1.05/2.1.00/03.0086 funding by the Ministry of Education of the Czech Republic.

REFERENCES

1. Locke B. R., Sato M. et al.: Ind. Eng. Chem. Res. *45*, 882 (2006).
2. Pastore Ch. M., Keikens P.: *Surface characteristics of fiber and textile. Surface science series*. *b94*, New York – Basel 2001.
3. Brablec A., Slavicek P., Stahel P., Cizmar T., Trunec D., Simor M., Cernak M.: Czech. J. Phys. *52* Suppl. D 491 (2002).
4. Simor M., Krump H., Hudec I., Rahel J., Brablec A., Cernak M.: Acta Physica Slovaca *54*, 43 (2004).
5. Neagoe G.: *PhD Thesis*. Masaryk University, Brno 2011.
6. Slobodskoi S. A. et al.: Vopr. Technol. Ulavlivania i Pererab. Prod. Koksovania, *1978*, 71.
7. Sharma A. K., Locke B. R., Arce P., Finney W. C.: Hazard. Waste Hazard. Mater. *10*, 209 (1993).

8. Grimonpre D. R., Sharma A. K., Finney W. C., Locke B. R.: Chem. Eng. J. *82*, 189 (2001).
9. Sunka P., Babicky V., Clupek M., Lukes P., Simek Schmidt J., Cernak M.: Plasma Sources Sci. Technol. *8*, 258 (1999).
10. Lukes P.: *Ph.D. Thesis*, Institute of Plasma Physics, Prague 2001.
11. Bruggeman P., Leys C., Vierendeels J.: J. Phys. D: Appl. Phys. *40*, 1937 (2007).
12. Bruggeman P., Verreycken T., Gonzalez M. A., Walsh J. L., Kong M. G., Leys C., Schram D. C.: J. Phys. D: Appl. Phys. *43*, 124005 (2010).
13. Gigosos M. A., Gonzalez M. A., Cardenoso V.: Spectrochim. Acta, Part B *58*, 1489 (2003).

O. Galmiz, A. Brabec, and Z. Navrátil *(Dep. of Physical Electronics, Faculty of Science, Masaryk University, Brno, Czech Republic):* **Some Aspects of Underwater Diaphragm Discharge Generated by HV Pulses at Atmospheric Pressure**

Underwater diaphragm discharge generated by HV pulses at atmospheric pressure has been studied by OES to estimate basic plasma parameters such as electron density and temperature of excited species for various experimental conditions. It was found that intensity of emitted H_α as well as temperature depends significantly on voltage and conductivity.

CHEMICAL ASPECTS OF STREAMER MECHANISM FOR NEGATIVE CORONA DISCHARGES

JURAJ HALANDA*[a], ANNA ZAHORANOVÁ[a], JOZEF KÚDELČÍK[b], MIRKO ČERNÁK[a,c]

[a] *Dep. of Experimental Physics, Comenius University, Mlynská dolina F2, 842 48 Bratislava, Slovak Republic,* [b] *Dep. of Physics, Faculty of Electrotechnical Engineering, University of Žilina, Univerzitná* 8215/1, *010 26 Žilina, Slovak Republic,* [c] *R&D Center for Low-Cost Plasma and Nanotechnology Surface Modifications, Faculty of Science, Masaryk University, Kotlářská 2, 611 37 Brno, Czech Republic*
juraj.halanda@gmail.com

Keywords: negative corona discharge, streamer mechanism

1. Introduction

When a sufficiently high negative voltage is applied to the point of a point-to-plane electrode system at pressures above of same 10 kPa, a negative corona discharge appears at the point cathode (see Fig. 1a), where the discharge current consists of the negative corona Trichel pulses (TPs, see Fig. 1b). Each TP is discerned by a peaked signal where in several nanoseconds the current rise to a maximum of (~ $1–10^2$ mA) before decreasing to a subsequent transient glow discharge stage[1–3]. As documented in refs.[1–4], quite surprisingly such peaked signal does not significantly depend on the secondary electron emission coefficient of the cathode material used. Typically, for any form of corona discharges, the interelectrode gap can be divided to a narrow (~ 0.1–1 mm, see Fig. 1a) visible ionization region and a dark low field drift region connecting the ionization region to with the low-field passive electrode.

The TP negative corona discharges operating in ambient air are widely used in electrostatic applications (corona precipitators, separators, and powder coating systems) as a simple source of negative ions. Also, chemical reactions both in corona exposed gases[5–14] and on surfaces[14–20] have been studied rather extensively. However, despite widespread use of the TP coronas, there is no reliable and generally accepted theoretical model of this phenomenon.

2. Models of Trichel pulses formation

The model of TPs formation, which is up to the present time most commonly used in engineering including the "chemical" applications, was developed by Loeb[21] and extended by Alexandrov[22]. According to this model the TP is initiated by electrons released from the cathode and proceeds by the Townsend ionization in initial electron avalanches.

The initial avalanches are produced between the cathode and some position distant from the cathode less

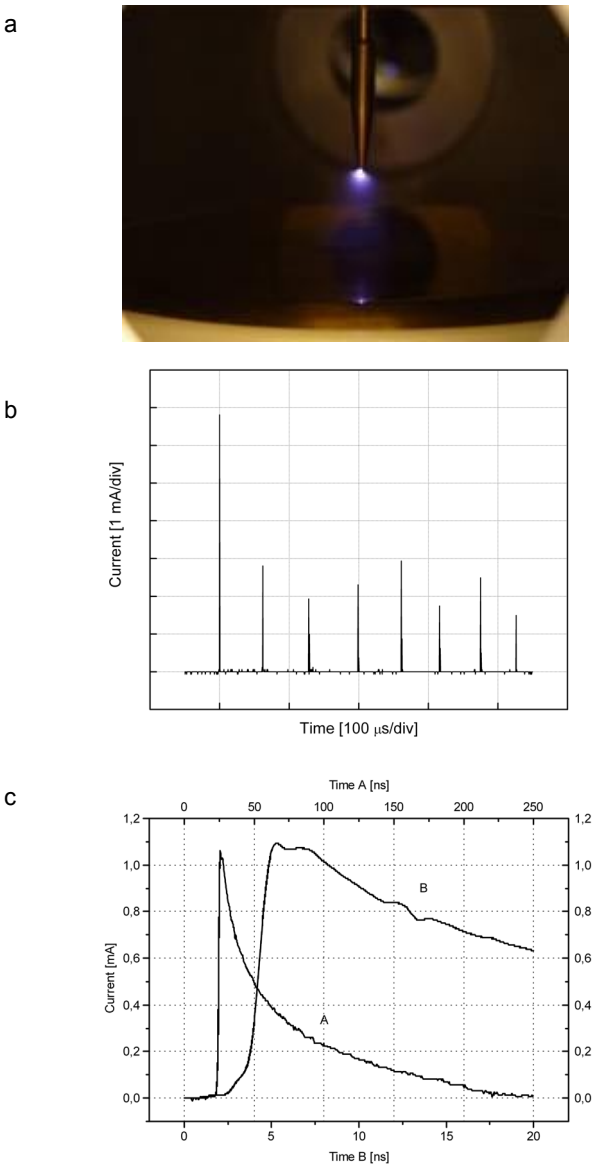

Fig. 1. **a) Negative corona discharge in a short point-to-plane gap, b) train of regular TPs measured in ambient air, c) leading edge of the regular TP in ambient air**

than 1 mm, where the ionization coefficient falls to zero. From the initial electron avalanches further generation of avalanches will result by secondary electron liberation at the cathode due to photoemission resulting in the fast TP current rise to the pulse maximum. Both Loeb and Alexandrov suggested that the TP current rise in ambient air cannot continue to values higher than 10^{-1} A because, in the time roughly equal to the short pulse rise time (see Fig. 1c), the electrons create a negative ion space charge through attachment to oxygen molecules at the perimeter (< 1 mm) of the ionizing zone. As a consequence, according to this theory, no free electrons can penetrate outside this narrow region. This is why it is generally accepted by the workers in the field of negative corona applications that the rest of the interelectrode space is filled solely with the negative ions.

However, the basic presumption of the Loeb-Alexandrov model on the current rise interruption due to the fast electron attachment is in sharp contrast to the fact that, when a step-wise voltage is applied to a negative corona gap in an electron nonattaching gas, the resulting glow corona formation is preceded by a peaked current signal of evidently the same mechanism as the fast TP rise and its initial decay in an electronegative gas, as O_2 and air[23–25]. Also, in the light of extensive results indication the mentioned independence of the TP rise time and magnitude on the cathode material[1–4], the fact that the Loeb-Alexandrov model, as well as the more recent computer simulation model by Morrow[26,27], are based on the presumption that the TP current rise is critically dependent on the cathode secondary emission, is a good reason to doubt about their validity.

In a contrast to the Loeb-Alexandrov model it has been suggested by several authors that the basic aspects of TPs formation can be explained on the basis of the streamer theory. According to this, the sequence of events leading to the TP formation can be envisaged as follows[2,25,28]:

At an initial stage of the development of a sequence of avalanches linked by the secondary emission from the cathode, the space charge created can shield itself from the external el. field, creating a streamer initiating plasma. If some "seed" electrons are presented just in front of the plasma, the avalanching in the locally enhanced field cause primary cathode- and anode-directed streamers to propagate. Thus, the feedback-to-cathode Townsend ionization mechanism fed by secondary electron emission from the cathode is supplanted by a faster feed-forward-to-gas streamer mechanism, where "secondary" electrons are created by photoionization in the gas. After an initial acceleration lasting for ~ 1 ns, velocity of the cathode-directed streamer increases exponentially to the order of 10^8 cm s^{-1} resulting in the TP rise due to the displacement current induced by the streamer movement in the cathode. The TP current rise is finished by the streamer arrival to the cathode and, subsequently, a low-current abnormal glow-discharge cathode spot is formed (Note that such process is theoretically analyzed in ref.[29]). The streamer-based model includes relevant physical factors that determine the development of Trichel pulses including the observed independence of the initial TP current peak on the electron detachment including and on the electron attachment and secondary electron emission (see refs.[23–25] and ref.[1–4], respectively). Contrary to the commonly held belief and in a sharp difference with the Loeb-Alexandrov model, the streamer-based model for TPs admits[2] the existence of a significant free electron current in negative corona discharges burning in ambient air even at distances from the cathode on the order of 1–10 mm. In fact, several indications for this can be found in refs.[14,30–32].

3. Conclusions

The above discussed and already experimentally well-verified streamer mechanism for TP formation strongly indicates the existence of free electrons in the drift region of negative corona discharges. Such free electrons, which can interact with the cold gas and induce reactions without back reactions in the drift region, may affect the chemical reaction in the corona gas volume as well as to induce surface reactions at the low-field anode.

This work was partly supported by the project R&D center for low-cost plasma and nanotechnology surface modifications CZ.1.05/2.1.00/03.0086 funded by the European Regional Development Fund and by the project 26240220042 supported by the Research & Development Operational Programme funded by the ERDF.

REFERENCES

1. Černák M., Hosokawa T.: Jpn. J. Appl. Phys. *27*, 1005 (1988).
2. Černák M., T. Hosokawa, S. Kobayashi, T. Kaneda: J. Appl. Phys. *83*, 5678 (1998).
3. Zahoranová A., Kúdelčík J., Paillol J., Černák M.: J. Phys. D: Appl. Phys. *35*, 762 (2002).
4. Zahoranová A., Šimor M., Černák M., Zahoran M., Kúdelčík J.: Czech. J. Phys. Suppl. D *52*, 886 (2002).
5. Eliasson B., Hirth M., Kogelschatz U.: J. Phys. D: Appl. Phys. *20*, 1421 (1987).
6. Abolmasov S. N., Kroely L., Roca P.: J. Phys. D: Appl. Phys. *41*, 165203 (2008).
7. Liu Ch., Marafee A., Hill B., Xu G., Mallinson R., Lobban L.: Ind. Eng. Chem. Res. *35*, 3295 (1996).
8. Kenkichi Nagato, Yasunori Matsui,Takahiro Miyata, Toshiyuki Yamauchi: Int. J. Mass Spectrom. *248*, 142 (2006).
9. Skalný J. D. et. al. : J. Phys. D: Appl. Phys. *37*, 1052 (2004).
10. Viner A. S., Lawless P. A., Ensor D. S., Sparks L. E.: IEEE Trans. Ind. Appl. *28*, 504 (1992).
11. Nashimoto K.: J. Imaging Sci. *32*, 205 (1988).
12. Pekarek S.: Eur. Phys. J. D *56*, 91 (2010).
13. Kurdel M., Morvová M.: Czech. J. Phys. *47*, 205 (1997).

14. Goldman M., Goldman A., Sigmond R. S.: Pure Appl. Chem. *57*, 1353 (1985).
15. Groza A. et. al. : Europhys. Lett. *68*, 652 (2004).
16. Napartovich A. P.: Proc. Int. Symp. on High Pressure Low Temperature Plasma Chemistry *1*, eds. H Wagner et al (Greifswald, Germany), 122, (2000).
17. Giacometti J. A.: IEEE Trans. Electr. Insul. *27*, 924 (1992).
18. Skalný J., M. Luknárová M., Dindošová D.: Czech. J. Phys. *38*, 329 (1988).
19. Goodman N., Hughes J. F.: J. Electrost. *60*, 69 (2004).
20. Machala Z., Tarabová B., Pelach M., Sipoldova Z., Hensel K., Janda M., Sikurova L.: Machala Z., Tarabová B., Pelach M., Sipoldova Z., Hensel K., Janda M., Sikurova L.: in Plasma for Bio-Decontamination, Medicine and Food Security, NATO Science for Piece and Security, Series A: Chemistry and Biology, 31 (2012)
21. Loeb L. B.: Electrical Coronas: Their Basic Physical Mechanism (Berkeley, CA: University of California) (1965).
22. Alexandrov G. N.: Sov. Phys. Tech. Phys. *8*, 161 (1963).
23. Černák M., Hosokawa T.: Appl. Phys. Lett. *52*, 185 (1988).
24. Černák M., Hosokawa T.: Jpn. J. Appl. Phys. *26*, L1721 (1987).
25. Černák M., Hosokawa T., Odrobina I.: J. Phys. D: Appl. Phys. *26*, 607 (1993).
26. Morrow R.: Phys. Rev. A *32*, 3821 (1985).
27. Morrow R.: Phys. Rev. A *32*, 1799 (1985).
28. Černák M., Hosokawa T.: Phys. Rev. A *43*, 1107 (1991).
29. Odrobina I., Černák M.: J. Appl. Phys. *783*, 635 (1995).
30. Černák M., Skalný J. D.: Czech. J. Phys. *34*, 926 (1984).
31. Leal Ferreira G. F., Oliviera O. N., Giacometti J. A.: J. Appl. Phys. *59*, 3045 (1986).
32. Gagarin A. G., Vigborchin V. Kh., Mitjuschin A. I.: Teplofiz. Vys. Temp. *4*, 823 (1983).

J. Halanda[a], A. Zahoranová[b], J. Kúdelčík[c], and Mirko Černák[a,c] *([a] Dep. of Experimental Physics, Comenius University, Bratislava, Slovak Republic; [b] Dep. of Physics, Faculty of Electrotechnical Engineering, University of Žilina, Žilina, Slovak Republic, [c] R&D Center for Low-Cost Plasma and Nanotechnology Surface Modifications, Faculty of Science, Masaryk University, Brno, Czech Republic):* **Chemical Aspects of Streamer Mechanism for Negative Corona Discharges**

It is explained that, contrary to the traditional Loeb-Alexandrov model for the negative corona current pulses formation, the more recent streamer-based model admits the existence of a significant free electron current in negative corona discharges burning in ambient air even at distances from the cathode on the order of 1–10 mm. The existence of such free electrons is in a sharp contrast to the commonly held belief that the low-field drift region of the discharge is filled solely with the negative ions. The importance of such free electrons for chemical reactions induced by negative corona discharges is discussed briefly.

CHEMICAL AND PHYSICAL EVALUATION OF HYDROPHOBIC pp-HMDSO LAYERS DEPOSITED BY PLASMA POLYMERIZATION AT ATMOSPHERIC PRESSURE

RICHARD KRUMPOLEC*[a], ANNA ZAHORANOVÁ[a], MIRKO ČERNÁK[a,b], DUŠAN KOVÁČIK[a,b]

[a] *Dep. of Experimental Physics, Faculty of Mathematics, Physics and Informatics, Comenius University, Mlynská dolina F2, 842 48 Bratislava, Slovak Republic,* [b] *R&D Center for Low-Cost Plasma and Nanotechnology Surface Modification, Faculty of Science, Masaryk University, Kotlářská 2, 611 37 Brno, Czech Republic*
krumpolec@fmph.uniba.sk

Keywords: plasma polymerization, hexamethyldisiloxane, glass, hydrophobic surface

1. Introduction

The deposition of various boundary layers is an important part of technology occurring in different areas. This considers great range of applications such as protective layers coatings, adhesion improvement, applications in Nano- & Bio- technology, and many other applications. The hydrophobic boundary layers deposition, e.g. by plasma polymerization could be one approach.

As "Plasma Polymerization", we consider the thin films deposition from mixture of monomers in plasma. It is possible to deposit various thin films with desirable physical and chemical characteristics using appropriate optimalization of operating parameters. Polymers formed by this technique, called as Plasma-Polymers, are generally highly branched and highly cross-linked due to radical fragmentation mechanism of polymerization. The resulting properties may be the high scratch resistance, insolubility as well as excellent adhesion to solid surfaces.

In this study we have worked with Hexamethyldisiloxane monomer (HMDSO $C_6H_{18}OSi_2$, $(CH_3)_3Si–O–Si–(CH_3)_3$). Therefore, the deposited plasma polymer was marked as pp-HMDSO. The chemical properties of obtained new polymer layers are presented.

2. Experimental setup

For plasma polymerization of hydrophobic polymer layers on the glass substrates a special reactor was constructed (Fig. 1). As the plasma source we used Diffuse Coplanar Surface Barrier Discharge[1,2] (DCSBD) fed by high voltage source (LIFETECH, s.r.o., Brno, Czech Republic).

In reactor chamber from plexiglass a movable cart which moved a sample above DCSBD plasma was placed.

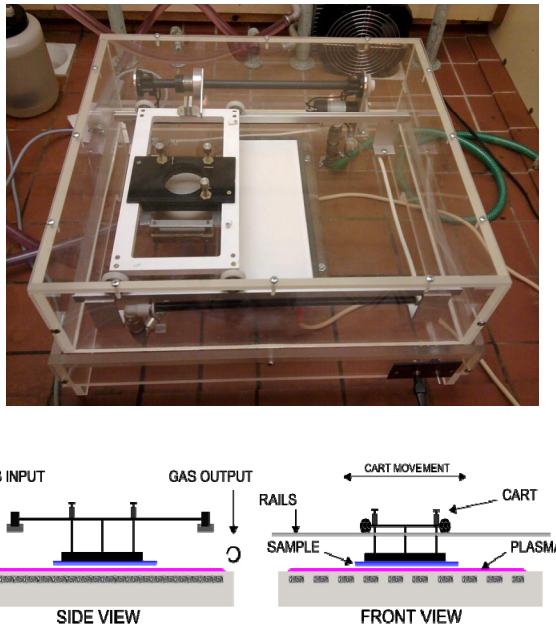

Fig. 1. **Reactor based on DCSBD for plasma polymerization**

The distance of sample's surface from ceramic surface of coplanar discharge could be adjusted as well as the velocity of the cart (Fig. 1).

As the glass samples for plasma polymerization the glass slides for optical microscopy with dimensions 25.85 × 75.9 × 1.0 mm were used. The as-received samples were inhomogeneous. To ensure the same surface properties of every glass sample they were cleaned before every experiment by this chemical cleaning procedure:

- 5 – minutes cleaning in acetone in ultrasonic bath,
- 5 – minutes cleaning in isopropyl-alcohol in ultrasonic bath,
- 5 – minutes cleaning in distilled water in ultrasonic bath.

After cleaning in ultrasound bath every sample was dried with nitrogen stream. For AFM, SIMS or XPS analyses we used smaller samples (the same material and cleaning procedure) with dimensions max. 10×10 mm.

The polymerization was carried out in dynamic mode for homogeneous plasma-polymerization treatment. The glass samples were polymerized 1 minute in N_2/HMDSO mixture vapour (concentration of HMDSO monomer admixture in nitrogen was set to $c = 0.147$ mmol l^{-1}). The input power to discharge was set up to 270 W. The distance of sample surface was set to 0.3 mm. After the entire layer deposition the samples were stored under ambient laboratory conditions. The deposited polymer layers were

hydrophobic with contact angles values of 90°–100° (measured for distilled water).

As the monomer for plasma polymerization a Hexamethyldisiloxane (HMDSO, as-received from Merck, Germany) with nitrogen (5.0) as a carrier gas were used.

A N_2/HMDSO mixture was carried out by system with two thermal mass flowmeters RED-Y (max. 10 l min^{-1} and 2 l min^{-1} respectively). The monomer temperature was controlled by thermocouple senzor.

3. Analytical methods

In order to investigate the morfology properties of deposited polymer layers SEM and AFM methods were used. SEM analysis was carried out by the Vega II SBH scanning electron microscope. The analyzed samples were non -conducting so they had to be coated with a thin Au-layer (~ 17–20 nm) with magnetron sputtering by BIO-RAD SEM Coating System (Microscience Division). The surface of plasma-polymer films was evaluated also by Atomic Force Microscopy (Solver P47-PRO).

The FTIR spectrum of polymer layers on glass substrates were recorded by BRUKER VECTOR 22 spectrometer using diamond Attenuated Total Reflection with Diamond/ZnSe polarization accessory from MIRacle™ (PIKE Technologies) The diamond was set at 45 degrees and other measurement settings were 20 scans, resolution 4 cm^{-1}, measuring range 4000–500 cm^{-1}.

The XPS spectrum used for component analysis of films was measured by Phoibos 100 XPS device from Specs company. The photoelectrons were detected by hemispheric analyzer in FAT regime. The photoelectron energy spectrum was calibrated according to energy of carbon bond C-C which characteristics energy is 284.5 eV. The spectra were analyzed and evaluated in CasaXPS software.

SIMS analysis was carried out on the TOF SIMS IV device (from ION-TOF Company, Münster, Germany). For ion bombardment of the sample's surface the bismuth ion gun producing Bi^+ ions (25 keV ion energy and current 1 pA) was used. The mass spectrum was analyzed in positively and negatively polarity on the total surface area of 100×100 μm^2. As the glass is dielectric, the electron gun for surface charge compensation was used.

4. Results

4.1. Morfology Analysis of Polymer Layers

The SEM analysis was performed on the samples stated as S1, S2, S3 which parameters are listed in the Table I. Sample S3 was treated after plasma polymerization by DCSBD plasma to study curing of deposited polymer film. The AFM operated in semicontact mode scanned the sample's surface on the scale of 100 μm^2. As the qualitative parameters for roughness rating (evaluation) R_q (RMS) and R_a (average roughness) were selected.

As the results show in Table II, the deposited polymer layers are smooth with $R_q < 1$ nm. The maximum roughness for every sample is under 10 nm except sample S3. We assume it is due to plasma post-treatment which caused increase of average roughness up to 19 nm.

Table I
List of analyzed samples and their treatment parameters

Sample	S1	S2	S3
Polymerization time, sec	60	30	60[a]
Input power, W	270	270	270
N_2/HMDSO mixture concentration, mmol l^{-1}	0.147	0.147	0.147

[a] The S3 sample was treated by N_2 plasma after plasma polymerization for 10 seconds to cure and stabilize the layer

Table II
Surface roughness of pp-HMDSO layers from Table I

Sample	R_q [nm]	R_a [nm]	Max. Roughness [nm]
S1	0.491	0.378	8.015
S2	0.679	0.543	7.159
S3	0.598	0.451	19.221
As-received glass	0.549	0.356	16.333

The SEM imaging revealed very smooth surface character even over maximum total area 700×700 μm^2 and all zooms from 300× to 100 000× in which the surface was scanned.

4.2. Chemical Analysis of Polymer Layers

FTIR analysis of polymer layer surfaces

FTIR spectrum of polymer layer on glass in the range 3600–1200 cm^{-1} can be seen in the Fig. 2. The broad wave number region of 3000–3600 cm^{-1} of infrared spectra is associated to valence vibrating states of primary (straight) amine functional groups of NH, NH_2 (ref.[3]). In the same region the peak associated with vibrating O-H and C-H states[4] was identified.

As we mentioned before, the monomer fragmentation goes on through radical mechanism[5]. The HMDSO molecule is broken to smaller units. Therefore on the layer surface we can identify the methyl CH_n groups, indicated by valence vibrational states of C-H in the band 2980–2850 cm^{-1} (ref.[6,7]).

Since used diamond ATR crystal technique we could not detect reliably the intensities in the range

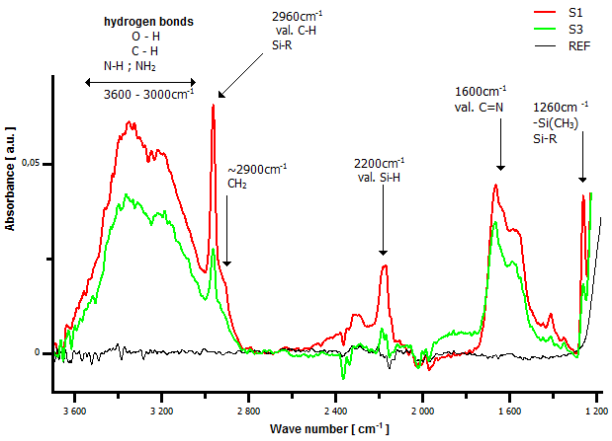

Fig. 2. **Selected FTIR spectrum of analyzed pp-HMDSO samples in the wavenumber range 3600–1200 cm^{-1}. REF = reference as-received glass sample**

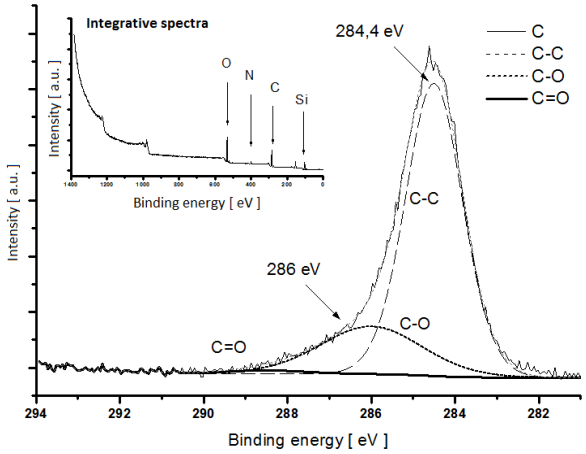

Fig. 3. **High-resolution XPS spectrum of C 1s for sample S1**

1950–2200 cm^{-1}, where e.g. typical C≡N bond at about 2200 cm^{-1} lies.

A significant increase of peak's amplitudes is also apparent in the range 950–1100 cm^{-1} from Si-O-Si bond and of the Si-H a Si-CH$_n$ states in the range 800–750 cm^{-1} respectively (Not shown in the Fig. 2).

XPS analysis of polymer layer surfaces

We interested in percentage proportion of elements creating the pp-HMDSO films on two samples S1 and S2 (with different time of polymerization). Namely the Si 2p, O 1s, C 1s a N 1s levels were studied as can be seen in the Fig. 3. In Fig. 4, the values of percentage proportion for sample S1 are compared to the XPS analysis of pure glass without hydrophobic treatment. The element composition for sample S2 with half polymerization time was quite the same as for sample marked as S1.

SIMS analysis of polymer layer surfaces

As expected, in the SIMS mass spectrum the most significant peaks came from CH$_x$ methyl groups bonded to SiO and SiO$_2$ groups respectively. The proportional distribution as $I_C < I_{CH} < I_{CH2} < I_{CH3}$ we observed in the mass spectrum of every sample. The I_x is intensity associated to the peak of X element. The intensities were calculated as the Corrected Area.

In addition to methyl groups bonded to Si or SiO we detected also amine (e.g. C$_x$H$_y$NO, SiCH$_x$N$_y$) and OH groups bonded to SiO$_2$, SiO or Si. The organic character of deposited films is confirmed also by organic functional groups as well as C_H, C_{H2}, C_{H3}, and more difficult C$_x$H$_y$ fragments respectively. The intensity of Si$^+$ ion decreases in sequence from sample S3 to sample S1. In case of sample S2 this is causes by higher organic C$_x$H$_y$ groups bonded from monomer due to longer polymerization time while decreasing of Si$^+$ ion detected on sample S1. As the

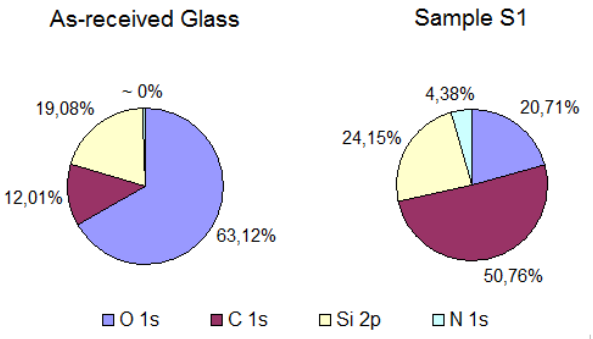

Fig. 4. **Percentage proportion of oxygen, carbon, silicon and nitrogen for sample S1 compared with as-received glass sample**

direct result of plasma post-treatment of pp-HMDSO film the organic C$_x$H$_y$ groups are wiped off (Fig. 5), because of lower energy bonds compared to the silicon and oxygen atoms. And further, it results in highest peak Si$^+$ ion for sample S3 compared to samples S1 and S2.

In the SIMS mass spectrum it was evidently visible the fragmentation series of $Si-O_x-C_n-H_{3n}-\{CH_3\}_n$ and $Si-O_x-C_n-H_{3n}-\{CH_2\}_n$ respectively.

The mechanical properties of pp-HMDSO layers were evaluated by Fischerscope H100 nanoindentor. The S1 sample was approximately 150 nm thick, while microhardness was 7 GPa, with elastic module of 70 GPa.

The stability of hydrophobic coatings was monitored of 120 hours after plasma polymerization and any "Ageing Effect" was observed. The average contact angle remained constant with significant decrease of value dispersion. Moreover the coated samples pass through the 120 minutes boiling test in distilled water.

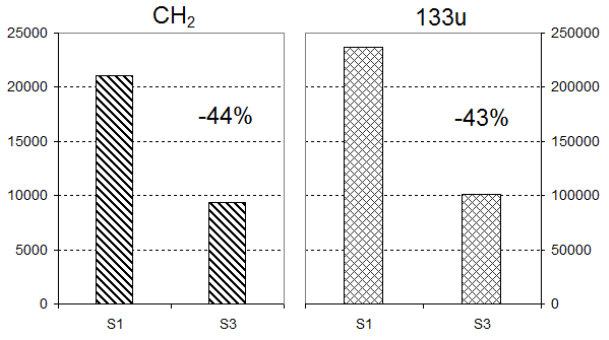

Fig. 5. **Removal of organic C_xH_y groups by plasma post-treatment. Decrease of intensity for CH_2 and heavier 133u with $(CH_2)_n$ organic groups peak fragment without and after plasma post-treatment (S1 vs. S3 samples). The symbol "u" refers Atomic Unit Mass**

5. Discussion

Trunec et al.[7] used for thin layer deposition of polymer pp-HMDSO layers on glass substrates nitrogen plasma generated by APGD discharge. Depending on the monomer concentration they observed the filamentary discharge or homogeneous plasma respectively. In the case of samples deposited in filamentary DBD they observed the sharp peaks with average height of up to 150 nm. In homogeneous regime of plasma generation they deposited the layers with average roughness of 7.9 nm, at deposition time 10 minutes.

According to the XPS analysis of our pp-HMDSO layers we conclude the percentage composition of carbon, oxygen, silicon and nitrogen is
n [%] (C : O : Si : N) = ~ 50 : 21 : 24 : 5.

For comparison, the authors in ref.[7] obtained this elements rate approximately in the ratio 41 : 26 : 15 : 17.

In the hexamethyldisiloxane molecule, the carbon to silicon atoms ratio is equal to 3. Based on the results of our XPS measurements of films we conclude this ratio decrease for the pp-HMDSO to value of 2. This change could be a consequence of the cross-linking during plasma polymerization process of the HMDSO molecule.[8]

As a result of plasma polymerization, the deposited pp-HMDSO films were characterized by high cross-linking with quite complex chemical structure. The most significant changes in FTIR absorbance spectrum of samples (compared to the pure glass) we observed at wave numbers 800–750 cm^{-1} (assigned to Si-O-Si; $Si-CH_n$), 1100–950 cm^{-1} (Si-O-Si; O-Si-O), 1260 cm^{-1} ($Si-CH_n$). Similarly, the highest IR intensity changes were observed at ~ 2960 cm^{-1} (assigned to valence vibration states of C-H, $Si-CH_n$) and around wave numbers of 2200 cm^{-1} (valence Si-H).

These observations are in good agreement with Szalowski´s et al. paper[9], where polymer coatings on glass in nitrogen plasma at atmospheric pressure were deposited too. In addition, the authors deposited polymer layers in the presence of substrate heating (~ 400 °C) and the total deposition time was 15 minutes.

Paulussen et al.[8] deposited the polymer layers on polished SiO_2 surface of silicon (deposition time 2 minutes) in nitrogen plasma generated by barrier discharge. They present the chemical composition of pp-HMDSO layers from XPS analysis as follows:
n [%] (C : O : Si : N) = ~ 50 : 24 : 24 : 2. As you can notice, it is similar rate as in our case presented earlier. Moreover, in the FTIR spectra were observed not only vibrations of $Si-(CH_3)_n$; $(CH_3)-Si-O-Si-(CH_3)$; C-O, but also from hydrogen – carbon and hydrogen – oxygen bonds C-H and O-H.

6. Conclusion

The possibilities to employ the plasma generated by DCSBD discharge for atmospheric pressure plasma polymerization of HMDSO monomer in nitrogen carrier gas were studied. The process of plasma polymerization is quite a complex, with a plenty of free parameters. The stable hydrophobic pp-HMDSO thin layers on the glass substrates were coated.

The polymer character of the coated layers was confirmed by the means of XPS, SIMS and FTIR analyses. After the XPS analysis the detail percentage of carbon, oxygen, silicon and nitrogen was obtained as n [%] (C : O : Si : N) = ~ 50 : 21 : 24 : 5. The AFM analysis, as well as SEM imaging, confirmed the smooth surfaces of polymer layers. The roughness of pure glass substrates is in the order of ~ 20 nm. Therefore the cleaned, high quality samples (not only glass) is important necessity for deposition at atmospheric pressure. This could be important for technology view of thin layer deposition. One negative and undesirable effect was observed during plasma polymerization – the direct deposition of pp-HMDSO polymer layer on the dielectric surface of coplanar discharge. The layer creates the additional dielectric barrier which implies the change of ignition voltage. On the other hand we have not observed any change in electrical characteristic of the discharge for HMDSO admixture of nitrogen working gas.

The DCSBD was successfully studied for plasma surface treatment, activation or cleaning of various types of materials[1,2]. In this study the hydrophobic coatings on glass substrates by plasma assisted polymerization were deposited. Our results show the possibility to employ DCSBD plasma for plasma assisted layer deposition. But we also see same drawback which should be solved in the future as we mentioned before. Apart from many advantages, the plasma polymerization approach also suffers from the serious disadvantage of high monomer and carrier gas consumption which are not efficient enough.

The authors express their thanks to M. Zahoran who performed SEM measurements and T. Plecenik for AFM analyses.

This work is the result of the project implementation: 26240220002 and 2622020004 supported by the Research & Development Operational Programme funded by the ERDF. Also, this research was partially supported by Comenius University in Bratislava under Grant UK No. UK/456/2012.

This research has been supported by the project R&D center for low-cost plasma and nanotechnology surface modifications CZ.1.05/2.1.00/03.0086 funding by European Regional Development Fund.

REFERENCES

1. Černák M. et al.: Eur. Phys. J. Appl. Phys. *47*, 22806 (2009).
2. Černák M. et al.: Plasma Phys. Control. Fusion *53*, 124031 (2011).
3. Milata V. et al.: *Applied Molecular Spectroscopy* – in slovak. STU in Bratislava, Bratislava 2008.
4. Gonzales-B. J. et al.: J. Appl. Polym. Sci. *62*, 375 (1996).
5. Fridman A.: *Plasma Chemistry*. Cambridge University Press, New York 2008.
6. Li K., Gabriel O., Meichsner J.: J. Phys. D: Appl. Phys. *37*, 588 (2004).
7. Trunec D. et al.: J. Phys. D: Appl. Phys. *37*, 2112 (2004).
8. Paulussen S., Goosens O., Vangeneugden D.: *International Symposium on Plasma Chemistry*: Abstracts and Full-Papers CD. *Taormina, Italy, June, 22-27, 2003* (R d'Agostino et al., ed.), Taormina, Italy 2003.
9. Szalowski-Sch K. et al.: Plasmas Polym. *5*, 173 (2000).

R. Krumpolec[a], A. Zahoranová[a], M. Černák[a,b], and D. Kováčik[a,b] *([a] Dep. of Experimental Physics, Faculty of Mathematics, Physics and Informatics, Comenius University, Bratislava, Slovak Republic; [b] R&D Center for Low-Cost Plasma and Nanotechnology Surface Modification, Faculty of Science, Masaryk University, Brno, Czech Republic):* **Chemical and Physical Evaluation of Hydrophobic pp-HMDSO Layers Deposited by Plasma Polymerization at Atmospheric Pressure**

This work deals with plasma polymerization deposition of hydrophobic layers onto glass substrates at atmospheric pressure. The hexamethyldisiloxane (HMDSO) organosilicon monomer was used as precursor for plasma polymerization in nitrogen working gas. The so-called Diffuse Coplanar Surface Barrier Discharge was used as a source of non-equilibrium non-thermal plasma. The pp-HMDSO thin films were studied by the means of SEM, AFM, FTIR, XPS and SIMS measurements. Our research revealed that smooth, polymer-like, hydrophobic and transparent in visible range thin films were deposited on the glass substrates. The results indicate that DCSBD discharge can be used for thin films deposition by the means of plasma polymerization process at atmospheric pressure.

THE EFFECT OF SURFACE CLEANING AND REMOVING OF ORGANIC CONTAMINANTS FROM SILICON SUBSTRATES AND ITO GLASS BY ATMOSPHERIC PRESSURE NON-THERMAL PLASMA

VERONIKA MEDVECKÁ*[a], ANNA ZAHORANOVÁ[a], DUŠAN KOVÁČIK[a,b], JÁN GREGUŠ[a]

[a] *Dep. of Experimental Physics, Faculty of Mathematics, Physics and Informatics, Comenius University, Mlynská dolina F2, 842 48 Bratislava, Slovak Republic,* [b] *R&D Center for Low-Cost Plasma and Nanotechnology Surface Modifications, Faculty of Science, Masaryk University, Kotlářská 2, 611 37 Brno, Czech Republic*
Veronika.Medvecka@fmph.uniba.sk

Keywords: DCSBD, silicon substrates, ITO glass, cleaning, organic contaminants

1. Introduction

Silicon is the most used material in semiconductor industry and photovoltaics. In the form of wafers, silicon serves as the basis for integrated circuits and multilayer technologies – Micro-Electro-Mechanical Systems (MEMS) or Silicon on Insulator (SOI). Semiconductor industry is affected by the miniaturization and what is accentuated is the purity, flatness and smoothness of substrate surface.

Indium tin oxide (ITO) is the solid solution of indium oxide (In_2O_3) and tin oxide (SnO_2) and it is heavily-doped n-type semiconductor. Due to high electrical conductivity and optical transparency in visible spectra, it is one of the most used transparent conductive oxides (TCO) as coating for many optical application – flat displays, organic or polymer light-emmiting diodes (OLED, PLED), IR-reflecting or Joule heating coating, gas sensors, etc.

In photovoltaics, 90 % of solar cells are produced from silicon[1]. Besides silicon and other semiconductors, solar cells are prepared from another materials able to generate electric charge by the light impact – thin films solar cells with organic light-absorbing dyes (DSSC), organic polymer materials[2,3] and semiconductors[4], etc. For improving of efficiency, new technologies are also used – multijunction, tandem, or quantum dot cells. Electrodes in the mentioned systems are often composed of TCO, mainly ITO thin film.

The preparation of semiconductor devices contains hundreds of steps and 10–15 % of them include cleaning and activation of surface. At present, the most used techniques are wet chemical cleaning methods. The standard model for cleaning of semiconductors was suggested and developed by Werner Kern in 1960. It is called RCA (ref.[5]), which is a type of wet chemical method using aggresive chemicals, which are toxic, environmentally unsuitable and non-biodegradable. At present, more economic and environmental alternative processes are investigated.

Many procedures in semiconductor industry are replaced by plasma. For cleaning of semiconductors low pressure plasma has been already used, but the necessity of vacuum equipment extends treatment time and enhances cost of method.

For this study a unique type of dielectric barrier discharge – Diffuse Coplanar Surface Barrier Discharge (DCSBD)[6] was used for removal of the organic contamination (2-propanol) from three types of silicon substrates. Moreover, comparative study of cleaning effectiveness of 2-propanol and DCSBD on the ITO glass samples was carried out. DCSBD produces non-thermal diffuse plasma in ambient air at atmosperic pressure. This type of plasma source was succesfully used for plasma treatment of nonwoven[7,8] , aluminium[9], wood[10], glass[11], or ozone production[12].

2. Experimental setup and samples

DCSBD consists of many parallel silver electrodes embedded in Al_2O_3 ceramics. DCSBD is powered by sinusoidal voltage with amplitude 15 kV (peak-to-peak) and frequency 16–18 kHz. More technical details are described in work of M. Šimor[13].

Experimental arrangement (Fig. 1) consist of static DCSBD discharge (Fig. 1-1) and moveable sample holder (Fig. 1-2) with possibility of treatment time adjusting in plasma in dynamic regime.

Silicon (111), N-type doped with phosphorus (ON Semiconductors, Czech Republic) with resistivity (33–45)·10^{-3} Ω m was used as a substrate. The diameter of the wafer was 100.0±0.5 mm and its thickness was 381±25 μm. Three types of silicon surfaces were prepared as follows:

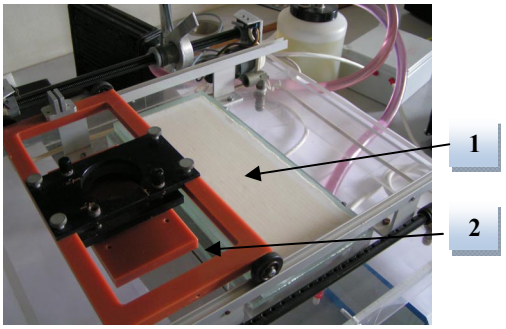

Fig. 1. **Experimental arrangement with main parts:** 1 – DCSBD, 2 – movable sample holder

a) "as received" silicon precleaned with acetone, 2-propanol and distilled water for 6 min in each liquid using sonication,
b) silicon pre-cleaned as in A), then thermally oxidized in O_2 atmosphere at 600 °C for 1 h
c) silicon pre-cleaned as in A), then rinsed in aqueous solution of hydrofluoric acid (HF/H_2O: 1/10 in volume).

Sample A was covered with a thin layer of native oxide. Thermal oxidation of sample B caused dehydration (removing of OH-groups) and increasing of oxide layer thickness. Immersion in HF dilution in sample C etches native oxide and creates hydrophobic H-terminated surface.

ITO glass samples (Präzisions Glas & Optik, GmbH, Germany) of CEC 015S type with ITO coating thickness of 120 nm were prepared on selected white float glass with thickness 1±0.1 mm and surface resistivity ≤ 15 Ω/□ (typical value 12,5 Ω/□).

3. Results and discussion

Isopopyl alcohol (IPA, 2-propanol, $(CH_3)_2CHOH$) was used for reproducable contamination of silicon samples. This chemical is often applied as a cleaning agent in electronics because of good dissolution of wide range non-polar compounds. IPA is also used as a solvent in other industrial processes, in medical application for disinfection, as fuel additives, etc.

The silicon samples marked A, B and C were rinsed in ultrasonic IPA bath for 3 min. In order to study the effect of the plasma treatment on the contamination removal, the samples were treated with DCSBD plasma in 0.3 mm distance from the Al_2O_3 ceramics. The input power was 300 W and the exposure time was 10 s. The parameters for plasma treatment were chosen according to previous research[14].

Attenuated Total Reflectance Fourier Transform Infrared Spectroscopy (ATR-FTIR) was performed with Bruker Vector 22 FT-IR spectrometer, equipped with additional Pike MIRacle™ accessories, working in the range from 4000 to 400 cm^{-1}. 20 scans were carried out with resolution of 4 cm^{-1}.

Si-O bond has weak ionic character[15] and it may exhibit very strong absorption in IR region. Relevant peaks and adequate bonds on silicon substrates are particularly Si-H bond and siloxanes. On each sample (A, B, C) peaks attributed to antisymmetric vibrations ν_{as}(Si-O-Si) (1105 cm^{-1}), valence vibrations Si-O-H (3700–3200 cm^{-1}) and H_2O bending in region from 1800 to 1400 cm^{-1} (ref.[16]) were observed. The peak at 611 cm^{-1} was identified as Si-Si bond[17]. On sample B – thermally oxidized silicon, it was possible to observe the characteristic peak (1240 cm^{-1}) of thermal oxide (Fig. 3) and with higher temperature of annealing its shift towards higher wavenumbers[13]. Si-H bonds[18], expected on H-terminated silicon (sample C) occure in region from 2280 to 2050 cm^{-1}. There was observed an area of IR absorption caused by CO_2 from air.

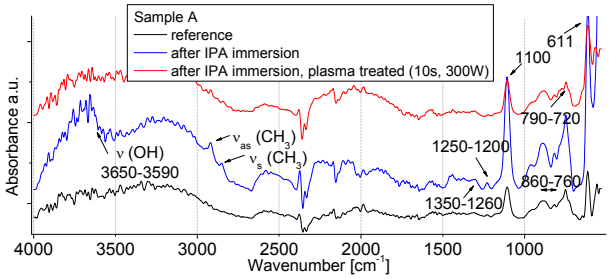

Fig. 2. **FTIR spectra of precleaned silicon (Sample A)**

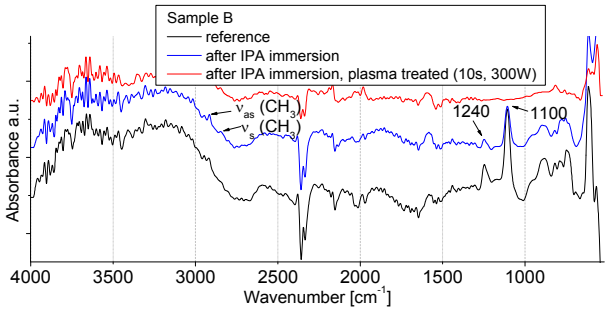

Fig. 3. **FTIR spectra of thermally oxidized silicon (Sample B)**

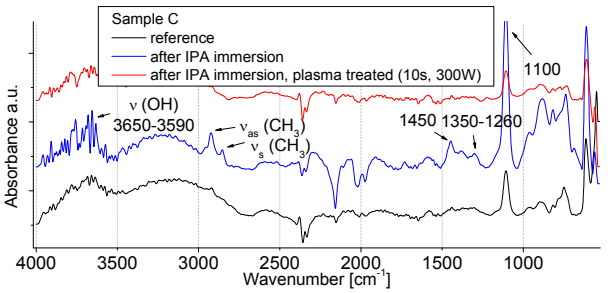

Fig. 4. **FTIR spectra of H-terminated silicon (Sample C)**

Changes after IPA immersion and plasma treatment were compared with IR spectra from the NIST database[19]. For alcohols and phenols, there are characteristic OH vibrations (3650–3590 cm^{-1}), for secondary alcohols such as the 2-propanol are specific deformation vibrations C-OH in region of 1350–1260 cm^{-1}. For H-bonds there is a shift to 1500–1300 cm^{-1} (ref.[20]). We can observe peak attributed to valence vibration C-O (1100 cm^{-1}) (ref.[20]) mainly in case of sample A (Fig. 2) and C (Fig. 4). It can overlap with the peak attributed to antisymmetric valence vibration of Si-O-Si – 1105 cm^{-1}. Organic contaminants on silicon are visible in region 600–1300 cm^{-1} (ref.[18]). In region 860–760 cm^{-1} there may exist valence vibrations Si-C (ref.[20]).

In case of sample C (Fig. 4) the peak at 1450 cm^{-1} was found. This peak was probably attributed to scissoring

deformation of CH_2 or antisymmetric deformation CH_3 (ref.[18]). Peaks of symmetric and antisymmetric valence vibrations of CH_3 (ref.[18,20]) was observable on each sample immersed in IPA. Intensity of peaks indicating IPA increased after IPA immersion and decreased after plasma treatment, mainly on samples A (pre-cleaned silicon) and C (H-terminanted silicon). Thermally oxidized silicon (Fig. 3) was relatively resistant to IPA contamination. The peaks were small after IPA ultrasonic bath and they decreased only slightly after plasma treatment. Moreover, peak observed at 1240 cm^{-1} (characteristic for thermally oxidized silicon) became extinct after plasma cleaning.

XPS signals were recorded using a Thermo Scientific K-Alpha XPS system equipped with a micro-focused, monochromatic Al Kα X-ray source (1486.6 eV). Measurement was carried out in argon (partial pressure $2 \cdot 10^{-7}$ mbar). The *Avantage* 4.75 software was used for digital acquisition and data processing. Spectral calibration was determined by using the automated calibration routine and the internal Au, Ag and Cu standards supplied with the K-Alpha system.

XPS measurements revealed increase of carbon compounds after IPA immersion and their decrease after plasma treatment. The effect of plasma treatment was compared on samples with and without IPA precleaning (Tab. I). The influence of plasma treatment was significant mainly in case of pre-cleaned (A) and H-terminated (C) silicon samples. During the preparation of thermal oxide (B) the organic contaminants are removed because of high temperature, therefore the thermally oxidized silicon is relatively resistant to IPA contamination. Fig. 5–7 show relative quantities of C-bonds obtained from deconvolution of C1s peak. The composition of bonds before and after plasma treatment indicated, that plasma is suitable for removal of IPA residues as well as for removal of other organic contamination mainly from samples A and C.

Table I
Chemical composition of silicon samples: IPA removing with plasma treatment (300 W, 10 s) measured with XPS

		Atomic concentration [%]			
		O1s	Si2p	C1s	N1s
Si precleaned (Sample A)	Reference	30	59	5	
	Ref + plasma	39	52	4	
	IPA	29	55	16	
	IPA + plasma	42	52	5	1
Si thermally oxidized (Sample B)	Reference	62	36	2	
	Ref + plasma	59	37	4	
	IPA	48	47	5	
	IPA + plasma	51	45	4	
Si H-terminated (Sample C)	Reference	10	70	11	9
	Ref + plasma	44	47	4	1
	IPA	56	23	20	1
	IPA + plasma	40	52	6	1

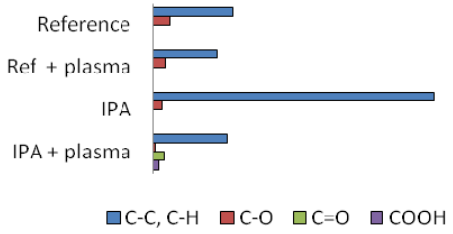

Fig. 5. **Relative quantities of C-bonds on precleaned silicon (A)**

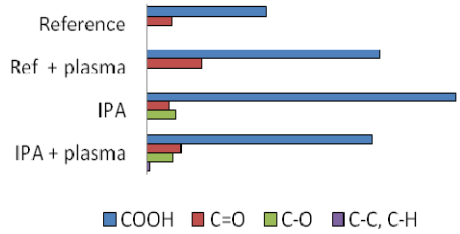

Fig. 6. **Relative quantities of C-bonds on thermally oxidized silicon (B)**

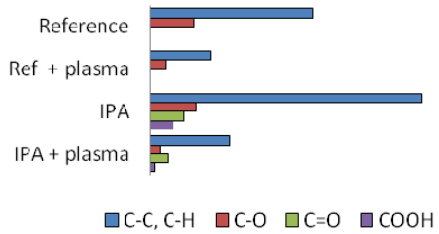

Fig. 7. **Relative quantities of C-bonds on H-terminated silicon (C)**

In this study we also compared cleaning effectiveness of IPA and plasma on ITO glass by XPS measurements. ITO glass was immersed in IPA for 5 min in ultrasonic bath and then was treated with plasma (300 W, 5 sec). Parameters for the plasma treatment of ITO glass were chosen with reference to previous research[21]. The sample without wet cleaning (reference sample) was studied also before and after plasma treatment. In Tab. II, it is shown that the content of carbon compounds decreased after IPA immersion and the oxygen content increased (due to increase of indium and tin oxides). In case of the reference sample without precleaning IPA caused partial removing of organic contaminants. The higher decrease of carbon compounds after plasma treatment of reference and IPA cleaned samples indicates that plasma removes organic contaminants as well as IPA residues. The relative quantities of C-bonds obtained from deconvolution of C1s peak are shown in Fig. 8. IPA removed contaminants with simple C-C, C-O bonds only partially. Plasma treatment caused better removal of both, contaminants with simple

Table II
Chemical composition of ITO glass-IPA removing with plasma treatment (300 W, 5s) measured with XPS

	Atomic concentration[%]			
	C 1s	In 3d	O 1s	Sn 3d
Reference	51	15	32	2
Ref + plasma	11	28	58	3
IPA	31	25	41	3
IPA + plasma	11	29	57	3

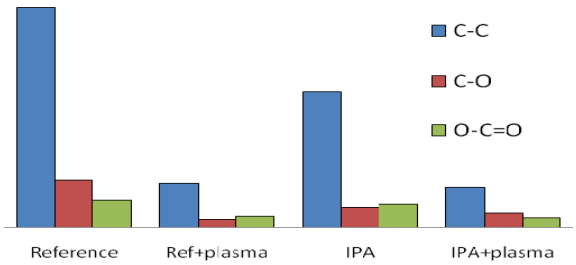

Fig. 8. **Relative quantity of C-bonds on ITO glass**

bonds and contaminations with more complicated bonds as O-C=O.

4. Conclusion

FTIR spectroscopy investigation of three type of silicon surfaces shows characteristic peaks indicating 2-propanol after IPA immersion and removing of IPA after plasma treatment using DCSBD. Only the thermally oxidized silicon was relatively resistant to 2-propanol.

Changes in chemical composition of surface measured by XPS approve increase of carbon compounds after IPA immersion and decline after plasma treatment, mainly on precleaned silicon and silicon rinsed in hydrofluoric acid. For comparison of cleaning effectiveness XPS measurement of ITO glass reference (as received) and IPA cleaned samples before and after plasma treatment was made. Changes in chemical composition indicate that plasma generated by DCSBD is suitable for organic contaminants removing and more effective than 2-propanol, which is often used for cleaning in electronics, semiconductor industry, medicine, etc.

This research has been supported by the project R&D center for low-cost plasma and nanotechnology surface modifications CZ.1.05/2.1.00/03.0086 funded by European Regional Development Fund., by the projects: 26240220002 and 2622020004 supported by the Research & Development Operational Programme funded by the ERDF and by UK grant UK/434/2012.

REFERENCES

1. Müller A., Ghosh M., Sonnenschein R., Woditsch P.: Mat. Sci. Eng., B *134*, 257 (2006).
2. Zunger A., Wagner S., Petroff P.M.: J. El. Mat. *22*, 3 (1993).
3. Chevaleevski O., Larina L.: Korean J. Chem. Eng. *18*, 403 (2001).
4. Brabec Ch. J.: Solar Energy Materials & Solar Cells *83*, 273 (2004).
5. Kern W.: J. Electrochem. Soc. *137*, 1887 (1990).
6. Černák M.: Patent WO 2007/142612 A1 2007, (2007).
7. Černák M., Černáková Ľ., Hudec I., Kováčik D., Zahoranová A.: Eur. Phys. J. – Appl. Phys. *42*, 22806 (2009).
8. Černáková Ľ., Szabová R., Wolfová M., Buček A., Černák M.: Fibres & Textiles in Eastern Europe *15*, 121 (2007).
9. Bónová L., Buček A., Plecenik T., Zahoranová A., Černák M.: Chem. Listy *102*, s1452 (2008).
10. Ondrášková M., Ráheľ J., Zahoranová A., Tiňo R., Černák M.: Plasma Chem. Plasma Proc. *28*, 203 (2008).
11. Buček A., Homola T., Aranyosiová M., Velič D., Plecenik T., Havel J., Sťaheľ P., Zahoranová A.: Chem. Listy *102*, s1459 (2008).
12. Šimek M., Homola T.: *28th ICPIG, Prague, Czech Republic, July 15-20, 2007* (Poster no. 3P10-29).
13. Šimor M., Ráheľ J., Vojtek P., Černák M., Brablec A.: App. Phys. Lett. *81*, 2716 (2002).
14. Zahoranová A., Medvecká V., Kováčik D., Plecenik T., Greguš J., Černák M.: *HAKONE XII, Trenčianske Teplice, Slovakia, 12.-17.9.2010,* Book of Contributed Papers (Országh, J., Papp, P., Matejčík, Š., ed.) p. 521.
15. Pauling L.: Am. Mineralogist *65*, 321(1980).
16. Amirfeitz P., Bengtsson S., Bergh M., Zanghellini E., Borjesson L.: J. Electrochem. Soc. *147*, 2693 (2000).
17. Vásquez-A. M. A., Águila Rodríguez G., García-Salgado G., Romero-Paredes G., Pena-Sierra R.: Revista Mexicana De Fi´sica *53*, 431 (2007).
18. Mayo D. W., Miller F.A., Hannah R. W.: *Course Notes on The Interpretation of Infrared and Raman Spectra.* J. Wiley, New Jersey 2003.
19. WebBook Chemie, NIST, [online] http://webbook.nist.gov/cgi/cbook.cgi?ID=C67630&Units=SI&Type=IR-SPEC&Index=3#IR-SPEC(4.5.2012).
20. Milata V., Segľa P., Brezová V., Gatial A., Kováčik V., Miglierini M., Stankovský Š., Šíma J.: *Aplikovaná molekulová spektroskopia,* Slovenská technická univerzita, Bratislava 2008.
21. Homola T., Matoušek J., Medvecká V., Zahoranová A., Kormunda M., Kováčik D., Černák M.: Appl.Surf. Sci. *258*, 7135 (2012).

V. Medvecká[a], A. Zahoranová[a], D. Kováčik[a,b], and J. Greguš[a] *([a] Dep. of Experimental Physics, Comenius University, Bratislava, Slovak Republic; [b] R&D Center for Low-Cost Plasma and Nanotechnology Surface Modifications, Faculty of Science, Masaryk University, Brno, Czech Republic):* **Effect of Surface Cleaning and Removing of Organic Contaminants from Silicon Substrates and ITO Glass by Atmospheric Pressure Non-thermal Plasma**

Plasma generated by DCSBD was investigated for cleaning and removing of organic contaminants from semiconductor materials. ITO glass used in photovoltaics and three types of most often used silicon surfaces in semiconductor industry – precleaned silicon, thermally oxidized silicon and H-terminated silicon was studied. The changes in chemical bonds on silicon surfaces were investigated by FTIR. Removing of IPA from silicon substrates was observed by XPS measurements. Effectivity of DCSBD as cleaning agent in comparison with isopropylacohol was investigated on ITO glass samples by XPS measurement.

MULTIFUNCTIONAL TRANSPARENT PROTECTIVE COATINGS ON POLYCARBONATES PREPARED USING PECVD

VALENTIN MOCANU[a]*, ADRIAN STOICA[a,b], LUKÁŠ KELAR[a], DANIEL FRANTA[a,b], VILMA BURŠÍKOVÁ[a,b], ROMANA MIKŠOVÁ[c], VRATISLAV PEŘINA[c]

[a] *Dept. of Physical Electronics, Masaryk University, Kotlářská 2, 611 37 Brno,* [b] *CEITEC, Central European Instituteof Technology, Masaryk University, Brno,* [c] *Nuclear Physics Institute, Academy of Sciences of the Czech Republic, 250 68 Rež near Prague, Czech Republic*
vallym@mail.muni.cz

Key words: multilayered coatings, protective, transparent, polycarbonate

1. Introduction

The advantageous properties (light weight, unique mechanical, thermal and electrical behaviour and high freedom of design) of plastics favoured the replacing of glass in a wide range of industries. The thermoplastic material can be manufactured by injection moulding to complex formed transparent elements. Optical characteristics of polycarbonate are a comparatively high refractive index of about 1.58 (500 nm) and a high dispersion (low Abbe number)[1]. The disadvantages of this material are high birefringence, low mechanical hardness, and sensitivity to UV radiation. Because of the known disadvantages of plastics compared to glass, such the softer surface and sensitivity to weathering, there is a high demand for development of protective coatings against degradation upon exposure to environment ultraviolet light. Various efforts are under way to develop scratch-resistant coatings based on silica and siloxanes by applying sol-gel or plasma -enhanced chemical vapor deposition (PECVD) processes[2–4]. The degradation of polycarbonate by global UV radiation has been well studied because polycarbonates are prone to yellowing[5–7].

When ultraviolet attack occurs the material may have a color shift, become chalky on the surface, and/or crack. There are a number of methods to reduce this problem. The addition of carbon black to the polymer will usually absorb most UV radiation. Chemical inhibitors are available for certain plastics, which improve the UV resistance. Paint and silicone coatings can also be used to completely cover exposed surfaces to sunlight (UV radiation). To remedy these limitations, various methods of producing hard transparent protective coatings are applied[8]. Existing wet chemical coating technologies consist of several steps, e.g. curing by UV radiation or oven drying. Among various techniques, plasma is a complex source of energy for surface modification, due to the large variety of components, such as excited and ionised particles, photons, radicals, with all of these species being capable of inducing chemical reactions, both in the plasma volume and at its interface with solid surfaces. There are two ways to plasma modify the surface properties of polymers, either by introducing new functional groups by surface grafting using noncoating plasmas, or by deposition of organic or inorganic films with the desired properties using coating plasmas[9].

We used the plasma-enhanced chemical vapour deposition method based on hexamethyldisiloxane (HMDSO) monomer and oxygen mixture to deposit protective films on polycarbonate surface.

Table I
Deposition parameters for the selected samples: n is the flow rate ratio $n= Q_{HMDSO}/(Q_{HMDSO} +Q_{O2})$, where Q_{O2} is the oxygen flow rate, Q_{HMDSO} is the monomer (HMDSO, $Si_2OC_6H_{18}$) flow rate, P is the applied power, U_b is the self bias voltage on the bottom substrate holder electrode, p is the average pressure, the relative error of the listed parameters is around 3%

No	Q_{O2} [sccm]	n	P [W]	U_b [V]	p [Pa]
VI01	5.2	0.66	50	–140	23.4
VI02	2.9	0.80	50	–175	14.5
VI03	5.2	0.66	50	–160	24.5
VI05	9.8	0.47	100	–185	36.4
VI06	20	0.31	100	–180	60.0
VI07	50	0.15	100	–111	111
VI09	4.9	0.64	100	–278	23.3
VI10	9.7	0.48	100	–216	39.0
VI11	9.7	0.47	50	–119	39.0
VI12	4.9	0.66	50	–196	23.0
VI13	4.7	0.66	75	–200	24.0
VI14	2.9	0.71	50	–240	15.0
VI15	4.9	0.52	50	–160	23.0
VI16	6.6	0.50	50	–150	31.0
VI17	9.7	0.52	50	–111	38.9
VI18	9.7	0.52	50	–107	38.0
VI19	7.0	0.60	50	–105	33.5
VI20	5.0	0.50	50	–192	24.8

2. Experimental

The films were prepared in low pressure r.f. glow discharges burning in mixtures of hexamethyldisiloxane (HMDSO, $Si_2OC_6H_{18}$) monomer with oxygen.

The deposition reactor consisted of a glass cylinder 310 mm in diameter, 210 mm in height. The cylinder was enclosed by two discs of stainless steel. The lower electrode was capacitively coupled to a high frequency generator that is working at the usual frequency of 13.56 MHz. The films were deposited by plasma enhanced chemical vapour deposition in two steps, first the plasma pretreatment, which was a mean for improving the adhesion of the films to the substrate, and the second step was the deposition itself. The summary of the most important operational parameters are given in Table I.

3. Results and discussion

The surface energy of the plasma-treated polycarbonate immediately after the treatment, as well as ageing effects, was studied by contact angle measurements performing surface free energy measurements. The surface free energy of the deposited films was calculated according Lifshitz-Van der Waals/acid-base approach. This method enables us to determine the electron-acceptor and electron-donor parameters of the surface tension which is a sum of its apolar and polar components:

$$\gamma = \gamma^{LW} + \gamma^{AB} \text{ , with } \qquad \gamma^{AB} = 2\sqrt{\gamma^{+}\gamma^{-}} \qquad (1)$$

Here LW indicates the total apolar (dispersive) Lifshitz-Van der Walls interaction and AB refers to the acid-base or electron-acceptor/electron-donor interaction according to Lewis.

The surface free energy can be calculated according to Young-Dupré equation expressed by terms as acid component γ^+ (acceptor effect) and basic component γ^- (donor effect). The values can be determined from contact angle measurement with three liquids two of which must have polar component γ^{AB} (ref.[9]). If we use more than three liquids, the total surface free energy and its components may be determined by means of acid-base regression model[9].

The liquids we used and their table notations are as follows: water (w), glycerol (g), ethylene glycol (e), diiodomethane (d), formamide (f), and α-bromonaphtalene (b) on polycarbonate.

The results of plasma treatment optimization are illustrated in Fig. 1. We studied not only the immediate effect of the surface treatment on the polycarbonate surface free energy but also its stability during storage. In case of 10 minute nitrogen treatment at 50 W we obtained the highest surface free energy, however, its decrease with time was quite fast. Moreover, the long plasma treatment sometimes caused a slight change in the polycarbonate substrate color. We have found out, that the color change occurred in case of a long time storage of the polycarbonate. The polycarbonate tends to absorb water and therefore its water content increases with time. Under vacuum conditions there is a high water desorption. Using optical emission spectroscopy, we have found out that occurrence of water fragments in the plasma causes increase of optical emission intensity in the UV part of the spectra, which can cause photodegradation of the PC samples. Also, long time treatment increases the surface roughness. Therefore, the optimum treatment time was determined as 1 minute and the optimum gas was hydrogen. If applied power of 50 W was used, the initial surface free energy γ_{tot} was high enough to achieve good adhesion. The decrease of γ_{tot} was slow and during the short treatment time color change or increase in surface roughness was observed. What we observed was the fact that the coatings deposited on the pretreated samples had a better adhesion to the substrate. This is correlated with the decrease of the contact angle values and with the increase of the surface total free energy.

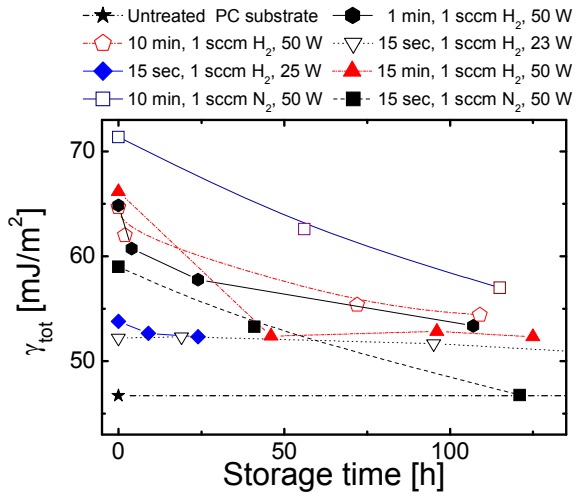

Fig. 1. **The dependence of the total surface free energy γ_{tot} on the storage time after plasma treatment in hydrogen or nitrogen.** The treatment time, gas flow and applied power are given in the graph

The values obtained from measurement of the contact angle for six liquids on thin films prepared from mixture of hexamethyldisiloxane and oxygen together with the values for the total surface free energy γ_{tot} and its components (γ^{LW}, γ^{AB}, γ^+, γ^-) are given in Table II. The results were obtained on films deposited on glass or polycarbonate substrate. The results listed in Table II. prove that the character of the thin film surfaces was possible to change from hydrophilic (for example VI15) to hydrophobic (for example VI12) .

In case of sample VI15, the polar component γ^{AB} as well as the acid γ^+ and base γ^- components were relatively high, compared to that of sample VI12. Sample VI12 had an almost purely apolar character, because the polar part of the surface free energy γ^{AB} was negligible.

Table II
Contact angle values Θ_i (suffix i denotes the liquid used: water – w, glycerol – g, ethylene glycol – e, diiodomethane – d, formamide – f, and α-bromonaphtalene – b) and total surface free energy γ_{tot} values together with their dispersive γ^{LW}, polar γ^{AB}, acid γ^{+} and base γ^{-} components for selected thin films. Film deposition conditions are given in Table I

Θ_w [°]	Θ_d [°]	Θ_g [°]	Θ_b [°]	Θ_e [°]	Θ_f [°]	γ_{tot} [mJ/m^2]	γ_{LW} [mJ/m^2]	γ_{AB} [mJ/m^2]	γ^+ [mJ/m^2]	γ^- [mJ/m^2]
VI15 on glass substrate										
43.56	55.71	41.46	31.16	33.55	–	45.96	34.19	11.78	0.96	36.07
VI13 on PC substrate										
83.79	58.48	79.97	34.67	58.64	57.65	34.91	34.13	0.78	0.03	5.81
VI12 on PC substrate										
86.74	62.01	81.02	49.67	67.29	69.65	29.6	29.11	0.49	0.01	6.35
VI08 on PC substrate										
49.82	47.52	41.85	30.59	–	–	47.15	34.46	12.69	1.5	26.77
VI01 on PC substrate										
80.6	62.47	76.39	49.98	66.27	60.43	30.97	28.95	2.02	0.11	9.23

The elemental composition, thickness and density, was determined by using the following nondestructive nuclear analytical methods[11], by RBS (Rutherford backscattering spectrometry) and ERDA (elastic recoil detection analysis).

The RBS is the only analytical method suitable for estimation of elemental composition in the whole depth of layers. The elements signals in RBS spectra overlap and this fact leads to great statistical uncertainty. We try to reduce this drawback by using enlarged non-Rutherford cross-section for proton projectiles scattered with C, O, Si. The conventional ERDA with 2.5 MeV alpha projectiles is suitable for hydrogen estimation up to depth 0.5–1 μm.

All spectra are at first evaluated severally and then each other interacted with regard for their definiteness. The right stopping powers depend on the precise composition of layers. For a detailed analysis of recorded experimental spectra, the codes GISA 3 (ref.[12]) and SIMNRA 6.06 (ref.[13]) were used.

Table III
Atomic composition of the prepared films obtained by RBS/ERDA

Sample	Si [%]	O [%]	C [%]	H [%]	O/Si ratio
VI06	21.46	59.41	0.13	19	2.77
VI07	29.86	51.15	0.48	18.5	1.71
VI08	30.23	52.52	0.75	16.5	1.74
VI10	27.27	58.51	0.72	13.5	2.15
VI15	27.12	54.72	1.66	16.5	2.02
VI16	27.11	54.7	1.9	18	2.02
VI19	20.43	32.85	20.72	26	1.61

The film deposited at relatively high negative self bias voltage and with HMDSO to total flow rate ratio around 0.5 or less exhibited SiO_2 – like properties. The carbon content in these coatings was low and the oxygen to silicon ratio was around 2 as it is in SiO_2 films (Table III) or more. In films prepared with n>0.5 and at relatively low negative self bias voltage the carbon and hydrogen content increased and these films showed polymer-like properties.

The instrumented indentation method and the Fischer scope H100 tester equipped with Vickers indenter was used to study the mechanical properties of the coating/substrate systems. The universal hardness HU can be defined as a measure of the material resistance against elastic and plastic deformation. From the loading/unloading curves it is possible to obtain the Martens hardness HM (measure of the resistance against elastic and plastic deformation). From the load-penetration curves (Fig. 2) it was possible to determine also the material resistance against plastic deformation H_{pl} (so called plastic hardness) or H_{IT} (so called indentation hardness) and the elastic modulus E_{IT} (Table IV).

The results in Table IV were obtained on films deposited on three different types of substrates (polycarbonate – pc, glass – gl, and silicon – si). The film thicknesses ranged from 3 to 5 μm. The substrate influence was negligible for silicon and glass substrates, but it is significant for polycarbonate, mainly in case of elastic modulus as it can be seen in Table IV. The results obtained on PC substrates characterise the resistance of film/substrate system against indentation at given indentation load. These parameters cannot be taken as the film characteristics. The results obtained on commercial paint used recently in the automotive industry for PC protection is included into graph and Table IV too.

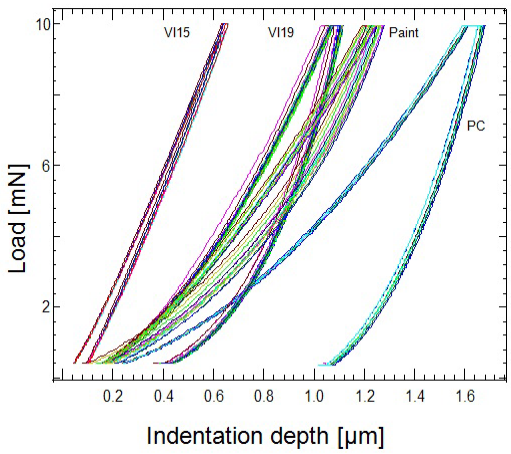

Fig. 2. **Comparison of the load-penetration curves obtained on noncoated PC and on PCs coated with films VI15, VI19 and commercial paint**

Jobin Yvon UVISEL phase-modulated spectroscopic ellipsometer was used to study the spectral dependences of prepared in films elipsin spectral range from 0.6 to 6.5 eV. Measurements were performed on five angles of incidence in the range 55° to 75°. The analysis of ellipsometric data of thick transparent films is generally difficult since it is not possible to use models assuming ideal layers and ideal apparatuses. Several effects, related to loss of coherence of light, become important for thick films even though they are not necessary to consider in the case of thin films. The final evaluation should take into account the effects of depolarization, which can be seen in spectral range from 0.6

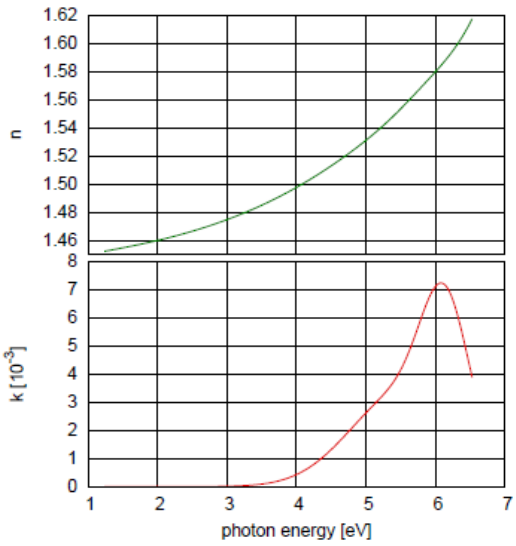

Fig. 3. **Spectral dependence of the refraction index n and the extinction coefficient k for sample VI19**

Table IV
Mechanical characteristics of the film-substrate systems on selected samples obtained using indentation tests with 10 mN of maximum load. HM is the Martens hardness, n_{IT} is the elastic to total deformation work ratio, H_{IT} is indentation hardness, E_{IT} is elastic modulus, h_{max} is the maximum indentation depth at maximum load of 10 mN, C_{r1} is the indentation creep deformation (expressed in percentage of h_{max}) reached during 5 s when the maximum load was kept constant, C_{r2} is the anelastic deformation (in percentage of h_{max}) reached during 5 s when the minimum load of 0.4 mN was kept constant. Abbreviation in sample name refer to the type of the substrate, i.e. pc – polycarbonate, gl – glass, si – silicon

No.	HM [GPa]	n_{IT} [%]	H_{IT} [GPa]	E_{IT} [GPa]	h_{max} [μm]	C_{r1} [%]	C_{r2} [%]
$VI06_{pc}$	0.16	55	0.32	3.1	1.56	2.4	–9
$VI07_{pc}$	0.17	52	0.33	3.5	1.49	2.7	–5
$VI08_{pc}$	0.14	52	0.25	3.0	1.68	2.2	–4
$VI10_{pc}$	0.15	59	0.29	3.3	1.57	2.3	–6
$VI15_{pc}$	0.70	92	11.8	18	0.74	0.9	–4
$VI16_{pc}$	0.69	91	10.8	18	0.74	0.9	–4
$VI19_{pc}$	0.21	88	0.82	3.7	1.35	1.4	–7
$VI06_{gl}$	3.33	65	8.54	68	0.35	1.2	–2
$VI07_{gl}$	3.67	60	8.27	79	0.32	1.5	–1
$VI08_{gl}$	3.03	60	6.93	63	0.35	1.6	–
$VI10_{gl}$	3.83	74	11.8	69	0.33	0.1	–
$VI16_{gl}$	3.43	70	9.80	69	0.33	0.9	–
$VI15_{si}$	3.48	68	9.50	70	0.33	0.7	–
$VI19_{si}$	0.59	93	2.24	11	0.80	0.5	–
Paint	0.27	64	0.56	5.4	1.18	2.9	–8
Substrates							
PC	0.12	41	0.19	3.1	1.74	2.9	–3
Glass	3.77	58	9.25	81	0.31	0.4	–
Si	7.32	62	13.3	18	0.28	–	–

to 1.25 eV and was caused by reflection of light from back side of the transparent silicon wafer.

In Fig. 3 an example of the dependence of the refractive index *n* and the extinction coefficient *k* on the photon energy obtained for film VI19 is shown. There is a strong increase in extinction coefficient in the spectral region from 4 to 6 eV, so the absorption of film VI19 increased in UV region. The thickness of the film VI19 was determined from ellipsometric measurements as t = 5320±20 nm.

4. Conclusion

Multifunctional thin films were prepared in r.f. capacitively coupled glow discharges using controlled ratios of mixtures between hexamethyldisiloxane with oxygen and hexamethyldisilazane with nitrogen on the polycarbonate substrates. By varying the discharge parameters

and the gas flow rates it was possible to change the character of films from hydrophobic (γ_{tot} =28 mJ m^{-2}) to hydrophilic (γ_{tot} = 47 mJ m^{-2}), from soft polymer-like (H_{IT} = 1 GPa, E_{IT} = 10 GPa) to hard SiO_x-like (H_{IT} = 11 GPa, E_{IT} = 80 GPa) films. The films were fully transparent for the visible light, the absorption in UV region for photon energy higher than 4.5 eV was observed for polymer-like films.

This research was supported by the Grant Agency of the Academy of Sciences of the Czech Republic under contract KAN311610701, by the project CZ.1.05/2.1.00/03.0086 'R&D center for low-cost plasma and nanotechnology surface modifications' funded by European Regional Development Fund and by the Ministry of Industry and Trade, contract FTTA5114 and by the Ministry of Education, Youth and Sports of the Czech Republic, contract MSM 0021622411

REFERENCES

1. Borcia C., Borcia G., Dumitrascu N.: Appl. Phys., A *90*, 507 (2008).
2. Sepeur S., Kunze N., Werner B., Schmidt H.: Thin Solid Films *351*, 216 (1999).
3. Zajickova L., Bursikova V., Janca J.: Vacuum *50*, 19 (1998).
4. Rats D., Hajek V., Martinu L.: Thin Solid Films *340*, 33 (1999).
5. Rivaton A.: Polym. Degr. Stab. *49*, 163 (1995).
6. Ram A., Zilber O., Kenig S.: Polym. Eng. Sci. *25*, 535 (1985).
7. Tjandraatmadja G. F., Burn L. S., Jollands M. C.: Polym. Degr. Stab. *78*, 435 (2002).
8. Benz G., Mutshler G., Schneider G.: Germany Patent DE 3413019 (1985).
9. http://www.makrolon.de. (7.9.2012)
10. Buršíková V., Sťahel P., Navrátil Z., Buršík J., Janča J.: *Surface Energy Evaluation of Plasma Treated Materials by Contact Angle Measurement*. Masaryk University, Brno 2004.
11. Wang Y., Nastasi M.: *Handbook of Modern Ion Beam Materials Analysis*, Second Edition. Materials Research Society, Warendale, Pensylvania 2009.
12. Saarilahti J., Rauhala E.: Nucl. Instrum. Methods Phys. Res. *B64*, 734 (1992).
13. Mayer M.: *SIMNRA User`suide, Technical report IPP 9/113*. Max-Planck-Institut fur Plasmaphysick, Garching, Germany 1997.

V. Mocanu[a], A. Stoica[a,b], L. Kelar[a], D. Franta[a,b], V. Buršíková[a,b], R. Mikšová[c], and V. Peřina[c] *([a] Dept. of Physical Electronics, Masaryk University, Brno, [b] CEITEC, Central European Instituteof Technology, Masaryk University, Brno, [c] Nuclear Physics Institute, Academy of Sciences of the Czech Republic, Rež near Prague, Czech Republic):* **Multifunctional Transparent Protective Coatings on Polycarbonates Prepared Using PECVD**

Thin transparent films on polycarbonate substrates were prepared using a capacitively-coupled radio-frequency discharge. The films were obtained from mixtures of hexamethyldisiloxane with oxygen. Varying the discharge parameters and the gas flow rates, multifunctional coatings wre prepared. The films were analysed using depth sensing indentation method, contact angle measurements, surface energy calculation, ellipsometry and spectrophotometry in order to determine the properties and functionality (hardness, fracture toughness, adhesion, internal stress, abrasion resistance, thickness, color, refractive index) of the obtained structures. The behavior of the coatings covers a wide range of material properties from inorganic to polymer-like coatings.

SILVER IONS BONDING ON POLYPROPYLENE BY UNDERWATER DOUBLE DIAPHRAGM DISCHARGE FOR ANTIMICROBIAL APPLICATIONS

GABRIELA NEAGOE*[a], ANTONÍN BRABLEC[a], JOZEF RÁHEĽ[a,b], VILMA BURŠÍKOVÁ[a,c]

[a] *Dep. of Physical Electronics, Faculty of Science, Masaryk University, Kotlářská 2, 611 37 Brno, Czech Republic,* [b] *Dep. of Experimental Physics, Comenius University, Mlynská dolina F2, 842 48 Bratislava, Slovak Republic,* [c] *CEITEC - Central European Institute of Technology, MU, 601 77 Brno, Czech Republic*
gabriela.pirpiliu@yahoo.com

Keywords: underwater discharge, antibacterial effect, silver, polypropylene

1. Introduction

Production of technical textiles is one of the fast growing sectors of the global textile industries. Textile materials used in the medical, health care and hygiene sectors are an important and expanding part of the industry, and they are usually referred to as biomedical textiles. This group of products demonstrates a great range of applications, from simple bandages to biocompatible implants and tissues; antibacterial wound treatment material, prosthetics and so called intelligent textiles.

The application of nonwoven fabrics varied in the wide range from hygienic products to medical fabrics and industrial applications. By appropriate surface treatments nonwoven polypropylene (PP) can be advanced in the biocompatible fabric and can acquire antimicrobial properties. Moreover, a new generation of dressing incorporating antimicrobial agents like silver and iodine has been studied[1].

For this study we used the underwater discharge generated in a diaphragm electrode configuration as the treatment technique for the PP nonwoven in a solution of silver salt ($AgNO_3$). Silver is a non-toxic, non-tolerant disinfectant that can significantly reduce many bacterial infections[2,3]. Bacteria have different membrane structures which allow a general classification of them as Gram-negative or Gram positive. The structural differences lie in the organization of a key component of the membrane, peptidoglycan. Gram negative bacteria exhibit only a thin peptidoglycan layer (~2–3 nm) between the cytoplasmic membrane and the outer membrane[4]; in contrast, Gram-positive bacteria lack the outer membrane but have a peptidoglycan layer of about 30 nm thick[5].

The possibility of combining the plasma chemical activity with the selectivity of processes in solutions[6] is an advantage of the discharge in water. It produces effectively hydrated electrons and hydroxyl radicals which can be used for material surface modification[7,8]. The obtained results indicate the unique capability of the underwater diaphragm discharge to activate the fabric and immobilize the particles on fibers surface within a single process step.

2. Experimental setup

The electrodes were connected to a pulsed HV power supply based on the double rotating spark gap. The maximum peak voltage was 40 kV DC. The maximum repetitive rate of pulses was 60 Hz. The duration of the electrical pulses was determined by the water conductivity. The distance between the diaphragms was 13 cm (Fig. 1).

Double diaphragm discharge is improving the treatment uniformly.

Polypropylene nonwoven fabrics of 50 grams per square meter (gsm) and 30 mm width supplied by PEGAS NONWOVENS s.r.o. (Czech Republic), was fed trough the slit with an adjustable speed. After treatment the samples were washed in a detergent solution in an ultrasonic bath for 20 minutes in order to remove weakly attached silver mictoparticles.

3. Results and discussion

The „Determination of antibacterial activity – Agar diffusion plate test“ method was used to study the antibacterial properties of the PP nonwoven textile.

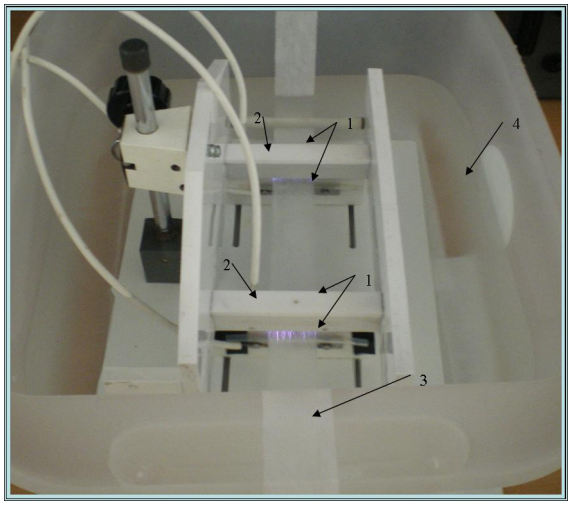

Fig. 1. **Experimental arrangement for Double Diaphragm Discharge:** 1 – electrodes; 2 – diaphragm; 3 – polypropylene nonwoven fabric; 4 – water-based solution

The samples were placed on a germ-containing agar plate and were inoculated with Gram-positive (*Staphylococcus aureus*) bacteria and Gram-negative (*Escherichia coli*) bacteria. In the images presented in Fig. 2 and Fig. 3, we can observe the antimicrobial effect of the washed and unwashed treated PP fabric against *S. aureus* and *E. coli*.

The antibacterial properties of the treated PP in solution of silver salt against *S. aureus* and *E. Coli* are presented in Tab. I and Tab. II.

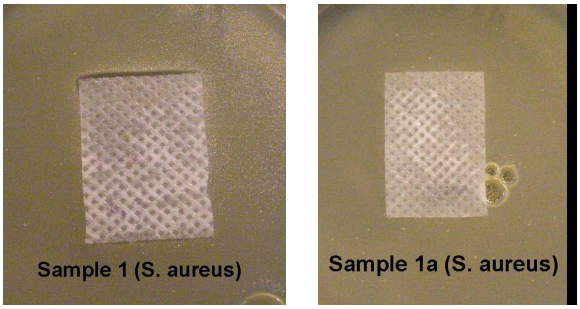

Fig. 2. **Images of the unwashed (sample 1) and washed (sample 1a) samples effect on *Staphylococcus aureus* bacteria**

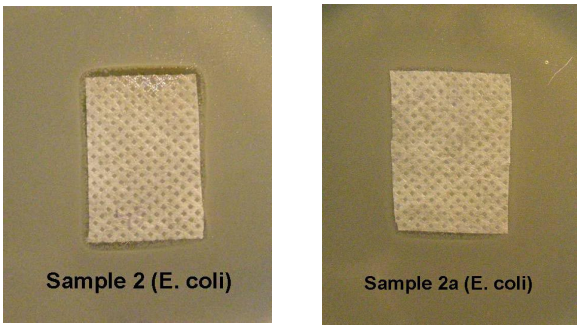

Fig. 3. **Images of the unwashed (sample 2) and washed (sample 2a) samples effect on *Escherichia coli* bacteria**

Table I
Antibacterial properties of the treated PP against *S. aureus*

Sample	Growth[a)]	Assessment
Ref – only PP	heavy	insufficient effect[b)]
Sample 1	none (inhibition zone = 0.5 mm)	good effect[c)]
Sample 1a (after washing)	none	good effect

[a] The growth of bacteria in the nutrient medium under the specimen, [b] no inhibition zone, compared to the control no growth reduction therefore insufficient effect, [c] no growth, the inhibition zone exceeding 1 mm or up to 1 mm (good effect)

Table II
Antibacterial properties of the treated PP against *E. coli*

Sample	Growth	Assessment
Ref – only PP	heavy	insufficient effect
Sample 2	none (inhibition zone = 1mm)	good effect
Sample 2a (after washing)	none	good effect

Samples 1a and 2a presented no inhibition zone and no growth of bacteria under the specimen. These samples were washed with detergent in an ultrasound bath for 20 min, as mentioned before. Samples 1, 2 (before washing) indicate an inhibition zone up to 1 mm and no growth of bacteria under the specimen. In case of the untreated PP, no inhibition zone and no growth reduction under the specimen were observed.

Fig. 4 and Fig. 5 show SEM micrographs of one of the treated samples in water solution of silver salt (σ = 6.54 mS cm^{-1}) before and after washing.

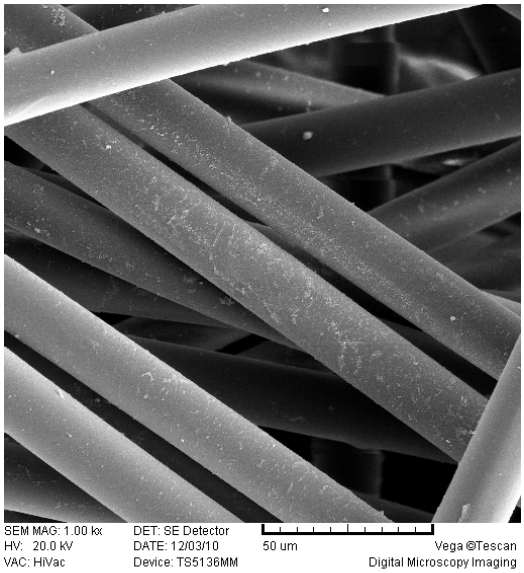

Fig. 4. **SEM micrographs of the sample treated in silver salt solution before washing**

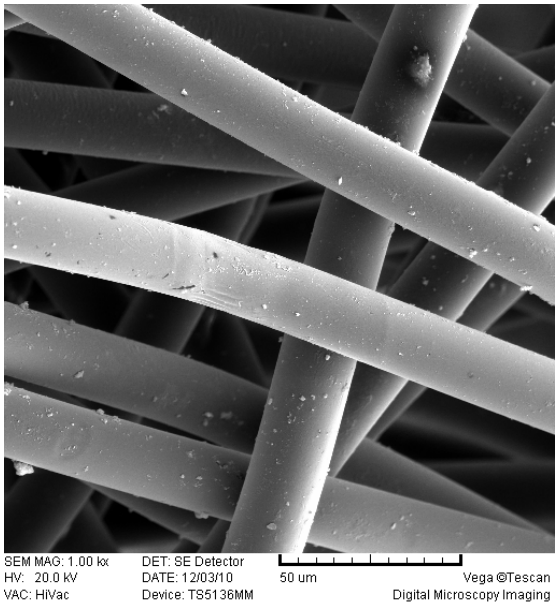

Fig. 5. **SEM micrographs of the sample treated in silver salt solution after washing**

From the Scanning Electron Microscop (SEM) images we can observe that the particles were not removed during washing and are uniformly spread on the textile surface, on both washed and unwashed samples.

The Energy Dispersive X-ray (EDX) analysis confirmed the presence of silver on the PP surface and no peaks of other impurities were detected. Similar results were obtained in different places on the samples.

4. Conclusion

SEM micrographs indicated that the silver crystals are well dispersed on the PP textile and the washing test confirmed that the particles are quite durably immobilized on the fibers surface. The EDX analysis confirmed the nature of the silver on the PP surface.

Performing Double Diaphragm discharge in the water solution of silver salt, we were able to immobilize the salts crystals on the surface of PP fibers. The „determination of antibacterial activity – Agar diffusion plate test" confirmed a good antimicrobial effect of PP nonwoven fabric with the immobilized salts crystals (no growth under the specimen and an inhibition zone up to 1 mm).

The observed antimicrobial effect for *S. aureus* and *E. coli* together with the fact that even after washing the fabric in ultrasonic bath the salt crystals are still attached on the fiber surface indicate that the Double Diaphragm discharge can be used advantageously for manufacturing of antimicrobial PP nonwovens in a single processing step.

This research has been supported by the Czech Science Foundation under the contact numbers 202/09/2064 and 104/09/H080 as well as by the project CZ.1.05/2.1.00/03.0086 'R&D center for low-cost plasma and nanotechnology surface modifications' funded by European Regional Development Fund.

REFERENCES

1. Schaller M., Laude J., Bodewaldt H., Hamm G., Korting H. C.: Skin Pharmacol. Physiol. *17*, 31 (2004).
2. Nakashima T., Sakagami Y., Ito H., Matsuo M.: Textile Res. J. *71*, 688 (2001).
3. Klaus-Joeger T., Joeger R., Olsson E., Granqvist C. G.: Trends Biotechnol. *19*, 15 (2001).
4. Murray R. G. E., Steed P., Elson H. E.: Can. J. Microbiol. *11*, 547 (1965).
5. Shockman G. D., Barret J. F.: Annu. Rev. Microbiol. *37*, 501 (1983).
6. Joshi R., Schulze R. D., Meyer-Plath A., Friedrich J. F.: Plasma Process. Polym *5*, 695 (2008).
7. Brablec A., Slavicek P., Stahel P., Cizmar T., Trunec D., Simor M., Cernak M.: Czech. J. Phys. *52* Suppl. D491 (2002).
8. Simor M., Krump H., Hudec I., Rahel J., Brablec A., Cernak M.: Acta Physica Slovaca *54*, 43 (2004).

G. Neagoe[a], A. Brablec[a], J. Ráhel'[a,b], and V. Buršíková[a,c] *([a] Dep. of Physical Electronics, Faculty of Science, Masaryk University, Brno, Czech Republic; [b] Dep. of Experimental Physics, Comenius University, Bratislava, Slovak Republic, , [c] CEITEC - Central European Institute of Technology, MU, Brno, Czech Republic):* **Silver Ions Bonding on Polypropylene by Underwater Double Diaphragm Discharge for Antimicrobial Applications**

An underwater plasma discharge is used for surface activation of polypropylene fabrics with subsequent immobilisation of silver particles. The „Textile fabrics – Determination of antibacterial activity – Agar diffusion plate test" was used to study the antibacterial properties of the treated PP nonwoven textile against *S. aureus* and *E. coli* bacteria. Distribution of the dispersed particles were measured by Scanning Electron Microscopy (SEM) and the chemical nature of crystals was confirmed by the Energy Dispersive X-ray (EDX) analysis of the sample.

ANTIBACTERIAL EFFECT OF COPPER IONS BONDED ON POLYPROPYLENE NONWOVEN BY UNDERWATER DOUBLE DIAPHRAGM DISCHARGE

GABRIELA NEAGOE*[a], ANTONÍN BRABLEC[a], ANNA ZÁHORANOVÁ[b], VILMA BURŠÍKOVÁ[a,c]

[a] *Dep. of Physical Electronics, Faculty of Science, Masaryk University, Kotlářská 2, 611 37 Brno, Czech Republik,* [b] *Dep. of Experimental Physics, Comenius University, Mlynská dolina F2, 842 48 Bratislava, Slovak Republik,* [c] *CEITEC - Central European Institute of Technology, MU, 601 77 Brno, Czech Republic*
gabriela.pirpiliu@yahoo.com

Keywords: underwater discharge, PP nonwoven, copper, antibacterial properties

1. Introduction

Underwater electrical discharges systems attract the attention of many research groups mainly for its proven eficiency in the wastewater remediations[1]. Recently emerged application for underwater electrical discharge offering a substantial economical and enviromental benefits compared with conventional wet chemical methods is the surface functionalization of textile materials (for example acid processing and alkaline hydrolysis)[2]. Only a small number of works has been published devoted to materials treatment by underwater plasma[3,4].

Underwater discharges generated in water solutions are effective sources of OH radicals, solvated electrons and number of others active species[5,6]. It is known that OH radicals can be used to incorporate hydroxyl groups in the structure of polymer materials, predominantly into polyaromatic polymers[7]. Together with solvated electrons OH radicals can take part in the formation of secondary active species such as H_2O_2, and O_3 which are strong oxidation and bleaching agents[1]. The aim of this work is to estimate the possibility of application of double diaphragm discharge system to processes of textile material treatment, and to evaluate the bactericidal effect of the polypropylene (PP) nonwoven treated in water solution of copper salt on *Staphylococcus aureus*.

The excellent physical and chemical properties of polypropylene (chemical resistance, low density, highest melting point in the family of olefin fibers, and moderate cost), compared to other fibers, make it an important fiber, increasingly used in industrial application.

Copper ions, either alone or in copper complexes, have been used for centuries to disinfect liquids, solids and human tissue. Bonding copper on polypropylene fibers or other polymeric materials enable the production of clothing, bedding and medical devices that possess biocidal properties.

In comparison with other methods, in the underwater diaphragm discharge we activate the surface and immobilize the particles in the same time.

2. Experimental setup

The discharge was generated in a narrow slit of 0.1×1×40 mm positioned between two metallic electrodes at 2 cm mutual distance. The distance between the diaphragms is 13 cm. The electrodes were connected to a pulsed HV power supply based on the double rotating spark gap. The maximum peak voltage was 40 kV DC. The maximum repetitive rate of pulses was 60 Hz. The duration of the electrical pulses was determined by the water conductivity.

The schematic of experimental setup is shown in Fig. 1.

The interfacial bonding between the particles and the PP fibers was observed by Scanning Electron Microscopy

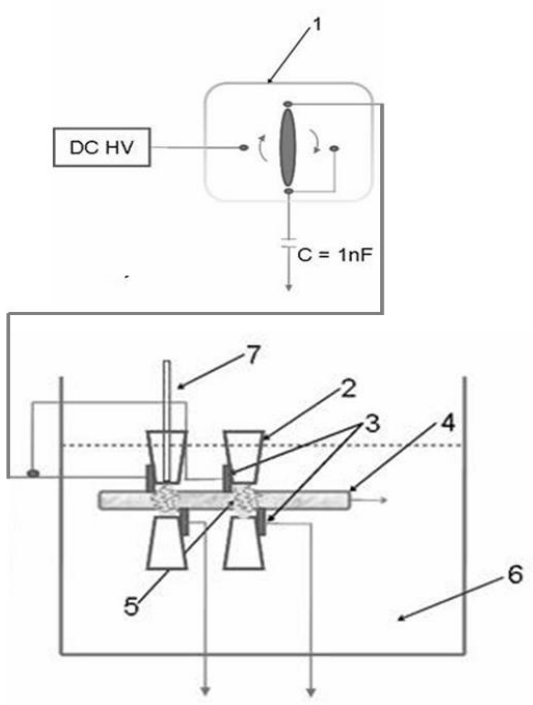

Fig. 1. **Double diaphragm discharge:** 1 – rotating spark gap; 2 – diaphragm; 3 – electrodes; 4 – textile; 5 – plasma; 6 – water solution; 7 – optical fiber

(SEM). The surface chemical compositions were analyzed by Energy Dispersive X-ray (EDX).

The ISO 20645 „Textile fabrics – Determination of antibacterial activity – Agar diffusion plate test“ was used to study the antibacterial properties of the PP nonwoven textile. The samples (treated and untreated) were placed on a germ-containing agar plate and were inoculated with Gram-positive (*Staphylococcus aureus*, ATCC 6538) bacteria. For this test i tis very important to have no growth of bacteria under the specimen and for better results also around the specimen (the so called inhibition zone).

3. Results and discussion

The polypropylene was treated in water solutions of $CuSO_4$, with different conductivities. Polypropylene nonwoven fabric of 50 gsm (grams per square meter) and 30 mm width was fed through the slit with an adjustable speed. After treatment we washed the sample in a detergent solution in Ultrasonic Bath for 15 minutes to see how many particles remain attached to the textile material.

Fig. 2 and Fig. 3 show SEM micrographs of one of the treated samples in water solution copper salt ($CuSO_4$) (σ = 6.73 mS cm^{-1}) before and after washing. We can observe that the particles were not removed during washing and are spread on the textile surface, on both washed and unwashed samples. Comparing the SEM micrographs of several samples, in different places on each sample, we observed that more than 70 % of these crystals were still attached even after the intense washing.

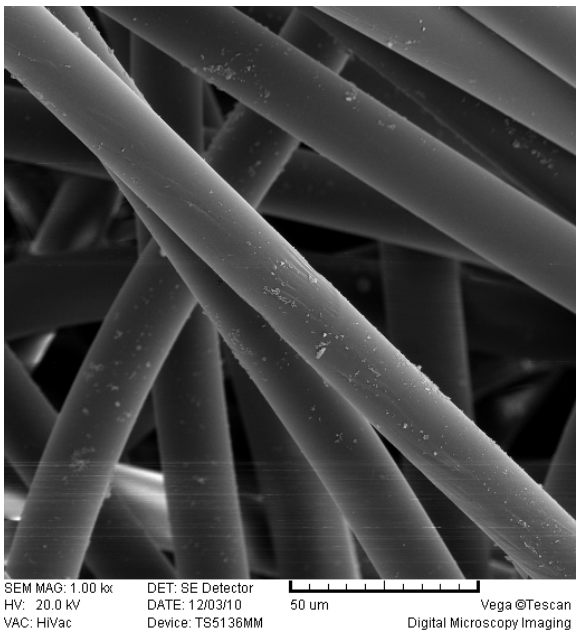

Fig. 2. **SEM micrographs of one spot on the sample treated in copper salt solution before washing**

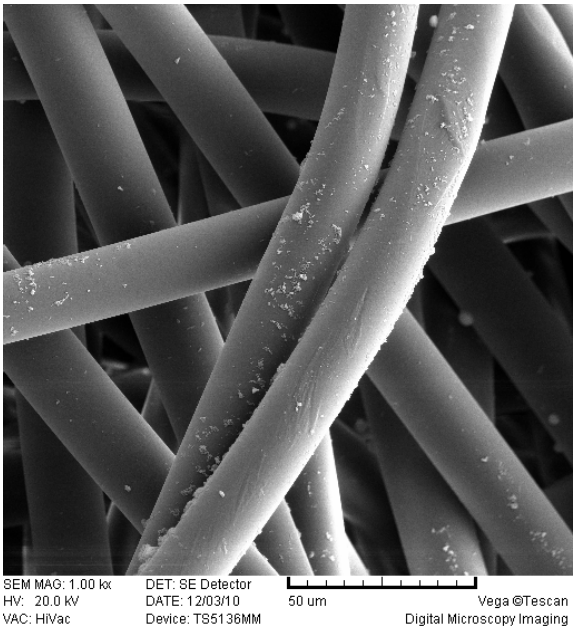

Fig. 3. **SEM micrographs of one spot on the sample treated in copper salt solution after washing**

The EDX analysis confirmed the presence of elemental cooper on the fabric fibers surface. Except the Au peak that appeared because of the initial coating of the samples with gold, no peaks of other impurities were detected.

In the image presented in Fig. 4, we can observe the different antimicrobial effect of the washed and unwashed treated PP fabric. Samples 11a and 12a (after washing) presented no inhibition zone and no growth of bacteria under the specimen. Sample 12 (before washing) indicate an inhibition zone up to 1 mm and no growth of bacteria under the specimen. In case of the untreated PP, no inhibition zone and no growth reduction under the specimen were observed.

Tab. I shows the antibacterial properties of the fabrics treated in solution of copper salt, where a) represents the growth of bacteria in the nutrient medium under the specimen, b) no inhibition zone, compared to the control no growth reduction therefore insufficient effect, c) no growth, the inhibition zone exceeding 1mm or up to 1 mm (good effect). All of the specimens exhibited excellent percentage reductions against *S. aureus*.

The assessment is based on the absence or presence of bacterial growth in the contact zone between agar and specimen and on the eventual appearance of an inhibition zone around the specimens.

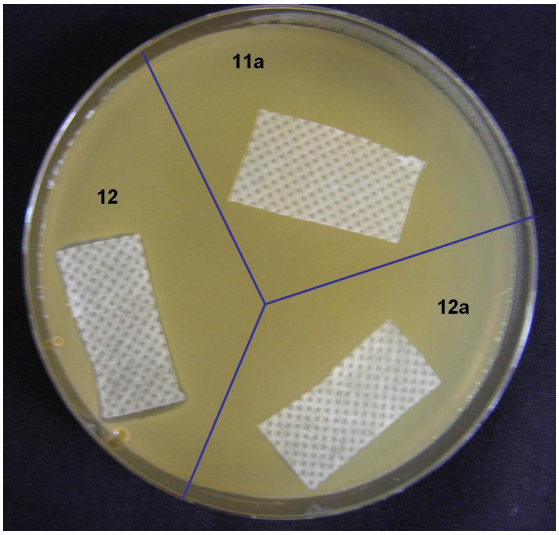

Fig. 4. **Photographic image of the incubation of *Staphylococcus aureus* on the nonwoven fabric after 24 h**: (sample 12) treated in solution of copper salt before washing; (sample 11a and 12a) after washing in ultrasound bath for 15 min

4. Conclusion

Our results indicated that underwater diaphragm plasma can immobilize copper crystals on the PP surface, copper being well known for its antibacterial properties. The „determination of antibacterial activity – Agar diffusion plate test" confirmed the antimicrobial effect of PP nonwoven fabric treated in $CuSO_4$ solution by underwater double diaphragm discharge against *S. aureus* (no growth under the specimen and an inhibition zone up to 1 mm). Also the fact that even after washing the fabric in ultrasonic bath the copper particles are covering more than 70 % of the fiber surface, allows us to consider that the diaphragm discharge can be potentially used in biomedical applications.

Table I
Antibacterial properties of the treated fabrics

Sample	Growth[a]	Assessment
Ref – only PP	heavy	insufficient effect[b]
11a (after washing)	none	good effect[c]
12	inhibition zone (1 mm)	good effect
12a (after washing)	none	good effect

This research has been supported by the Czech Science Foundation under the contact numbers 202/09/2064 and 104/09/H080 as well as as well as by the project CZ.1.05/2.1.00/03.0086 'R&D center for low-cost plasma and nanotechnology surface modifications' funded by European Regional Development Fund.

The work was also the result of the project implementation 26240220042 supported by the Research & Development Operational Programme funded by the ERDF.

REFERENCES

1. Locke B. R., Sato M. et al.: Ind. Eng. Chem. Res. *45*, 882 (2006).
2. Pastore Ch. M., Keikens P.: *Surface characteristics of fiber and textile*. *Surface science series*. *94*, New York – Basel, 2001.
3. Brablec A., Slavicek P., Stahel P., Cizmar T., Trunec D., Simor M., Cernak M.: Czech. J. Phys. *52* Suppl. D491 (2002).
4. Simor M., Krump H., Hudec I., Rahel J., Brabec A., Cernak M.: Acta Physica Slovaca *54*, 43 (2004).
5. Sunka P.: Physics of Plasmas *8*, 2587 (2001).
6. Malik M. A., Ghaffar A. Malik S. A.: Plasma Sources Sci. Technol. *10*, 82 (2001).
7. Steen M. L., Butoi C. I., Fisher E. R.: Langmuir *17*, *26*, 8156 (2001).

G. Neagoe[a], A. Brablec[a], A. Zahoranová[b], and V. Buršíková[a,c] *([a] Dep. of Physical Electronics, Faculty of Science, Masaryk University, Brno, Czech Republic; [b] Dep. of Experimental Physics, Comenius University, Bratislava, Slovak Republic, [c] CEITEC - Central European Institute of Technology, MU, Brno, Czech Republic):* **Antibacterial Effect of Copper Ions Bonded on Polypropylene Nonwoven by Underwater Double Diaphragm Discharge**

Underwater plasma discharge was used for surface activation of polypropylene fabrics with subsequent immobilisation of copper particles. Size and distribution of dispersed particles were measured by Scanning Electron Microscopy (SEM) and the chemical nature of crystals was confirmed by the Energy Dispersive X-ray (EDX) analysis of the sample. „Determination of antibacterial activity – Agar diffusion plate test" method was used to study the antibacterial properties of the PP treated and untreated nonwoven textile samples.

UNDERWATER DIAPHRAGM DISCHARGE, A NEW TECHNIQUE FOR POLYPROPYLENE TEXTILE SURFACE MODIFICATION

GABRIELA NEAGOE*[a], OLEKSANDR GALMIZ[a], ANTONÍN BRABLEC[a], JOZEF RÁHEĽ[a,b], ANNA ZÁHORANOVÁ[b]

[a] *Dep. of Physical Electronics, Faculty of Science, Masaryk University, Kotlářská 2, 611 37 Brno, Czech Republic,* [b] *Dep. of Experimental Physics, Comenius University, Mlynská dolina F2, 842 48 Bratislava, Slovak Republic*
gabriela.pirpiliu@yahoo.com

Keywords: underwater discharge, PP nonwoven, surface energy, contact angle

1. Introduction

Surface modification of textile materials extends over a wide range of alterations to provide desired single or multi-features for various applications. It is a highly focused area of research in which alterations to physical and/or chemical properties lead to new textile products that provide new applications or satisfy specific needs. These processes can involve numerous chemicals, some of which are toxic to humans and hazardous to the environment. In an effort to eliminate these harmful chemicals and waste products, surface modification and finishing via plasma treatment has become an attractive alternative.

Polypropylene (PP) is being increasingly used for industrial applications thanks to its beneficial properties and ability to be recycled. However, PP has a very low surface free energy, resulting in poor wettability and bonding strengths. To overcome this shortcoming, various techniques have been employed to modify the surface of polypropylene materials[1–3]. Plasma treatment is one of the most important surface modification techniques and has proven to be an environmentally friendly technique in the textile industry.

Plasma treatment of PP proceeds by a free-radical mechanism, which introduces a wide variety of oxidized functional groups onto the surface of the treated polymer. These oxidized functional groups may include C–OH, C=O, COOH, C–O–C, epoxy, ester, or hydroperoxide, and they are responsible for the changes in the polymer surface properties. The general effects of plasma treatment on the fiber surface are oxidation, generation of radicals, and etching.

During the last few years a lot of attention has been attracted by this field of underwater plasmas and its application in a variety of fields[4–8]. Important applications for these types of discharges had been restricted to the areas of water purification, sterilization, UV sources and shock wave generation.

Investigation of underwater discharges generated in water solutions at atmospheric pressure have shown effective production of OH radicals, solvated electrons and a number of others active species[8,9]. This primary source of radicals is often localised in a small region related to the size of the plasma discharge. Those radicals are highly reactive. Their oxidation potentials are one order of magnitude higher than usual chemical substances used to sterilise or to remove pollutants from the liquid phase.

Electrical breakdown in liquids is generally preceded by events called streamers. The two possible mechanisms for streamer initiation need to be considered: the first is due to electron avalanche which causes electrons to be injected in the liquid and drift to the cathode, and the other is due to the formation of micro-bubbles which cause gaseous cavities to be formed that give rise to electrical breakdown in the gas bubbles. The electric field around the electrode, or the streamer channel, is highly increased, which causes an intense field emission current that eventually vaporizes the water. Streamer discharge phenomena in water are known to be influenced by various factors, such as gap geometry, water conductivity, pulse duration and amplitude of the applied voltage[10].

2. Experimental setup

Distilled water was used as a working medium. The underwater plasma treatment was performed using two versions of experimental arrangement: single diaphragm (SD) discharge and double diaphragm (DD) discharge illustrated in Fig. 1. The detail of the discharge treating the textile is shown in Fig. 2.

The electrodes and the slit (diaphragm) were positioned under the water level. The electrodes were con-

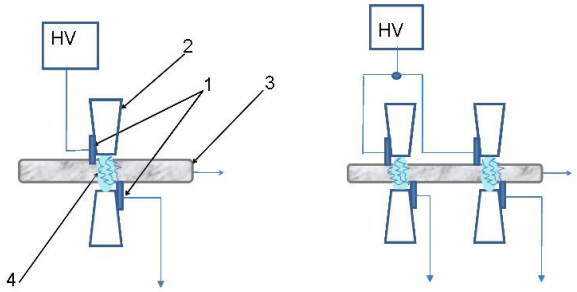

Fig. 1. **SD discharge (left) and DD discharge (right):** 1 – electrodes; 2 – diaphragm; 3 – polypropylene nonwoven fabric; 4 – discharge

Fig. 2. **Detail of the discharge**

nected to a pulsed HV power supply based on the double rotating spark gap. The maximum peak voltage reached a value of 40 kV DC and the maximum repetitive rate of pulses was 60 Hz.

Polypropylene nonwoven fabric of 50 gsm (grams per square meter) and 30 mm width was used for this experiment.

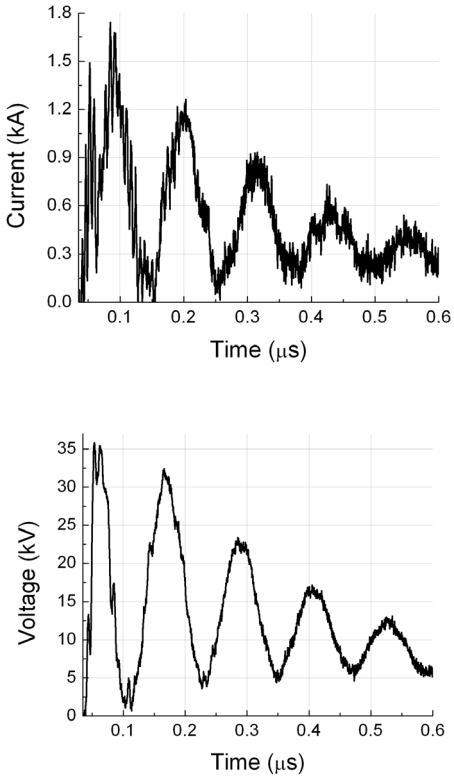

Fig. 3. **Waveforms of the discharge current and applied voltage pulses in distilled water**

The discharge was generated using a diaphragm electrode, where a narrow slits of 0.1×1×40 mm was positioned between two metallic electrodes at 2 cm mutual distance. The arrangement for double diaphragm is similar with the single diaphragm, but in this case we have two diaphragms in the same basin, the material undergoing two successive treatments. The distance between the diaphragms is 13 cm.

To keep optimal characteristics of the discharge the current and voltage measurements were done using the LeCroy WaveRunner 6100A (1GHz, 2GSa/s) Oscilloscope. Typical waveforms of the voltage and discharge current pulses are shown in Fig. 3.

We performed standard Optical Emission Spectroscopy (OES) to check the plasma discharge by means of the parameters[11]. The spectra profiles were measured by means of the Triax HR550 spectrometer, Jobin – Yvon (grating 1200 grooves, focal length 550 mm, CCD detector cooled by Peltier). The standard Griem's table (which takes into account the impact broadening by electron and quasi-static broadening by ions) of H_α line was used to determine electron temperature and density from H_α line profile[12]. The detailed description of the procedure is presented in (ref.[13]). Typical profile of H_α is shown in Fig. 4.

The total surface free energy (SFE) was determined from the measurements of the contact angles between the test liquids and the PP surfaces using a sessile drop technique. The system developed in our laboratory enables the observation of a solid–liquid meniscus directly by a CCD camera and the contact angles are determined from the CCD snapshots (Fig. 5); more information can be found in (ref.[14]).

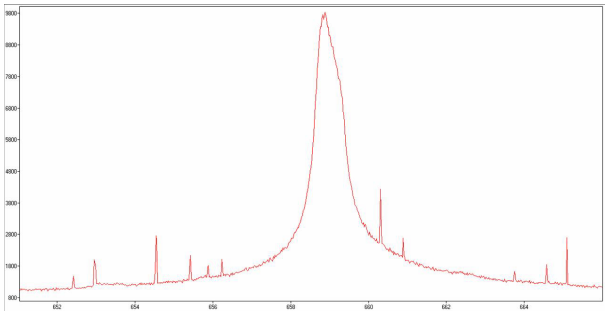

Fig. 4. **H_α line profile – original data, no filtering**

Fig. 5. **Snapshots of drops (diiodomethane) before (left) and after (right) treatment**

3. Results and discussion

The electron density changes from $1 \cdot 10^{22}$ m^{-3} to $2 \cdot 10^{24}$ m^{-3} while the electron temperature was practically constant $4 \cdot 10^4$ K in all experimental conditions studied. The error of the measured electron density was less than 5 %. The error of electron temperature was much higher, which is due to the weak dependence of the line profile on the electron temperature.

Given the nature of the plasma discharge (thin plasma filaments), the textile material is not uniformly treated in single diaphragm configuration. We noted that the wettability of the fabric was increased when the fabric was passing through two diaphragms. The second diaphragm proved to be an efficient tool for improving the wettability (Fig. 6) and not damage the fabrics. The optimum speed of PP through the diaphragms was 23 cm min^{-1} and the applied voltage was 25 kV.

The SFE (Kwok – Neumann model) of the untreated PP was 13.71 mJ m^{-2}. After double diaphragm treatment the SFE was increased to 31.51 mJ m^{-2}.

Contact angles between test liquids and polymers were measured in order to determine the total SFE using a sessile drop technique. Liquid drops on the plasma-activated polymer surface were imaged by the CCD camera and the contact angle was measured. The volume of each drop was 4 μl. Contact angles were measured for at least 10 drops for each liquid (Tab. I). The following six liquids were used: distilled water (H_2O), diiodomethane (CH_2I_2), formamide (CH_3NO), 1,2-ethanediol ($C_2H_6O_2$). Error of every measured angle is lower than 0.6°.

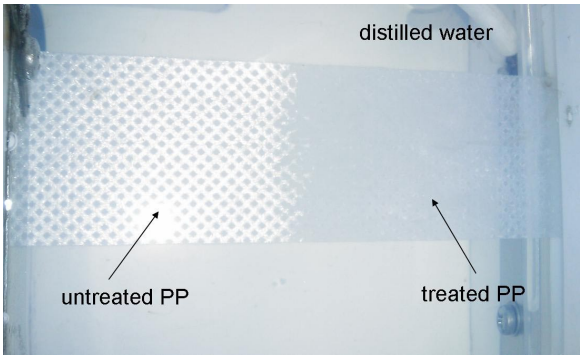

Fig. 6. **PP nonwoven treated by double diaphragm discharge (right) and untreated (left) immersed in distilled water**

Table I
Contact angles of liquids (in degrees) for untreated, single treated and double treated samples

Treatment type	H_2O	CH_2I_2	CH_3NO	$C_2H_6O_2$
untreated	110°	91°	107°	102°
SD	98°	70°	96°	78°
DD	89°	22°	53°	29°

The ageing of surface properties was also studied. The samples were stored in dry air and the SFE was measured during the time. The SFE did not change significantly during the time. The maximum decrease in the SFE was about 2 mJ m^{-2} after 14 days and afterwards the properties of the samples were stable.

4. Conclusion

It was found that the underwater diaphragm discharge (SD and DD configuration) can be used as possible application for surface modification of PP nonwoven. Double diaphragm discharge has increased the uniformity of the PP treatment.

It is shown that underwater diaphragm discharge treatment increases surface wettability of polypropylene nonwoven significantly. This is the result of an increase in surface free energy. Higher surface wetting is shown by a lower contact angle. Also, we observed that the ageing for 14 days has no significant effect on the surface free energy of the treated sample.

The results showed no thermal damage of PP after plasma treatment.

Surface modification by underwater plasma treatment has opened up new possibilities in relation to wettability and adsorption of nonwoven materials.

This research has been supported by the Czech Science Foundation under the contact numbers 202/09/2064 and 104/09/H080 as well as by the project CZ.1.05/2.1.00/03.0086 'R&D center for low-cost plasma and nanotechnology surface modifications' funded by European Regional Development Fund.

The work was also the result of the project implementation 26240220042 supported by the Research & Development Operational Programme funded by the ERDF.

REFERENCES

1. Slobodskoi S. A. et al.: Vopr. Technol. Ulavlivania i Pererab. Prod. Koksovania, *1978*, 71.
2. Sharma A. K., Locke B. R., Arce P., Finney W. C.: Hazard. Waste Hazard. Mater. *10*, 209 (1993).
3. Grimonpre D. R., Sharma A. K., Finney W. C., Locke B. R.: Chem. Eng. J. *82*, 189 (2001).
4. Monte M., De Baerdemaeker F., Leys C., Maximov A. I.: Czech J. Phys. *52*, Suppl. D, 724 (2002).
5. De Baerdemaeker F., Simek M., Clupek M., Lukes P., Leys C.: Czech J. Phys. *56*, Suppl. B, 1132 (2006).
6. Lukes P., Clupek M., Babicky V., Janda V., Sunka P.: J. Phys. D: Appl. Phys. *38*, 409 (2005).
7. Locke B. R., Sato M., Sunka P., Hoffmann M., Chang J.: Ind. Eng. Chem. Res. *45*, 882 (2006).
8. Sunka P., Babicky V., Clupek M., Lukes P., Simek Schmidt J., Cernak M.: Plasma Sources Sci. Technol.

8, 258 (1999).
9. Lukes P.: *Ph.D. Thesis*, Institute of Plasma Physics, Prague 2001.
10. Bruggeman P., Leys C., Vierendeels J.: J. Phys. D: Appl. Phys. *40*, 1937 (2007).
11. Bruggeman P., Verreycken T., Gonzalez M. A., Walsh J. L., Kong M. G., Leys C., Schram D. C.: J. Phys. D: Appl. Phys. *43*, 124005 (2010).
12. Griem H. R.: *Spectral line broadening by plasma*. Academic Press, New York 1974.
13. Brablec A., Slavíček P., Sťahel P., Čižmár T., Trunec D., Šimor M., Černák M.: Czech. J. Phys. *52*, Suppl. D 491 (2002).
14. http://www.advex-instruments.cz/

G. Neagoe[a], O. Galmiz[a], A. Brablec[a], J. Ráhel[a,b], and A. Záhoranová[b] *([a] Dep. of Physical Electronics, Faculty of Science, Masaryk University, Brno, Czech Republic; [b] Dep. of Experimental Physics, Comenius University, Bratislava, Slovak Republic):* **Underwater Diaphragm Discharge, a new Technique for Polypropylene Textile Surface Modification**

Underwater single and double diaphragm discharge were used for surface modification of polypropylene nonwoven. The discharge was generated in distilled water. Optical Emission Spectroscopy (OES) was used to determine temperature and density of the plasma electrons. The total surface free energy (SFE) was determined from the measurements of the contact angles. It was found that the double diaphragm arrangement improved the uniformity and wettability of PP treatment.

Chem. Listy *106*, s1475−s1481 (2012) CEPLANT

STEEL SURFACE TREATMENT AND FOLLOWING AGING EFFECT AFTER COPLANAR BARRIER DISCHARGE PLASMA IN AIR, NITROGEN AND OXYGEN

VADYM PRYSIAZHNYI[a,*], JINDŘICH MATOUŠEK[b], MIRKO ČERNÁK[c]

[a] *Faculty of Science, Masaryk University, Kotlarska 2, 611 37 Brno, Czech Republic,* [b] *Department of Physics, Faculty of Science, J. E. Purkinje University, Ceske mladeze 8, 400 96 Usti nad Labem, Czech Republic,* [c] *Faculty of Mathematics, Physics and Informatics, Comenius University, Mlynská dolina, 842 48 Bratislava, Slovak Republic*
mr.vodik@gmail.com

Keywords: steel surface; air plasma treatment; DCSBD; aging effect; hydrophobic recovery.

1. Introduction

Non-thermal atmospheric plasma surface processing is a hot topic for applied research nowadays. Despite all the complications to fully understand the plasma chemistry, it is already used in many industrial applications. Main reasons are its benefits, such as environmentally friendly technology, low cost of maintenance, and easy implementation of plasma in production lines (compared with low-pressure plasma treatments). Due to the wide range of possibilities to change plasma chemistry (by adding gas mixtures, changing electrode geometry or discharge type), it attracts more attention for applications without high requirements for treatment on nanosize level, like adhesion improvement, increase quality of painting for automotive, construction or aerospace industries. Surface pre-treatment of steel for these kinds of applications is often required. From the variety of surface modifications of steel we are particularly interested in low-cost surface pre-treatment for painting/adhesion enhancement. Different pre-treatment methods were developed for surface modifications, such as sol-gel[1], electrochemical[2], laser[3] or surface coating by adhesive layer (e.g. chromization[4]).

Different plasma sources and approaches were used to study the effects of plasma pre-treatment of steel surface. Low-pressure plasma treatment for metal surface modifications was studied first[5]. It was typically used to implant additives in surface to modify material (nitriding of steel[6]) or to deposit a coating onto the surface (low-pressure polymerization[7]). Nowadays low-pressure treatment of steel is not considered for large scale metal industry because of its high maintenance costs.

Several atmospheric pressure plasma sources have been developed for surface modifications[8–10]. Plasma treatments using cheap gases (like air, nitrogen, argon or oxygen) are at high interest as they are economically beneficial[11]. The use of plasma jet systems for metal surface treatments was reported in several works[12,13]. For flat surface treatments the use of plasma jet has more complications, like insufficient homogeneity or long treatment duration.

Dielectric Barrier Discharge (DBD) plasma sources are proven to be efficient for flat surface pre-treatments[14]. There are many examples when DBD plasmas are used in surface treatment of textiles, plastics, wood and metals. An important issue of plasma pre-treatment, when no coating is deposited while plasma is in contact with surface, is its non-permanent character or so-called aging effect.

The typical parameter that can evaluate pre-treatment efficiency is surface wettability or its quantitative parameter, the surface free energy (SFE). In most cases the surface free energy is increasing as a result of the surface pre-treatments using atmospheric pressure plasmas[15]. Aging effect (or hydrophobic recovery) can be defined as a decrease of the SFE to lower values (not always original value before plasma treatment) after several hours or days[16]. As a consequence, the aging effect may play important role when a time delay between technological steps is necessary. The detailed study of aging effect was done for polymer surfaces, where it is an important technological issue[17,18]. But even though the presence of aging effect after plasma treatment of metal substrates was shown[19,20], this topic is still not clear enough.

Air humidity is another important parameter, which needs to be taken into account when ambient air plasma treatments are considered. When non-thermal (cold) plasmas at atmospheric pressure are used for the surface treatments, the humidity affects the chemical reactions in plasma volume[21]. The effect of humidity on plasma parameters for dielectric barrier discharges (DBDs) was studied and generation of $-NO_x$ radicals in plasma volume was measured and modeled theoretically[22,23]. However, we are not aware of any results explaining in more details the effect of humidity on the plasma treatment of steel.

This work describes the characteristics of common low-carbon steel after surface DBD plasma treatments, the increase of wettability after the plasma treatments and the explanation of the following aging effect of plasma treated steel surfaces. Plasma treatments were done using the Diffuse Coplanar Surface Barrier Discharge (DCSBD), which generates surface barrier discharge plasma with higher power density that conventional volume DBD plasma sources.

A detailed study of aging effect, i.e. decrease of the surface free energy while storing the plasma treated surfaces, and influence of humidity was performed by the surface free energy and X-ray photoelectron spectroscopy techniques.

2. Experimental

Steel samples were cut from steel sheets (1.0330 steel; 1 mm thick; Fe – max. 99.19 %, C – max. 0.12 %, P – max. 0.045 %, S – max. 0.045 %, Mn – max. 0.6 %). After cutting (for the surface free energy the samples had size 10 cm × 3 cm, for the X-ray photoelectron spectroscopy samples had size 1 cm × 1 cm), a two steps cleaning process was performed for all the samples. During the first step, chemical degreasing using dust-free tissue was done to remove metal dust particles or leftovers of grease. In the second step, the samples were cleaned in ultrasonic bath for 5 minutes in isopropanol; cleaned in ultrasonic bath for 5 minutes in acetone. Subsequently the samples were dried with flow of compressed air and stored at least one day in laboratory air before plasma treatments.

The Diffuse Coplanar Surface Barrier Discharge (DCSBD) source was used for steel surface treatments[24]. This plasma source is a type of surface barrier discharge. It allows generating highly non-equilibrium high-power density plasma in form of a thin planar layer with thickness of about 0.3−0.5 mm as it is shown in Fig. 1a. The coplanar electrodes were produced on the alumina ceramics that have size 26 cm × 9.3 cm. Silver metal electrodes were evaporated on the bottom side in etched channels 1.5 mm wide, with 1 mm distance in between them. The plasma was generated on 20 cm × 8 cm area, where thirty eight metal stripes were produced, as it is shown in Fig. 1b.

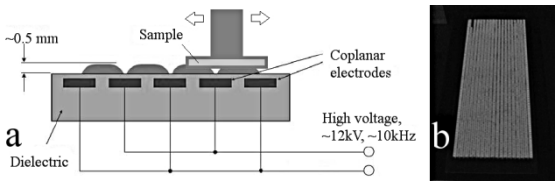

Fig. 1. **(a) Schema of DCSBD plasma source and (b) image of the discharge running in ambient air with exposition time 1/1000 s**

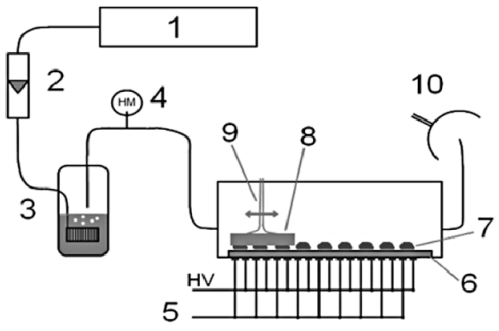

Fig. 2. **Schema of experimental setup.** 1 – air compressor, 2 – gas flow meter, 3 – bubbler, 4 – humidity meter, 5 – high voltage, 6 – Al_2O_3 ceramic, 7 – plasma layer, 8 – sample, 9 – movable sample holder, 10 – gas exhaust

Table I
Surface tension (σ_l) and its polar (σ_l^{polar}) and dispersive (σ_l^{disp}) part for test liquids used

	σ_l	σ_l^{polar}	σ_l^{disp}
Distilled water	72.6	21.6	51
DMSO	44	36	8
50% K_2CO_3 in water	103.8	34	69.8

The plasma surface modifications were performed at room temperature by moving the sample above the DCSBD electrode system with a constant speed. Dry, ambient and humid air, nitrogen and oxygen were used as a plasma gas. The humidity of air was set from less than 2 % RH to more than 90 % RH. The plasma treatment time was 5 s, 40 s and 100 s.

The distance between the sample and the DCSBD electrode was set to 0.35 mm. The applied power, which was measured by Energy Check 3000 from Voltcraft, was set to 340 W. This value corresponds to the power density of 1.9 W cm^{-2}. A schema of the experimental setup is shown in Fig. 2.

The wettability was estimated by measuring the surface free energy (SFE) of steel surface using sessile-drop method. The SFE measurements were performed by a Surface Energy Evaluation System (supplied from Advex Instruments, Czech Republic). This method requires to measure values of contact angles using a few test liquids with well-defined properties. For current measurements the volume of each drop was 2 μl and the average value of at least 6 droplets was calculated for each test liquid and for each sample. Distilled water, dimethyl sulfoxide (DMSO) and 50 % solution of K_2CO_3 in deionized water were used as test liquids. The total surface tension and its polar and dispersive parts for the different liquids are presented in Table I (ref.[25,26]). The Owens-Wendt regression model was used to calculate the surface free energy using measured values of contact angles[27].

The X-ray photoelectron spectroscopy (XPS) measurements were done to evaluate the changes in chemical composition and bond structure occurred on the steel surface after plasma treatments. The XPS measurements were performed using a spectrometer equipped with a hemispherical analyzer operated in FAT mode (Phoibos 100 from company Specs). The Al K_{alpha} X-ray source (1486.7 eV) was operated at 200 W. The survey spectra were recorded at pass energy 40 eV with an energy step of 0.5 eV, while the high-resolution XPS spectra at pass energy 10 eV with an energy step of 0.05 eV. All spectra were referenced to the peak of aliphatic C-C bond at 285 eV. A Shirley-type background was subtracted from all spectra prior to data processing. Binding energies and peak fitting routines were performed by CasaXPS software.

3. Results and discussion

3.1. Surface wettability

The results of the SFE measurements showed the significant increase of the surface free energy of treated steel surfaces compared to the untreated ones. One of the reasons for the increased wettability can be the change of the surface roughness. However, the results of AFM measurements that were done on the steel substrates didn't show changes in the surface morphology and estimated surface roughness was not altered after the plasma treatment (the peak-to-peak values of the steel surface substrates was approximately 2 μm on the areas without visible scratches for both untreated and treated samples). Therefore, the observed changes in the surface wettability are related to the changes in surface composition/surface chemical structure.

As an example, the increase of the surface free energy as a function of treatment duration in ambient air is shown in Fig. 3. In this and further figures with SFE measurements the total height of the bar stands for the value of the surface free energy (white part of bar corresponds to its dispersive component and grey part of bar corresponds to the polar component). The increase of the SFE is due to the increase of its polar component, as shown in Fig. 3. For such cases a generation of polar functional groups on the surface can be expected. Taking into account that the treatment was done in air, these functional groups might be the OH ones.

Aging effect of plasma treated steel surfaces was measured up to 7 days after the plasma treatments, showing a decrease of the surface wettability while storage. The results of the SFE measurements (plasma treatment time 40 s) in air after 1, 2, 3, 4 and 7 days of storage in ambient air are shown in Fig. 4. The hydrophobic recovery of the plasma treated steel surfaces was reaching the saturation after about 2 days of storage. The changes in ratio between polar and dispersive component immediately after the plasma treatment and after storage in air for two days for different plasma durations are presented in Fig. 5. Note the different character of aged surfaces treated in dry (Fig. 5a) and wet air (Fig. 5b). Polar component changes with increasing of the treatment time in an inverse way. In dry air, for longer treatment duration the polar component of the SFE was decreasing. In wet air, the value of polar component was growing for higher treatment durations. Proposed assumption about generated OH groups allows explaining measured data. Higher number of OH groups is conserved on the surface for the samples stored in wet air, because of water vapors presented in wet air. Also higher number of polar groups will remain on the surface after longer treatment, because higher number of groups was generated on steel surface by plasma. Smaller number of OH groups was conserved on the surface during storage in dry air.

To examine the aging effect, additional series of measurements were done for treated steel samples in ambient air, nitrogen and oxygen. After treatment the samples were stored in ambient air and vacuum. To ensure the aging process is finished it was decided to store samples for 4 days (see Fig. 4). The samples were stored in ambient air at room temperature with humidity ~40 % RH. Vacuum storage was done in the oil-free vacuum chamber with pressure about 10^{-3} Pa.

The results of these measurements are presented in Fig. 6, Fig. 7 and Fig. 8 for plasma treatment in air, nitrogen and oxygen, respectively. The following observations were found after these measurements.

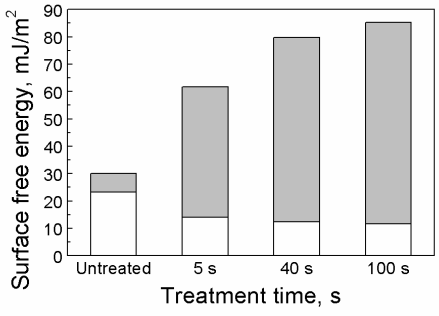

Fig. 3. **Change of the SFE for steel sheets (total bar height) after the air DCSBD plasma treatment.** Treatment conditions: ambient air, 40 s

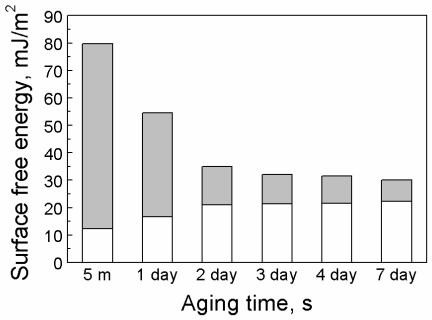

Fig. 4. **Aging effect of plasma treated steel sheets depending on a storage time in laboratory air.** Treatment conditions: ambient air, 40 s

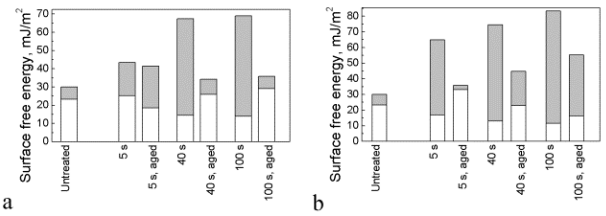

Fig. 5. **Changes in SFE depending on a treatment gas, treatment time and aging conditions. (a) plasma treatment in dry air, (b) plasma treatment in wet air.** Aging done in ambient air for 2 days

1) The values of the SFE are in the same range of 65–70 mJ m^{-2} for 5 s plasma treatments and 76–82 mJ m^{-2} for 40 s treatments.

2) The proportion of polar-to-dispersive component of the SFE measured on the plasma treated steel surfaces after the treatment in all gases are roughly the same.

3) The treatment in air and oxygen gave similar results, while the measurements on the samples treated in nitrogen show higher value of dispersive component for short treatment times of 5 s.

4) Based on the obtained data it can be assumed that the most important impact on the surface wettability has the post-treatment surface reactions.

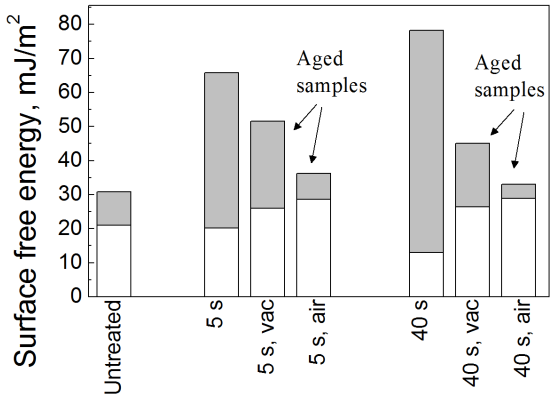

Fig. 6. **Changes of the SFE after air DCSBD treatment of steel surfaces with subsequent aging for 4 days in ambient air and vacuum**

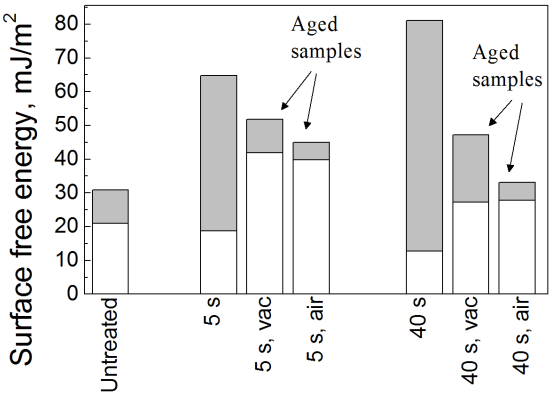

Fig. 7. **Changes of the SFE after nitrogen DCSBD treatment of steel surfaces with subsequent aging for 4 days in ambient air and vacuum**

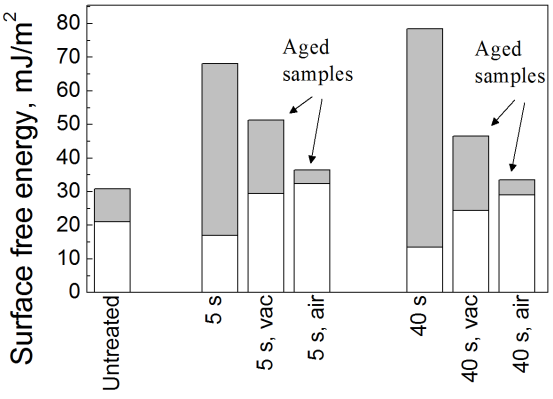

Fig. 8. **Changes of the SFE after oxygen DCSBD treatment of steel surfaces with subsequent aging for 4 days in ambient air and vacuum**

3.2. Surface chemical composition and bond structure

In our previous study[28] it was shown that more than 10 s treatment times is needed to obtain homogeneous treatment on aluminium. Therefore, most of the samples measured by the XPS technique were treated for 40 s. The surface composition depending on treatment conditions are presented in Tab. II. Note that the increase of iron and oxygen concentration is mostly due to reduction of carbon content after the plasma treatment.

As expected, the content of atomic iron was lowest for oxygen plasma treatment (highest oxidation is expected), followed by the air and nitrogen treatments.

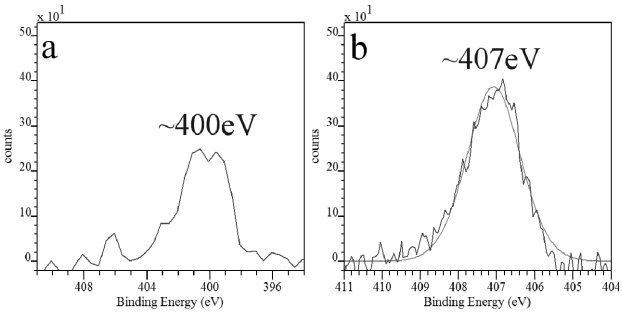

Fig. 9. **High-resolution N 1s peak on steel surface: a) weakly bonded nitrogen, plasma treatment in nitrogen for 40 s; b) nitrate group, plasma treatment in ambient air for 40 s**

Table II
Surface composition of steel samples after plasma treatment in various gases for 40 s

	Fe [at%]	O [at%]	C [at%]	N [at%]	Mn [at%]
Untreated	7	42	49	–	1
Dry air	16	63	16	3[a]	2
Ambient air	16	61	15	6[a]	4
Wet air	16	60	13	10[a]	1
Oxygen	10	60	25	2[b]	3
Nitrogen	22	61	11	2[b]	4

[a] Nitrate group, [b] weakly bonded nitrogen due to presence of residual air

The presence of N 1s peak in the XPS spectra measured on the plasma treated steel surfaces was evidenced. The content of atomic nitrogen was proportional to air humidity (see Tab. II). N 1s peak had two subcomponents at binding energies 400 eV and 407 eV. The first one (Fig. 9a) is corresponding to weakly bonded nitrogen[29] and was found on the steel substrate after nitrogen and oxygen plasma treatment. Most probably its presence is due to residual air of the plasma reactor. The second component (Fig. 9b) is corresponding to the nitrate ($–NO_x$) group. It was identified by the shift of binding energy[30] of the N1s peak to the value of 407 eV. The results allow us to assume that $–NO_x$ functional groups were generated on the steel surface during the humid air plasma treatment, which is in a good agreement with literature about air DBD plasma chemistry[31], where nitrate radicals are one of the intermediate products of complex series of chemical reactions.

The XPS measurements were performed on aged samples to determine the role of aging environment. The samples treated in ambient air, nitrogen and oxygen were stored for 4 days in (i) oil-free vacuum chamber, where the pressure was not exceeding $2 \cdot 10^{-5}$ Pa and (ii) ambient air. The changes in atomic composition after storage are shown in Table III, Table IV and Table V for DCSBD plasma treatments in ambient air, nitrogen and oxygen, respectively. The following observations were established:

1) Decrease of carbon content was measured for longer plasma treatment duration for treatments in air, nitrogen and oxygen. This proves the plasma treatment has the cleaning effect. Unlike for polymer surfaces, longer treatment duration is needed to obtain the cleaning effect after the DBD plasma (i.e. higher energy impact to unit surface). For instance, polymer surface oxidation can be achieved in fractions of a second.

2) Aging in air is leading to the highest re-adsorption rates of airborne hydrocarbon contaminants, while the situation is opposite for plasma treated samples after storage in vacuum.

3) The nitrate groups created after the plasma treatment in ambient air remain on the surface after storage in vacuum.

Table III
Surface composition of plasma treated steel in air and aged in different conditions for 4 days

	Fe [at%]	C [at%]	O [at%]	N [at%]	Mn [at%]
Untreated	7	49	42	–	1
5 s	9	23	58	5[a]	5
40 s	16	15	61	6[a]	3
aged, air	17	21	57	–	5
aged, vacuum	12	19	61	3[a]	5

[a] Nitrate group

Table IV
Surface composition of plasma treated steel in nitrogen and aged in different conditions for 4 days

	Fe [at%]	C [at%]	O [at%]	N [at%]	Mn [at%]
Untreated	7	49	42	–	1
5 s, N_2	15	27	54	2[b]	3
40 s, N_2	22	11	61	2[b]	4
aged, air	18	18	60	1[b]	3
aged, vacuum	22	16	59	1[b]	2

[b] Weakly bonded nitrogen due to presence of residual air

Table V
Surface composition of plasma treated steel in oxygen and aged in different conditions for 4 days

	Fe [at%]	C [at%]	O [at%]	N [at%]	Mn [at%]
Untreated	7	49	42	–	1
5 s, O_2	12	22	62	2[b]	2
40 s, O_2	10	22	63	2[b]	3
aged, air	21	18	59	–	3
aged, vacuum	12	21	63	2[b]	3

[b] Weakly bonded nitrogen due to presence of residual air

Table VI
Assignment of the Fe $2p_{3/2}$ peak components

Component	Binding energy [eV]	FWHM [eV]
Fe	707.0	2.0
FeO	709.6	2.2
FeOOH	711.8	3.4
Fe_2O_3	710.8	2.4

In order to study the changes in the bond structure, the high resolution Fe $2p_{3/2}$ peak was fitted by 4 components according to literature[32] (the Fe $2p_{3/2}$ spectra are not shown here). Component at 707.0 eV can be attributed to Fe in metallic state. This component decreased after all types of treatments while the increase of the oxygen containing groups bonded to Fe was observed after the plasma treatment.

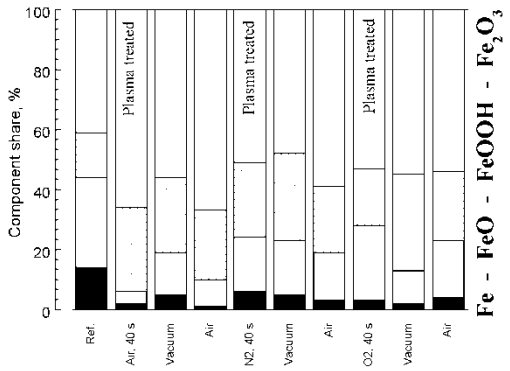

Fig. 10. **Ratio for Fe $2p_{3/2}$ components depending on plasma gas atmosphere and following aging in different environments after 4 days of storage**

The Fe $2p_{3/2}$ components and the probable chemical species related to them are listed in Tab. VI. Overall results for different treatment atmospheres and aging conditions are presented in Fig. 10. The x-axis should be understood as follows: "Ref." means untreated sample, bars marked "Plasma treated" represents the ratio of iron components after the plasma treatment, bars with mark "Vacuum" and "Air" represent the ratio of iron components for samples stored for 4 days in vacuum and air, respectively.

The increase of oxide (Fe_2O_3) and hydroxide (FeOOH) content after plasma treatment was observed for all treatment conditions. Also, independent on carbon content, the amount of atomic iron is lower for plasma treated samples. No obvious regularities between amount of FeOOH and surface wettability were found as opposed to plasma treated aluminium surfaces[33]. The increase of hydroxide component, though, shows that the assumption of generated OH groups was correct, but reduced wettability is due to hydrocarbon re-adsorption.

4. Conclusions

The effects of plasma gas (including air humidity) and aging environment on the coplanar barrier discharge plasma treatment of low-carbon steel surface was reported. The plasma treatment was done using the Diffuse Coplanar Surface Barrier Discharge (DCSBD) and resulted in significant increase of the surface free energy. For the typical plasma treatment conditions the surface free energy was growing from 29 mJ m^{-2} to over 75 mJ m^{-2}.

The aging effect of the plasma treatment was measured for storage in air and vacuum. The obtained results from the SFE measurements were explained using the results of XPS technique. It is apparent that plasma treatment leads to surface cleaning from hydrocarbon contaminants and generation of hydroxyl, nitrate and iron oxide. Changes in wettability can't be explained only by relative quantities of atomic carbon or iron hydroxides on the steel surface. Based on the measured results it is reasonable to suppose that both contaminants and ratio between oxide/ hydroxide components defines the surface wettability of steel. Generation of $-NO_x$ groups on steel surface after plasma treatment in humid air was shown. The nitrate surface groups are not stable in air and their stability is higher in vacuum.

This research has been supported by the project CZ.1.05/2.1.00/03.0086 'R&D center for low-cost plasma and nanotechnology surface modifications' funded by European Regional Development Fund, by the Grant Agency of the Academy of Sciences of the Czech Republic under contract KAN311610701 and by the Czech Science Foundation (Projects No. 104/08/0229 and 202/09/2064).

REFERENCES

1. Metroke T. L., Parkhill R. L., Knobbe E. T.: Prog. Org. Coat. *41*, 233 (2001).
2. Jegannathan S., Sankara Narayanan T. S. N., Ravichandran K., Rajeswari S.: Surf. Coat. Technol. *200*, 4117 (2006).
3. Pereira A., Cros A., Delaporte P., Marine W., Sentis M.: Appl. Surf. Sci. *208–209*, 417 (2003).
4. Wang Z. B., Lu J., Lu K.: Acta Mater. *53*, 2081 (2005).
5. Sapieha S., Cerny J., Klemberg-Sapieha J. E., Martinu L.: J. Adhesion *42*, 91 (1993).
6. Liang W.: Appl. Surf. Sci. *211*, 308 (2003).
7. Yasuda H., Matsuzawa Y.: Plasma Process. Polym. *2*, 507 (2005).
8. Plasma Treat Open Air. http://www.plasmatreat.com/plasma-technology/openair-atmospheric-plasma-technique.html (7.12.2012).
9. PlasmaSpot. http://www.vitoplasma.com/en/30 (7.12.2012).
10. Corotec Corporation. http://corotec.com/products/plasmajet-specs.html (7.12.2012).
11. Roth J. R.: *Industrial Plasma Engineering: Principles*. Taylor & Francis, University of Tennessee, Knoxville, USA, 1995.
12. Kim M. C., Song D. K., Shin H. S., Baeg S.-H., Kim G. S., Boo J.-H., Han J. G., Yang S. H.: Surf. Coat. Technol. *171*, 312 (2003).
13. Tang S., Kwon O.-J., Lu N., Choi H.-S.: Surf. Coat. Technol. *195*, 298 (2005).
14. Goossens O., Dekempeneer E., Vangeneugden D., Van de Leest R., Leys C.: Surf. Coat. Technol. *142–144*, 474 (2001).
15. Mantel M., Wightman J. P.: Surf. Interface Anal. *21*, 595 (1994).
16. Roth J. R., Chen Z. Y.: Acta Metal. Sin. *14*, 391 (2001).
17. Morent R., De Geyter N., Leys C., Gengembre L., Payen E.: Surf. Coat. Technol. *201*, 7847 (2007).
18. O'Connell C., Sherlock R., Ball M. D., Aszalos-Kiss

B., Prendergast U., Glynn T. J.: Appl. Surf. Sci. *255*, 4405 (2009).
19. Kim M. C., Yang S. H., Boo J.-H., Han J. G.: Surf. Coat. Technol. *174–175*, 839 (2003).
20. Shin D. H., Bang C. U., Kim J. H., Hong Y. C., Uhm H. S., Park D. K., Kim K. H.: IEEE Trans. Plasma Sci. *34*, 1241 (2006).
21. Benstaali B., Boubert P., Cheron B. G., Addou A., Brisset J. L.: Plasma Chem. Plasma Process. *22*, 553 (2002).
22. Tochikubo F., Uchida S., Yasui H., Sato K.: Jpn. J. Appl. Phys. *48*, 076507 (2009).
23. Iskenderova K., Chirokov A., Gutsol A., Fridman A., Kennedy L., Sieber K. D., Grace J. M., Robinson K. S.: *15th International Symposium on Plasma Chemistry, Orléans, France, 9–13 July 2001*. Symposium Proceedings II, 443.
24. Černák M., Černáková L'., Hudec I., Kováčik D., Zahoranová A.: Eur. Phys. J. Appl. Phys. *47*, 22806 (2009).
25. Kwok D. Y., Neumann A. W.: Adv. Colloid Interface Sci. *81*, 167 (1999).
26. *Potassium Carbonate Handbook, Technical Data for Potassium Carbonate*, Armand Products, Table 10, www.armandproducts.com/pdfs/k2so3P33_46.pdf.
27. Rudawska A., Jacniacka E.: Int. J. Adhes. Adhes. *29*, 451 (2009).
28. Prysiazhnyi V., Vasina P., Panyala N. R., Havel J., Cernak M.: Surf. Coat. Technol. *206*, 3011 (2012).
29. Gredelj S., Gerson A. R., Kumaring S., Cavallaro G. P.: Appl. Surf. Sci. *174*, 240 (2001).
30. *NIST X-ray Photoelectron Spectroscopy Database*, *Version 3.5*. National Institute of Standards and Technology, Gaithersburg, 2003, http://srdata.nist.gov/xps/.
31. Herron J. T., Green D. S.: Plasma Chem. Plasma Process. *21*, 459 (2001).
32. Yamashita T., Hayes P.: Appl. Surf. Sci. *254*, 2441 (2008).
33. Prysiazhnyi V., Zaporojchenko V., Kersten H., Černák M.: Appl. Surf. Sci. *258*, 5467 (2012).

V. Prysiazhny[a], J. Matoušek[b], and M. Černák[c]
([a] Faculty of Science, Masaryk University, Brno, Czech Republic, [b] Department of Physics, Faculty of Science, J. E. Purkinje University, Usti nad Labem, Czech Republic, [c] Faculty of Mathematics, Physics and Informatics, Comenius University, Bratislava, Slovak Republic): **Steel Surface Treatment and Following Aging Effect after Coplanar Barrier Discharge Plasma in Air, Nitrogen and Oxygen**

The results on plasma treatment of low-carbon steel sheets by Diffuse Coplanar Surface Barrier Discharge are reported. Significant increase of the surface free energy from 29 mJ m^{-2} to over 75 mJ m^{-2} after the plasma treatment was observed. A detailed X-ray photoelectron spectroscopy study was performed to understand the reasons for increased wettability as well as following hydrophobic recovery. Based on the obtained results it was found that the aging effect is related to the transformation in the bond structure between Fe, O and OH and re-adsorption of hydrocarbon contaminants from air. The presence of surface nitrate groups was measured after the treatments in humid air plasma as well.

MODELLING OF REACTIVE MAGNETRON SPUTTERING WITH FOCUS ON CHANGES IN TARGET UTILIZATION

TEREZA SCHMIDTOVÁ*, PETR VAŠINA

Deartment of Physical Electronics, Faculty of Science, Masaryk University, Kotlářská 2, 611 37 Brno, Czech Republic
dorain@physics.muni.cz

Keywords: reactive magnetron sputtering, modelling, target utilization

1. Introduction

The deposition of thin films by reactive magnetron sputtering is frequently used in many industrial applications. For growing of oxides or nitride thin films reactive gases are commonly added to the deposition chamber. To set the desired experimental conditions for the deposition process, it is natural to adjust the reactive gas flow rather than the partial pressure of the reactive gas. It is simpler and easier to perform, however, the process controlled by the supply flow of the reactive gas exhibits undesirable hysteresis behaviour.

The reactive gas added to the deposition chamber causes the forming of the compound molecules on the target surface which are being removed by the sputtering. The local composition of the target results from the balance between the creation and the destruction of the compound molecules. These processes are sometimes in a simplified way referred to as the target poisoning and the target cleaning. The origin of the hysteresis behaviour lies in the difference in the sputtering yield of metal atom from the clean and from the compound part of the cathode surface[1]. If the reactive gas supply flow is low, the resulting fraction of the compound molecules on the target surface is low, too. The process runs in the so-called metallic mode. If the reactive gas supply flow is increased up to a certain value, the newly generated conditions force the partial pressure of the reactive gas to increase often very dramatically. The process conditions are changed and the transition from the metallic to the compound mode occurs[2–4]. In order to acquire the reverse decrease of the partial pressure of the reactive gas it is necessary to substantially decrease the reactive gas supply flow.

In the magnetron configuration, the presence of the magnetic field causes a formation of a high density plasma in a shape of a toroid in front of the magnetron target and thus the sputtering of the target is very non-uniform[5–8]. Although it would be highly desirable to utilize the target material completely, due to the non-uniformity of the discharge current density, it is infeasible. The scale coefficient of the target usage by sputtering is a factor of the target utilization. The target utilization is a relative quantity proportional to the amount of the target material that is sputtered under certain conditions during the deposition. In practic, the target utilization is determined by the relative change in the weight of the target after it becomes depleted at the racetrack part of the target by sputtering. Nowadays, target manufacturers can reshape the targets to increase the target utilization simply by adding more material to the racetrack area.

In the case of the sputtering in the non-reactive atmosphere, the target erosion profile copies the profile of the discharge current density over the target area. Therefore, also by reshaping of the magnetic field structure over the target a higher target utilization can be achieved. At present, a wide range of magnetic field configurations exits on the market. Standard configurations are two pole magnetics with the target utilization approximately 30 %, but above standard multi pole magnetics that deform and flatten the structure of the magnetic field over the target area that gives the target utilization approximately 60 % can be found. By an increase of the target utilization, the cost of the target material for deposition of the thin film can be reduced. In the case of precious metals a considerable saving can be made.

If a reactive gas is added into the sputtering process, the conditions in the whole deposition chamber including the target surface change. Simultaneous poisoning and cleaning of the target causes the compound fraction in the target parts with lower discharge current density to be higher than in the racetrack part which is sputtered more intensively. The target composition is becoming non-uniform and due to the difference between sputtering yields of the metal atoms from the clean parts of the target and from the parts covered by the compound, the sputtering rate of the target is changing, too. It can be expected that the target utilization at different conditions during the reactive sputtering deposition process can be at least slightly reduced compared to the situation without any presence of the reactive gas. The goal of this paper is to predict the scale of these changes in the target utilization during the evolution of the reactive sputtering deposition process. Particularly, the role of the profile of the discharge current density on the changes of the target utilization during the reactive magnetron sputtering is studied.

2. Model specifications

The reactive magnetron sputtering process is usually simulated by models based on the well known Berg model[9–11] which is a parametric model describing the behaviour of the sputtering process. It has been used to state

very interesting predictions and to explain some non-trivial observations. Just to mention the most recent research; for example it states that the hysteresis can be reduced or even eliminated not only by an increase of the pumping speed[12–14] but also by a reduction of the target erosion zone[15], the model was also used to predict the temporal evolution of reactive magnetron sputtering[16], etc. The original Berg model and its successors assume the uniform discharge current density and consequently, they cannot predict the target utilization. Assuming the uniform discharge current density, the target utilization is always independent of the experimental conditions. Recently, we intentionally extended on Berg model in order to accommodate the non-uniform discharge current density[17]. Therefore it allows the investigation of the reactive sputtering of targets exposed to different discharge current density profiles at different process conditions. For purposes of this paper two Gaussian profiles of the discharge current density are closely studied (see Fig. 1). Both show the maximum value at the half radius of the target and values of FWHM are 0.02 m and 0.04 m, which correspond to the target utilization in pure metallic mode (i.e. without any presence of the reactive gas in the deposition chamber) of 30 % and 60 %, respectively.

The process conditions that are studied in details are represented by the points of interest during the evolution of the sputtering process, see Fig. 2. Point A is the situation without any reactive gas and it is denoted as the pure metallic mode, point B is set at 1 sccm of the reactive gas to represent the metallic mode, the moment just before the transition between metallic and compound mode (M-C transition) corresponds to point C, point D is the situation just after the metallic to compound mode transition and point E is chosen at 4.5 sccm of the reactive gas to represent the compound mode. Note that points A, B and E are fixed on the flow of the reactive gas but points C and D are

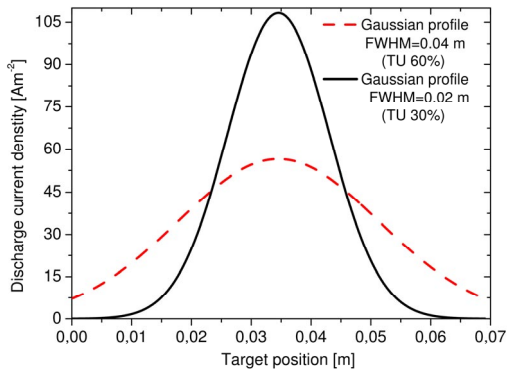

Fig. 1. **Two Gaussian profiles of the discharge current density over the target radius.** The maximum is placed at half radius of the target and the FWHMs are 0.02 m and 0.04 m. Corresponding target utilizations in pure metallic mode are 30 % and 60 %, respectively

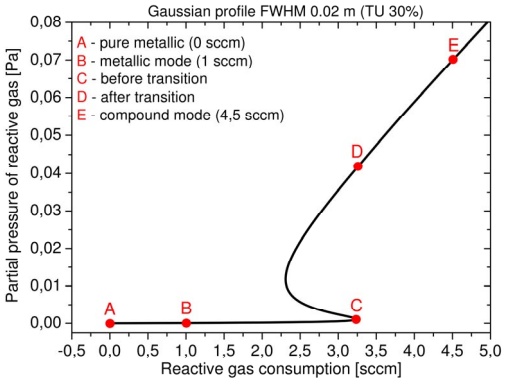

Fig. 2. **Declaration of the points of interests in the plot of the partial pressure of the reactive gas as a function of the reactive gas supply flow for the profile with FWHM = 0.02 m**

variable depending on the moment of the transition, which occurs for the different profiles of the discharge current density at different reactive gas supplies.

3. Results and discussion

3.1. Modelling of the lateral target composition

Modelled lateral variations of the compound fraction at the target for two studied Gaussian discharge current density profiles are shown in Fig. 3. The edges of the target and its centre are parts which are least sputtered and therefore the compound fraction in these areas is very high even for relatively low supply flow of the reactive gas. Different situation occurs at parts with higher values of the discharge current density; those parts of the target are sputtered more effectively so the metal composition of the target is mostly preserved. These target parts are generally called the target racetrack. In the metallic mode, the compound fraction at the racetrack area is very low for both discharge current density profiles – bellow 5 %. The most remarkable change of the target composition takes place during the M-C transition. The compound fraction at the centre of the racetrack is increased dramatically by the M-C transition - for the profile with FWHM 0.02 m by almost 4.5 times and for the profile with FWHM 0.04 m by 3.5 times.

Note that the discharge current density profile is always assumed to be the same in the model, independent of the reactive gas supply flow. Therefore the key variable determining the erosion profile of the target and consequently the target utilization is the profile of the target composition. The relatively flat profile of the compound fraction in the most sputtered area of the target – such as that corresponding to the metallic mode in Fig. 3 – indicates that the target erosion profile and thus the target utili-

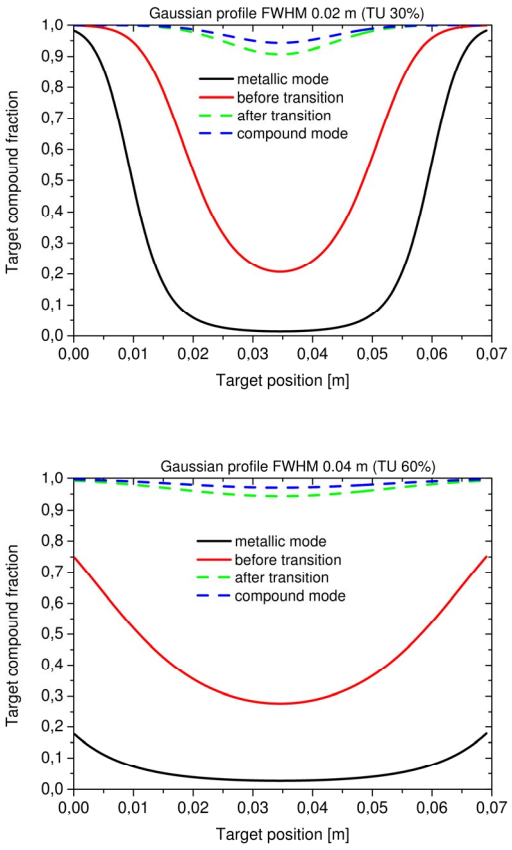

Fig. 3. **Dependency of the compound fraction over the target radius.** Upper and lower graphs correspond to Gaussian profiles of discharge current density with FWHM equal to 0.02 m and 0.04 m, respectively

zation in metallic mode should be only very slightly different from that in the pure metallic mode.

3.2. Modelling of the racetrack shape at different conditions

The target erosion rate can be computed taking into account simultaneously the discharge current density profile and the evolution of the target composition over the target position. The computed target erosion rate was normalized to reach 1 in the most sputtered area of the target in order to compare the racetrack shapes at different process conditions (points B, C, D and E). Moreover, this normalization enables us to visualize the shape of the originally flat target just at the moment when it gets depleted by the sputtering in its racetrack part. Modelled racetrack shape is plotted in Fig. 4. The target utilization can be deduced from modelled racetrack shape of the target.

Fig. 4 shows that the highest target utilization corresponds to the situation when no reactive gas is introduced into the deposition chamber. In that case, the racetrack profile corresponds to the profile of the discharge current density. For a reactive gas introduced into the deposition chamber, the radial evolution of the target composition intervenes in the computation of the racetrack profile.

Different compound fractions of the target are reached for different situations during the sputtering process (see Fig. 3) and the target get sputtered differently too, see Fig. 4. By an increase of the reactive gas supply in the deposition chamber, the target gets progressively covered by the compound mainly in the central parts of the target and at the edges. Since the forming compound is hard to sputter, the profile of the racetrack shrinks. Increasing the reactive gas supply further to higher values, the compound fraction increases even at the racetrack part of the target and the racetrack profile shrinks even more.

For both Gaussian discharge current density profiles, the target utilization is the lowest for the situation shortly before the M-C transition. When the system undergoes the M-C transition, the partial pressure of the reactive gas increases, the target gets almost fully covered by the compound. Although the target erosion rate is lower after M-C transition; resulting profile of the racetrack after the transition is broader than before the transition. For extremely high supplies of the reactive gas, the target is almost fully covered by the compound and the profile of the racetrack is almost identical to the profile of the discharge current density. In that case the target utilization reaches the value corresponding to the pure metallic mode.

For better visualization of the racetrack changes and therefore the changes in the target utilization during the sputtering process evolution, the ratio of the target erosion rates is plotted in Fig. 5 for the Gaussian profile with FWHM = 0.02 m. Values of the target erosion ratio give information on how many times more or less the target is sputtered in the specific position at the target compared to the sputtering in the reference situation. After the addition of the reactive gas, the centre of the target and its edges are

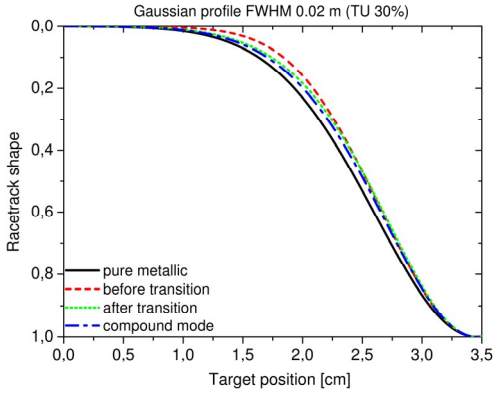

Fig. 4. M**odelled shape of the racetrack in the metallic mode (B), before (C) and after M-C transition (D) and in the compound mode (E).** Upper and lower graphs correspond to Gaussian discharge current density profile with FWHM = 0.02 m and 0.04 m, respectively

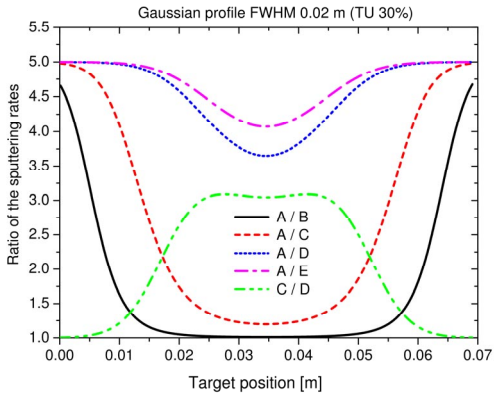

Fig. 5. **Ratio of the target erosion rates at different conditions computed for the Gaussian profile of the discharge current density with FWHM = 0.02 m**

always sputtered 5 times less compared to the pure metallic mode (A) but the racetrack exposed to the relatively high discharge current is sputtered differently depending on the conditions in the reactor. The factor 5 comes from the ratio between the sputtering yield of the metal atom from the clean and from the compound part of the target.

However, more interesting information about the target utilization is provided by the shapes of the ratio plots rather than the absolute values. It is the flatness and the curvature of the plot that is very important for the changes in the target utilization at different process conditions in the reactor. If the ratio of the target erosion rates for two different situations is very flat in the area exposed to a relatively high discharge current density, it means that the target erosion shape is mainly preserved and the target utilization is kept almost the same. This is the case of the ratio plot corresponding to the situation before and after the M-C transition (C/D) for the Gaussian profile with FWHM = 0.02 m in Fig. 5. In this case, the ratio in the racetrack area is around 3, which means that the target material is approximately 3 times less removed from the racetrack than its outer parts from the target centre. But the flatness of the ratio plot indicates that the ratio is the same in the important part of the target. It means that despite the fact that the target at condition corresponding to the point D is depleting about 3 times longer than at the conditions corresponding to the point C; the amount of the target material removed from the target after being depleted at the racetrack is finally approximately the same.

We can conclude that although almost all process parameters change drastically by the transition, the target utilization is not significantly influenced by the transition. In Fig. 5, parts of the curves with high slope point out places where the target erosion rate is changing the most. The continuous compound forming by the reactive gas flow onto the target and its counter effect the continuous sputtering are simultaneous processes resulting in a laterally non-uniform target composition. The progressive shrinking of the racetrack profile with added reactive gas can be well observed from the curved corresponding to A/B and A/C curves in Fig. 5.

3.3. Evolution of the target utilization for different discharge current density profiles

Two particular Gaussian discharge current density profiles with FWHM = 0.02 m and with FWHM = 0.04 m corresponding to the target utilization 30 % and 60 % in the pure metallic mode (point A) were investigated.

Let us investigate the changes in the target utilization in the situation shortly before and shortly after the metallic to compound mode transition as a function of the target utilization magnitude in the pure metallic mode. To quantify the changes in target utilization the Gaussian discharge current density profiles with various target utilization varying from 15 % up to 75 % were modelled by changing the FWHM of Gaussian profile. The changes in the target utilization are expressed as the relative proportion of the target utilization in the studied situation (C and D) to the target utilization in the pure metallic mode (A) for the same discharge current density profile. The ratio of the target utilization in the situation C and D is plotted, too. The results are shown in Fig. 6.

Comparing the situation before the M-C transition with the pure metallic mode the difference in TU is around 8 % independent on the discharge current density profile. If the target is sputtered more economically – in other words by a very broad profile of the discharge current density (TU in the pure metallic mode 50 % or higher) – the changes in the target utilization between the pure metallic mode (A) and the situation after the M-C transition (D) are low, around 5 %. For less economical sputtering by a very sharp and narrow profile of the discharge current density (TU in the pure metallic mode below 30 %) the changes in the target utilization can reach almost 8 %.

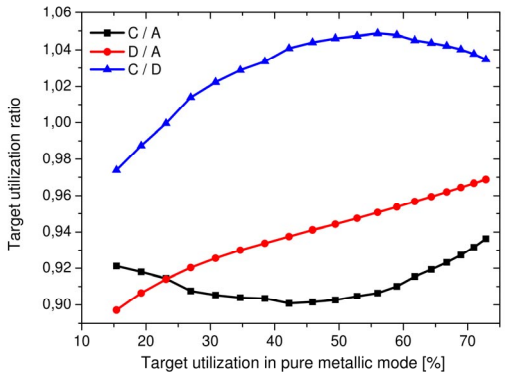

Fig. 6. **The relative proportion of the target utilization in the studied situation (C and D) to the target utilization in the pure metallic mode (A) for various Gaussian discharge current density profiles.** The ratio corresponding to the situation C and D is plotted, too

Comparing the ratio for the situations shortly before and shortly after the M-C transition, it is clear that the transition does not cause any abrupt change in the target utilization. It affects the target utilization maximally by 4 %. Note that the target utilization after the M-C transition is greater than before the transition for all the discharge current density profiles used in practise (those giving the target utilization in the pure metallic mode at least 25 %). Only for very sharp discharge current density profiles, the racetrack shrinking continues even by the transition.

Designed magnetron sputtering source used in practice should have the target utilization in pure metallic mode at least 30–40 %.

4. Conclusion

Changes in the target utilization during the evolution of the magnetron sputtering deposition process were modelled using the extended model of the reactive magnetron sputtering assuming Gaussian discharge current density profiles. The model is a natural extension of the well known Berg model that presumes a uniform discharge current density over the whole target and thus it is not suitable for the investigation of the target utilization.

The role of the target poisoning on the lateral evolution of the target composition and the changes in the racetrack shape with increasing amount of the reactive gas were discussed particularly for two different profiles of the discharge current density. These profiles were chosen to represent the typical magnetic field configuration available on the market – two pole magnetics with target utilization in the pure metallic mode around 30 % and well designed multi pole magnetics that deform and flatten the structure of the magnetic field over the target area to reach the target utilization of 60 %. For both studied profiles, the parts of the target sputtered by low discharge current density are poisoned even for relatively low reactive gas supply flow while the racetrack subjected to high discharge current density is cleaned more effectively by sputtering.

Consequently, the relatively low compound fraction is preserved at the racetrack even for the supplies of the reactive gas close to the supply corresponding to the M-C mode transition. The target poisoning and the target cleaning are continuous and simultaneous processes. The target utilization and the shape of the racetrack for different conditions during the sputtering are modelled and the effect of racetrack shrinking is reported. Shortly before the M-C mode transition the relative compound fraction in the racetrack starts to grow. However, although almost all process parameters change drastically by the M-C transition, the target utilization is not significantly influenced.

To quantify the changes in target utilization for broader range of current density profiles, the Gaussian discharge current density profiles with various target utilization in pure metallic mode varying from 15 % up to 75 % were modelled by changing the FWHM of the Gaussian profile. For the set of the standard input parameters, the differences of the target utilization in the situation shortly before the M-C transition from the pure metallic mode of about 8 % profile were found. This value has been found to be almost independent on the discharge current density profile.

For all studied profiles, the influence of the transition on the target utilization is relatively low – about 4 % – compared to other quantities changing by the transition. Despite that the erosion rate of the target is lower after M-C transition, the resulting profile of the racetracks after the transition is broader than before the transition and consequently the target utilization increases by the transition, too. It could seem surprising that the racetrack does not shrink any more by the transition but it gets broader not realizing that by the transition, the racetrack gets almost fully and equally covered by the compound.

This research has been supported by GACR contracts 104/09/H080, 205/12/0407 and R\&D center project for low-cost plasma and nanotechnology surface modifications CZ.1.05/2.1.00/03.0086 funded by European Regional Development Fund.

REFERENCES

1. Ranjan R., Allain J. P., Hendricks M. R., Rujic D. N.: J. Vac. Sci. Technol. A *19*, 1004 (2001).
2. Tsiogas C. D., Avaritsiotis J. N.: J. Appl. Phys. *71*, 5173 (1992).
3. McMahon R., Affinito J., Parsons R. R.: J. Vac. Sci. Technol. *20*, 376 (1982).
4. Safi I.: Surf. Coat. Technol. *127*, 203 (2000).
5. Schiller S., Heisig U., Goedicke K., Schade K., Teschner G., Hennenberg J.: Thin Solid Films *64*, 455 (1979).
6. Guttler D., Grotzschel R., Moller W.: Appl. Phys. Lett. *90*, 3502 (2007).
7. Moller W., Guttler D.: J. Appl. Phys. *102*, 094501 (2007).
8. Guttler D., Moller W.: Plasma Sources Sci. Technol. *17*, 025016 (2007).
9. Berg S., Blom H.O., Larsson T., Nender C.: J. Vac. Sci. Technol. A *5*, 202 (1987).
10. Berg S., Larsson T., Blom H. O., Nender C.: J. Appl. Phys. *63*, 4267 (1988).
11. Berg S., Nyberg T.: Thin Solid Films *476*, 215 (2005).
12. Larsson T., Blom H.O., Nender C., Berg S.: J. Vac. Sci. Technol. A *6*, 1832 (1988).
13. Kadlec S., Musil J., Vyskocil H.: J. Phys. D: Appl. Phys. *19*, L187 (1986).
14. Musil J., Kadlec S., Vyskocil J., Poulek V.: Surf. Coat. Technol. *39/40*, 301 (1989).
15. Nyberg T., Berg S., Helmersson U., Hartig K.: Appl. Phys. Lett. *86*, 164106 (2005).
16. Kubart T., Kappertz D., Nyberg T., Berg S.: Thin Solid Films *515*, 421 (2006).
17. Vasina P., Hytkova T., Elias M.: Plasma Sources Sci. Technol. *18*, 025011 (2009).

T. Schmidtová and P. Vašina *(Dep. of Physical Electronics, Faculty of Science, Masaryk University, Brno, Czech Republic):* **Modelling of Reactive Magnetron Sputtering with Focus on Changes in Target Utilization**

Target utilization is a parameter determining the usage of the target material for sputtering deposition. It is defined by the relative change in the weight of the target after it becomes depleted at the racetrack by the sputtering. In the case of the sputtering in the non-reactive atmosphere, the target erosion profile copies the profile of the discharge current density. Adding reactive gas into the deposition chamber the target utilization results simultaneously from the discharge current density profile and from the evolution of the target composition. A modified Berg model is used to determine the target utilization during the evolution of the reactive magnetron sputtering deposition process. The shrinking followed by the broadening of the racetrack is reported as the flow of the reactive gas is increased. We quantify these changes in the racetrack profile and the target utilization and we propose a physical interpretation.

ACTIVATION OF SILICON SURFACE IN ATMOSPHERIC OXYGEN PLASMA

DANA SKÁCELOVÁ, PAVEL SŤAHEL, MIRKO ČERNÁK

Department of Physical Electronics, Faculty of Science, Masaryk University, Kotlářská 2, 611 37 Brno, Czech Republic
danka@physics.muni.cz

Keywords: DCSBD, Si wafer, activation, oxygen plasma

1. Introduction

Surface pre-treatment of silicon is a very important process in semiconductor industry. The final properties and utilization of silicon wafers greatly depend on the initial surface conditions[1].

Simple plasma treatment could replace a demanding chemical bath. Various methods, such as Chemical vapor deposition (CVD) or Plasma-enhanced chemical vapor deposition (PECVD)[2] are widely used at present. Nevertheless, the atmospheric pressure plasmas, such as plasma jets[3,4], tend to be appealing in the semiconductor device fabrication.

The aim of this study is to investigate a new technology for plasma treatment of silicon wafer surface. Crystalline silicon surface was treated in Diffuse Coplanar Surface Barrier Discharge (DCSBD) which represents applicable plasma source operating in various gases.

By means of contact angle measurement the modification of c-Si wafers surface with orientation (111) or (100) in oxygen plasma was investigated. Additionally, the effect of orientation and different pre-cleaning procedure were investigated.

2. Experimental setup

Plasma treatment was realized by dielectric barrier discharge in coplanar arrangement, the so-called DCSBD[5–8].

This type of discharge is characterized by the large area of thin layer of atmospheric non – isothermal low temperature plasma on the surface of Al_2O_3 ceramic barrier with embedded metallic electrodes. This geometry ensures the pure plasma without any contaminations from electrodes.

Silicon samples were placed on a movable holder in the discharge chamber in oxygen atmosphere. The discharge chamber was blowen through by oxygen with flow $Q[O_2] = 6$ L min^{-1}.

As a substrate polished n – type, doped with phosphorous, Si (111) having resistivity (33–45)·10^{-3} Ω cm and polished n – type, doped with antimony Si (100) having resistivity (5–18)·10^{-3} Ω cm purchased from ON Semiconductor, Czech Republic,s.r.o. were used.

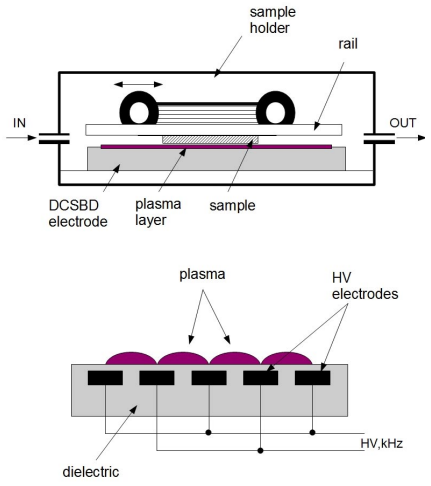

Fig. 1. **Experimental apparatus of DCSBD and the cross section of the electrode**

Before plasma treatment two different cleaning methods were used. The group of samples was cleaned by isopropyl alcohol and cyclohexan (1:1), native oxide layer was retained. Another group of samples was additionally immersed in 1% HF solution for 45 s at the room temperature to remove native oxide layer.

Immediately after cleaning the samples were treated in plasma for 5 s at 350 W.

Contact angle measurements were realized by Surface Energy Evaluation System (SEE System)[9]. Surface free energy γ^{TOT} was calculated by Acid – base model. Water, glycerol and diiodomethane were used as the measuring liquids.

3. Results

The properties of silicon surface before plasma treatment and after plasma treatment are summarized in Tab. I and Tab. II. It is evident that before plasma treatment the water contact angle (WCA) strongly depends on the cleaning procedure and crystallographic orientation of silicon. Etching in HF solution makes the surface more hydrophobic due to H terminating of dangling bonds.

However, after plasma treatment WCA markedly decreased to less than 5° independently on the orientation

Table I
Surface properties of the silicon samples before plasma treatment

	WCA	γ^{TOT}	γ^{LW}	γ^{AB}
(100) IPA cleaned	38.6	56.7	41.0	15.5
(100) HF etched	84.6	48.8	47.9	0.9
(111) IPA cleaned	38.7	53.8	36.3	17.5
(111) HF etched	65.6	52.3	45.9	6.4

and cleaning process. The improving of wettability after plasma treatment is caused by creating hydroxyl OH groups on the surface, which are responsible for hydrophilic properties of silicon[10]. This fact was successfully confirmed due to increasing of acid-base component γ^{AB} of surface free energy in case of all investigated samples (Tab. II).

Table II
Surface properties of the silicon samples after plasma treatment

	WCA	γ^{TOT}	γ^{LW}	γ^{AB}
(100) IPA cleaned	4.5	60.4	42.5	17.8
(100) HF etched	3.5	62.5	42.7	19.7
(111) IPA cleaned	5.6	61.5	42.7	18.8
(111) HF etched	4.0	61.8	42.5	19.4

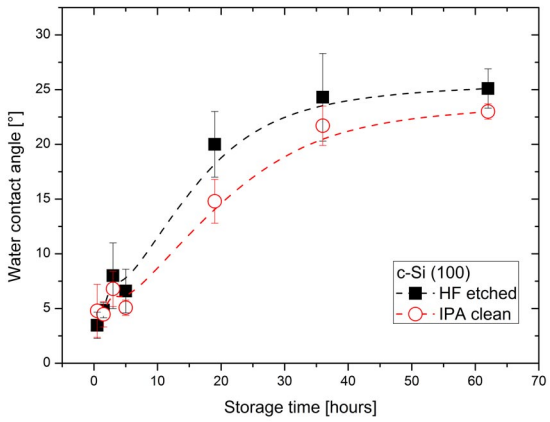

Fig. 2. **Ageing effect of treated c-Si (100)**

Moreover, the ageing effect of oxygen plasma modification was investigated. Fig. 2 and Fig. 3 show the change of water contact angle for (100) and (111) oriented plasma treated c-Si samples during exposure to ambient condition. In principle, within about one day the water

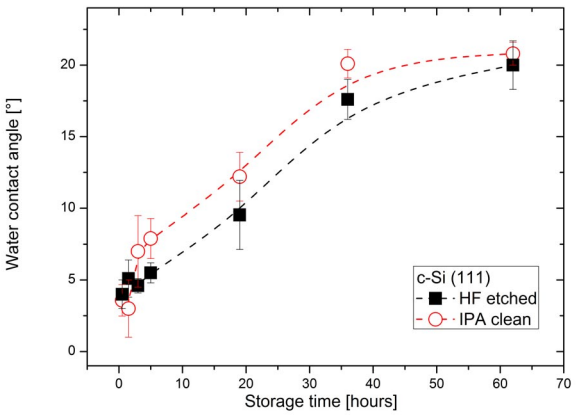

Fig. 3. **Ageing effect of treated c-Si (111)**

contact angle achieved the value that changed further slightly. All samples tend to achieve almost the same constant value of WCA within 40 hours. This phenomenon is caused by the loss of OH groups on the surface and adsorption of contamination from air.

5. Conclusion

In the current work, the modification of silicon surface wafer in oxygen atmospheric plasma was studied. DCSBD was used to plasma modification of crystalline silicon samples in orientation (111) and (100) and different pre-cleaning process. Furthermore, the ageing effect of plasma treated samples was studied.

Contact angle measurement proved the appreciable improving of wettability after plasma treatment independent on crystallographic orientation of cleaning process.

This research has been supported by the project R&D center for low-cost plasma and nanotechnology surface modifications CZ.1.05/2.1.00/03.0086 funded by European Regional Development Fund.

REFERENCES

1. Siffert P., Krimmel E. : *Silicon: evolution and future of a technology*. Springer-Verlag, Berlin 2004.
2. Rossnagel S. M., Westwood, W. D., Cuomo J. J.: *Handbook of Plasma Processing Technology: Fundamental, Etching, Deposition and Surface Interactions*. Noyes Publication, New York 1989.
3. Habib S. B., Gonzales E., Hicks R. F.: J. Vac. Sci. Technol. *A 28*, 476 (2010).
4. Dani I., Mäder G., Grabau P., Dresler B., Linaschke D., Lopey E., Kaskel S., Beyer E. : Contrib. Plasma Phys. *49*, 662 (2009).
5. Šimor M., Ráhel´ J., Vojtek P., Černák M., Brablec

A.: Appl. Phys. Lett. *81*, 2716 (2002).
6. Skácelová D., Sťahel P., Haničinec M., Černák M.: Acta Tech. *56*, T356 (2011).
7. Buček A., Homola T., Aranyosiová M., Velič D., Plecenik T., Havel J., Sťahel P., Zahoranová A.: Chem. Listy *102*, 1459 (2008).
8. Černáková L., Szabová R., Wolfová M., Buček A., Černák M.: Fibres Text. East. Eur. *15(5-6)*, 121 (2007).
9. Buršíková V., Sťahel P., Navrátil Z., Buršík J., Janča J.: *Surface Energy Evaluation of Plasma Treated Materials by Contact Angle Measurement*. Masaryk university, Brno 2004.
10. Zhang X. G.: *Electrochemistry of Silicon Surface and Its Oxide*. Kluwer Academic Publisher, New York 2003.

D. Skácelová, P. Sťahel, and M. Černák *(Department of Physical Electronics, Faculty of Science, Masaryk University, Brno, Czech Republic):* **Activation of Silicon Surface in Atmospheric Oxygen Plasma**

In this contribution, the surface modification of crystalline silicon surface in oxygen atmosphere was investigated. Moreover the effect of crystallographic orientation and surface pre-cleaning of silicon surface were studied. c-Si wafers (100) and (111) oriented were cleaned in isopropyl alcohol or etched in HF solution and afterwards treated in Diffuse Coplanar Surface Barrier Discharge.

Wettability, changes of surface properties and ageing effect of plasma treated surface were studied by means of contact angle measurement.

It was proved that modification of c-Si surface in oxygen plasma improves the wettability independently on crystallographic orientation and initial cleaning process.

MECHANICAL STABILITY OF THE P-I-N SOLAR CELLS STUDIED BY INDENTATION METHOD

VILMA BURŠÍKOVÁ[a,b], PETR SLÁDEK*[c], PAVEL SŤAHEL[a]

[a] Department of Physical Electronics, Faculty of Science, Masaryk University, Kotlářská 2, 611 37 Brno, [b] CEITEC, Central European Institute of Technology, Masaryk University, 601 77 Brno, [c] Department of Physics, Chemistry and Vocational Education Faculty of Education, Masaryk University, Poříčí 7, 603 00 Brno, Czech Republic
sladek@jumbo.ped.muni.cz

Keywords: solar cells, mechanical stability, hardness, elastic modulus, interfacial fracture toughness

1. Introduction

The mechanical stability of the solar cells may play a crucial role in their technological application and their determination is of great importance. One of the most suitable methods of characterization of mechanical properties of thin films is the indentation technique. Besides the film hardness, the method also enables to determine also other important material properties such as the film elastic modulus, the plastic and elastic part of the indentation work, the fracture toughness of the film and the film substrate interface.

The aim of the present work was to describe the determination of the above listed parameters for typical p-i -n silicon solar cells.

2. Experimental part

The studied p-i-n solar cells were deposited by RF glow discharge in ARCAM reactor[1]. In Fig. 1 the structure of the studied solar cells is shown. The solar cells consist of several layers. At first, an about 10 nm thick p-doped a-SiC:H layer was deposited, followed by 10 nm thick a-SiC:H layer and 12 nm thick standard buffer a-Si:H layer. The subsequent thick intrinsic i(a-Si:H) layer and the following 12 nm thick buffer a-Si:H layer was finally coated by a 20 nm thick n-doped n(a-Si:H) layer. All layers were deposited at 180 °C.

In case of the structured coatings, the interfacial fracture toughness of the particular interfaces is one of the most important parameters for the mechanical stability of the solar cells.

The depth sensing indentation (DSI) method by means of Fishercope H100 tester, equipped with Vickers indenter was used for determination of the mechanical properties of the films. In the case of the Fischerscope H100 tester the applied load is registered as a function of indentation depth both during loading and unloading. The maximum applied load could be changed in the range from 1 mN to 1 N. The sensitivity of the depth measurement is approximately ± 1 nm. In order to minimize the experimental errors, each measurement was repeated at least 9 times.

On the basis of the DSI method the universal hardness *HU* (also called Martens hardness *HM*) as a measure of the material resistance against elastic and plastic deformation may be obtained. *HU* is calculated as the contact pressure (ratio of the applied load *L* to the immediate contact area *A*). In our case, the Vickers technique based on the indentation of square-based diamond pyramid with face angle $\alpha = 136°$ was used. The so called plastic hardness HU_{pl} is obtained as the ratio of the maximum applied load and the area of the remained indentation print A_d. The loading and unloading curves enable to determine the elastic and plastic part of the indentation work (W_e and W_{pl}), the effective elastic modulus $Y = E/(1–\nu^2)$, where E is the Young's modulus and n is the Poisson's ratio of the films and the hardness of the film[2].

The indentation may introduce substantial cracks and adhesive failures into the thin films. By the analysis of the morphology of the indentation prints, it is possible to determine material characteristics as the fracture toughness of the films and the resistance of the film-substrate interface against delamination. The fracture toughness of the coating-substrate interface could be estimated from the analysis of the energy dissipated during the indentation[3]. During the deformation, the total deformation work is transformed into elastic strain energy W_{el}, energy dissipated due to plastic deformation W_{pl}, energy dissipated due to fracture W_{fr} and thermal energy W_{th}. The area between

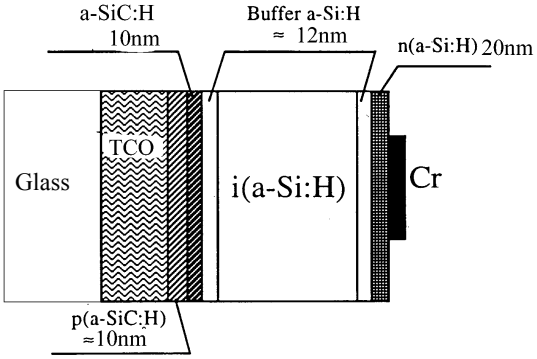

Fig. 1. **Schema of the studied solar cells**

the loading and unloading curves gives the total amount of the dissipated energy. The energy dissipated in the propagation of the delamination crack can be related to the interfacial fracture energy W_{fr}. The interfacial energy release rate G_{int} can be obtained on the basis of the indentation work W_{fr} needed for creation of delaminated area with radius c (Fig. 1). The interfacial fracture toughness K_{int} was calculated according to the following formulas:

$$G_{\text{int}} = \frac{W_{fr}}{\pi c^2}, \quad \frac{1}{E_{\text{int}}} = \frac{1}{2}\left(\frac{1}{E_f} + \frac{1}{E_s}\right) \tag{1}$$

$$K_{\text{int}} = \sqrt{G_{\text{int}} E_{\text{int}}} \tag{2}$$

Here E_{int} is the so called interfacial elastic modulus defined by Hutchinson and Suo[4]. E_f is the film elastic modulus and E_s the substrate elastic modulus.

The morphology of the film surface and the indentation prints was studied by means of Zeiss – Neophot optical microscope, a Nicon SMZ - 2T optical stereomicroscope, a Philips SEM 505 scanning electron microscope and by AFM.

3. Results and discussion

The analysis of the load-penetration curves was done for several p-i-n solar cells with different thicknesses. Because of the complicated structure of the solar cells the measurements were made for several different indentation depths (i.e. several different applied loads) in order to map the mechanical properties from near surface up to film-substrate interface.

In Fig. 2 the load-penetration curves carried out at maximum load L = 10 mN for 3.4 μm thick p-i-n solar cell

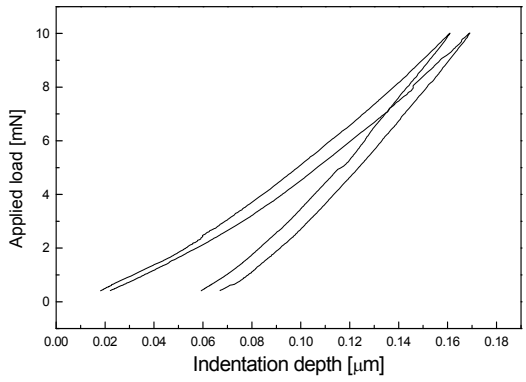

Fig. 2. **Load-penetration curves measured for 3.4 μm thick p-i-n solar cell.** The maximum load was L = 10 mN

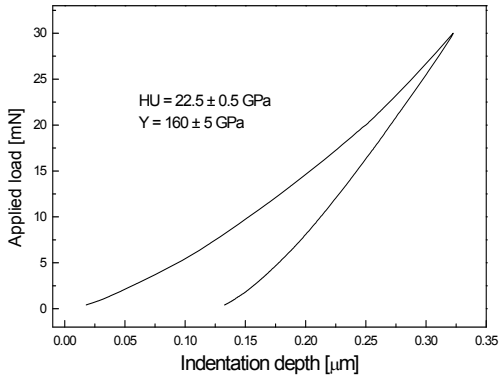

Fig. 3. **Load-penetration curves measured for 3.4 μm thick p-i-n solar cell.** The maximum load was L = 30 mN. The loading and unloading time was 60 s

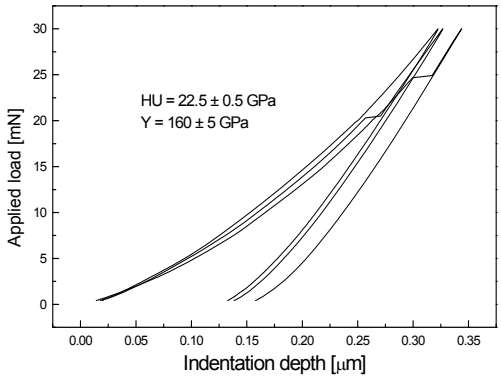

Fig. 4. **Load-penetration curves measured for 3.4 μm thick p-i-n solar cell.** The maximum load was L = 30 mN. The loading and unloading time was 20 s

are shown. The time of the loading and unloading was t = 20 s. The measured plastic hardness HU_{pl} was 25 ± 5 GPa, the universal hardness was 7.7 ± 0.7 GPa and the elastic modulus 160 ± 10 GPa. The load-penetration curves and the experimental values were scattered due to the interfacial effects such as interfacial microcracks. The effect of microcracks could be observed in Fig. 2 as jumps on the curve. These microcracks were created at the first two interfaces between the n-doped a-Si:H and the buffer a-Si:H layer or between the buffer layer and the intrinsic layer.

With increasing loading time, i.e. decreasing deformation rate, the cracks were not created. This effect was observed also for higher applied loads. An example is shown in Fig. 3. The maximum load was 30 mN and the loading time was 60 s. The universal hardness was

7.7 ± 0.5 GPa. The plastic hardness HU_{pl} was 22.5 ± 0.5 GPa and the elastic modulus was $Y = 160 \pm 5$ GPa. The load penetration curves made with low deformation rate were smooth without jumps as it is shown in Fig. 3. On the other hand high deformation rates (loading time $t = 20$ s) caused sudden deformations appearing on the load-penetration curve as jumps. This effect is shown in Fig. 4. The maximum applied load was the same as in Fig. 3. These jumps indicate sudden slips or creation of microcracks at the interface. At higher loads (higher indentation depths) the jumps appear also at low deformation rates due to the influence of the bottom interfaces.

At higher applied loads the 0.9 μm thick solar cell showed also the indentation induced delamination around the indentation prints. In Fig. 8 the indentation prints made at 0.5 N are shown. Due to film transparency there is clearly shown the indentation induced separation (delamination) of the film from the substrate at the film-substrate interface.

Measuring the radius of the delaminated area, we can determine the fracture toughness of the film-substrate interface according to equations (*1*) and (*2*). The calculated interfacial fracture toughness of the 0.9 μm thick solar cell was $K_{ic} = 7.2 \pm 0.5$ MPa $m^{1/2}$.

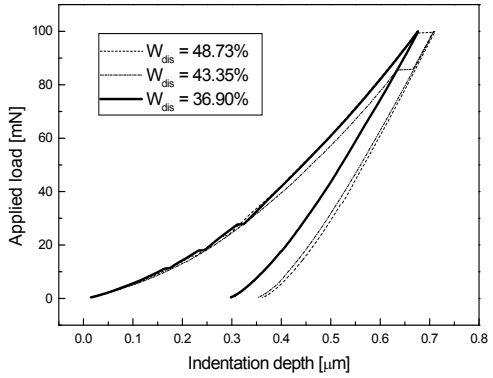

Fig. 5. **Load-penetration curves measured for 3.4 μm thick p-i-n solar cell.** The maximum load was L=100 mN. The loading and unloading time was 60 s. In the graph the total irreversibly dissipated parts of deformation work are given in percents

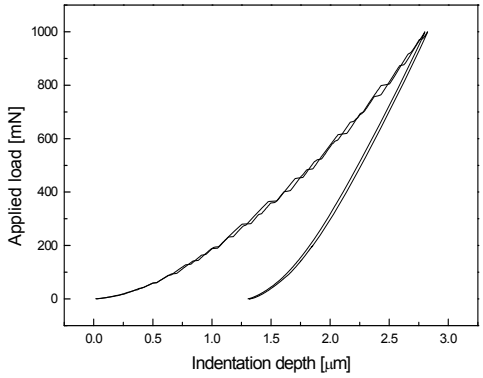

Fig. 6. **Load-penetration curves measured for 3.4 μm thick p-i-n solar cell.** The maximum load was L = 1 N. The loading and unloading time was 60 s

Table I
Determination of the deformation work made with applied load 100 mN. W_{tot} is the total, W_{el} is the elastic and W_{ird} is the irreversibly dissipated work. W_{int} is the work for interfacial deformation

W_{tot} [nJ]	W_{el} [nJ]	W_{ird} [nJ]	W_{int} [nJ]
26.6	16.8	9.8	~0
27.0	16.5	10.5	0.7
27.1	16.3	10.7	0.9
28.1	15.9	12.2	2.4
30.2	15.5	14.7	4.9

The DSI technique enables us to quantitatively determine the indentation work, which was needed for the plastic, elastic and interfacial deformation. The determination of the particular parts of the total indentation work is shown in Fig. 5.

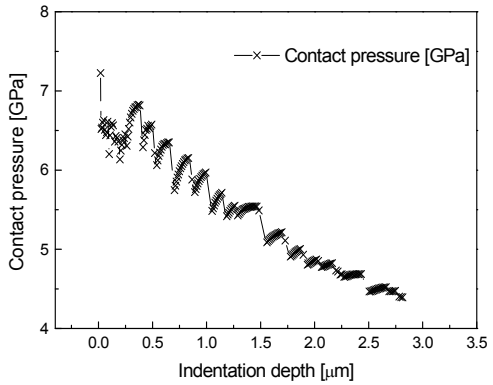

Fig. 7. **The dependence of the contact pressure between the indenter and the thin film-substrate system on the indentation depth measured for 3.4 μm thick p-i-n solar cell.** The maximum load achieved at the end of the loading was L = 1 N. The loading and unloading time was 60 s

4. Conclusion

The depth sensing indentation technique was used for characterization of the mechanical properties of the p-i-n solar cells. Cells of several different thicknesses were studied. Detailed analysis of load-penetration curves obtained at applied loads ranging from 10 to 1000 mN and for two deformation rates was done. The determination of important material parameters such as plastic and universal hardness, elastic modulus, the irreversibly dissipated deformation work and the interfacial fracture toughness was shown. The possible deformation mechanism of structured thin films resulting loading curves by steps was described.

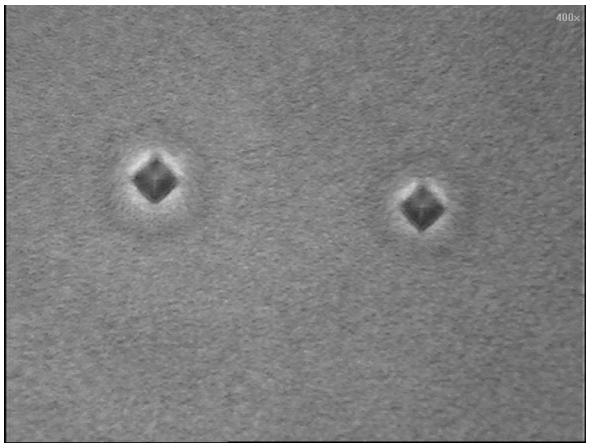

Fig. 8. **Optical micrographs of the indentation prints made in the 0.9 μm thick solar cell with applied load L = 0.5 N**

This research was supported by the Grant Agency of the Academy of Sciences of the Czech Republic under contract KAN311610701 and by the project CZ.1.05/2.1.00/03.0086 'R&D center for low-cost plasma and nanotechnology surface modifications' funded by European Regional Development Fund.

REFERENCES

1. Roca i Cabarrocas P., Chévrier J. B., Huc J., Loret A., Parey J. Y., Schmitt J. P. M.: J. Vac. Sci. Technol. *A9*, 2331 (1991).
2. Pharr G. M., Oliver W. C., Brotzen F. R.: J. Mater. Res. *7*, 613 (1992).
3. Malzbender J., et.al.: Mater. Sci. Eng. R *36*, 47 (2002).
4. Hutchinson J. W., Suo Z.: Adv. Appl. Mech. *29*, 63 (1992).

V. Buršíková[a,b], P. Sládek[c], and P. Sťahel[a]
([a] Department of Physical Electronics, Faculty of Science, Masaryk University, Brno, [b] CEITEC, Central European Institute of Technology, Masaryk University, Brno, [c] Department of Physics, Chemistry and Vocational Education Faculty of Education, Masaryk University, Brno, Czech Republic): **Mechanical Stability of the P-I-N Solar Cells Studied by Indentation Method**

The main priorities when preparing the p-i-n amorphous silicon based solar cells are the efficiency as well as the optoelectronic stability of the cells. However, for the final applications, a good mechanical and thermomechanical stability is not of the second order of importance. The large internal mechanical stress, weak adhesion can result the deterioration of the solar cell (cracking, delamination).

The objective of our study was to investigate the mechanical properties of p-i-n amorphous silicon based solar cells by means of depth sensing indentation technique (Fisherscope H100). The instrumented indentation method combined with the study of the morphology of the indentation prints enable us to determinate microhardness, fracture toughness of the interface with substrate and internal stress.

DIFFUSE COPLANAR SURFACE BARRIER DISCHARGE FOR CLEANING AND ACTIVATION OF GLASS SUBSTRATE

VLASTA ŠTĚPÁNOVÁ, DANA SKÁCELOVÁ, PAVEL SLAVÍČEK*, MIRKO ČERNÁK

Department of Physical Electronics, Faculty of Science, Masaryk University, Kotlářská 2, 611 37 Brno, Czech Republic
ps94@sci.muni.cz

Keywords: barrier discharge, DCSBD, plasma cleaning, AFM

1. Introduction

The aim of our research is the cleaning and activation of glass by environmental friendly methods. Glass can be cleaned by several types of discharges[1,2] at low pressure and at atmospheric pressure, too. This article presents the results of glass cleaning by Diffuse Coplanar Surface Barrier Discharge (DCSBD)[3,4] at atmospheric pressure in ambient air. The advantage of this method is that in this way the non-ecological cleaning using toxic chemicals can be avoided. Borosilicate glass was used as a substrate.

2. Experimental set-up

Diffuse Coplanar Surface Barrier Discharge (DCSBD) is a special type of dielectric barrier discharge (DBD)[5] plasma source operated at atmospheric pressure[6,7]. DCSBD electrode system was made by parallel metallic electrodes embedded in Al_2O_3 ceramic (see Fig. 1). This construction enables to create a thin layer of non-isothermal cold plasma with large surface area. The sample holder is mounted on the rails in order to enable the movement of samples in accurately adjustable distance over the dielectric barrier in plasma layer. The photo of DCSBD at atmospheric pressure in ambient atmosphere is shown in Fig. 2.

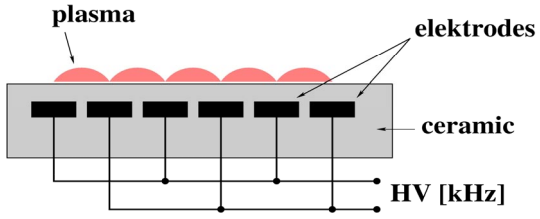

Fig. 1. **Scheme of Diffuse Coplanar Surface Barrier Discharge**

Plasma treatment was realized in air at atmospheric pressure. The discharge power was 300 W. The distance between the sample surface and the ceramic plate was 0.2 mm.

The size of the substrates was 18 × 18 × 0.1 mm. The studied samples were cleaned in isopropyl alcohol before plasma treatment.

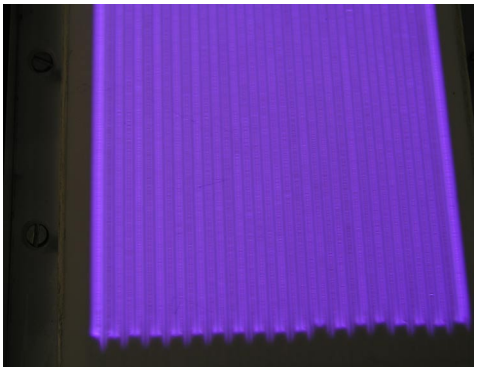

Fig. 2. **Photo of the Diffuse Coplanar Surface Barrier Discharge**

3. Measurement methods

The roughness of glass surface has been evaluated using Atomic Force Microscope (AFM). Measurements have been performed by AFM, type CP-II Veeco – scanning probe microscope. By this measurement we have investigated the dependence of the exposition time of glass in plasma on the change of its surface roughness. The measurement was carried out in contact mode. The data from the AFM measurement have been evaluated by the help of Gwyddion software[8].

The contact angle[9,10] of water has been studied using Surface Energy Evaluation system (SEEsystem). SEEsystem is an instrument for measurement of the contact angle and for the calculation of surface free energy. Using this system we verified the wettability change of the glass before and after the plasma treatment. We measured the contact angle between the liquid and the tested material, in our case deionised water and glass surface.

4. Results and discussion

The time dependence of the roughness has been measured by means of AFM. The time of exposition in plasma ranged from 1s to 2 min. The obtained results are presented in Table I and Fig. 3. In Table I the time dependence of the root mean square (RMS) roughness[11,12] parameter is shown.

Table I
RMS roughness and time of plasma treatment

Time of plasma treatment [s]	RMS [nm]
0	0.68
1	0.89
5	1.25
10	1.25
25	1.27
60	7.30
120	13.0

Short time exposition in plasma caused only slight increase of the surface roughness. The maximum roughness was in order of nanometre magnitude in this case. The long time exposition of the glass surface in plasma increased the roughness by almost two orders of magnitude.

The results of the roughness of glass after plasma treatment obtained using AFM and evaluated by Gwyddion software are shown in Figs. 4, 5, 6 and 7. Fig. 4 presents the roughness of glass surface after 10 s of plasma treatment. 3D image of glass surface after 10 s of plasma treatment is shown in Fig. 5. The maximum of the surface roughness did not exceed the nanometre level.

The roughness of the glass substrate after 120 s plasma treatment is presented in Fig. 6 and the 3D model is presented in Fig. 7. The maximum of roughness increased of one order of magnitude, it reached several tens of nanometres.

Typical surface profiles of plasma treated glass obtained by AFM measurements and evaluated by Gwyddion software are shown in Fig. 8 and Fig. 9. In Fig. 8 the results obtained after short treatment times (1 s, 5 s, 10 s) are presented. On the other hand, Fig. 9 presents long plasma treatment times (25 s , 60 s).

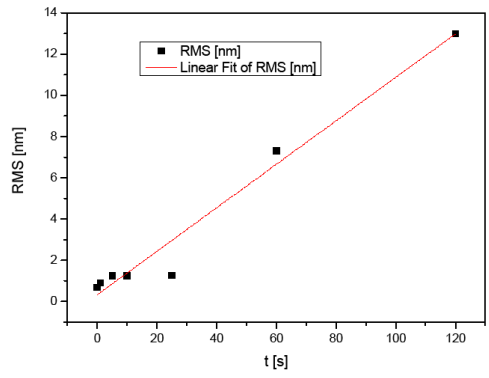

Fig. 3. **Time dependence of plasma treatment on the surface roughness.** The graph shows, that short plasma treatment s up to 20 s duration have no significant effect on roughness of the glass surface

SEE system was used to study the wettability change of the glass surface. The contact angle between deionised water and glass surface was measured. The results for the sample of glass before plasma treatment and after short

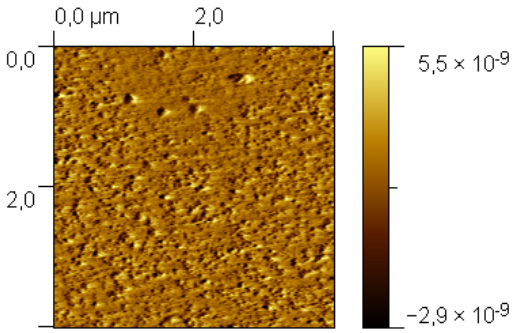

Fig. 4. **AFM image of plasma treated glass.** The treatment time was 10 s

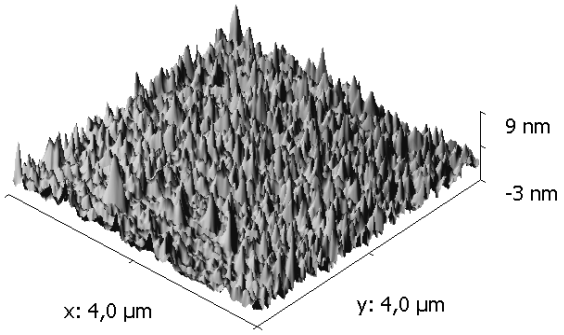

Fig. 5. **3D AFM image of plasma treated glass.** The treatment time was 10 s

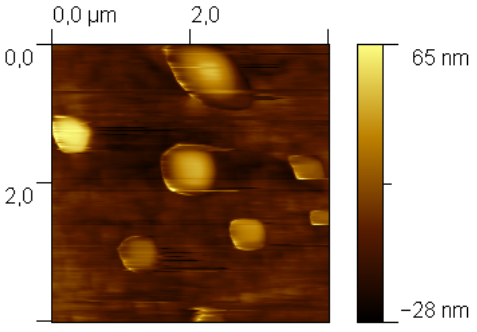

Fig. 6. **AFM image of plasma treated glass.** The treatment time was 120 s

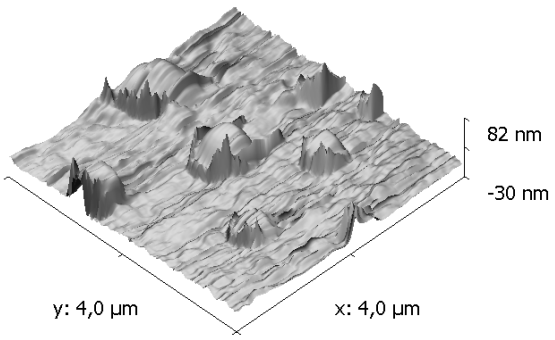

Fig. 7. **3D AFM image of plasma treated glass.** The treatment time was 120 s

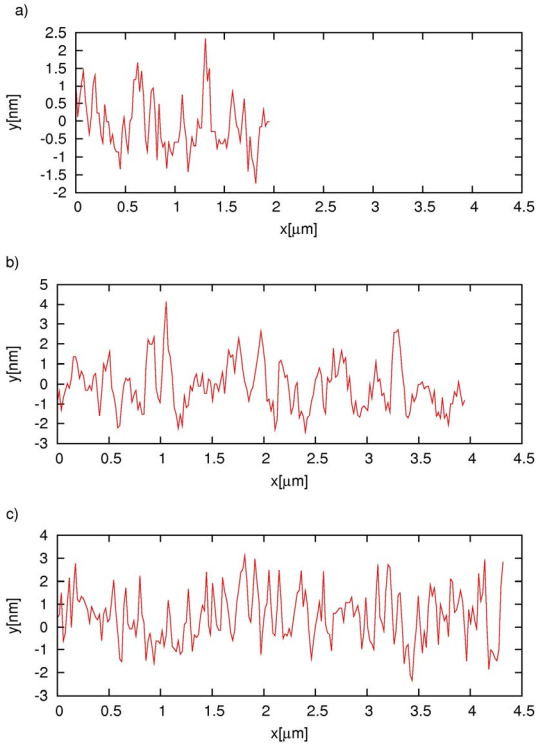

Fig. 8. **Surface profiles of plasma treated glass obtained by a short time plasma treatment: (a) 1 s, (b) 5 s, (c) 10 s**

time plasma treatment are shown in Fig. 10 and Fig. 11. Already after a short time of treatment in DCSBD the change of wettability is evident. Before the plasma treatment the contact angle was 30° (Fig. 10) and after 5s of plasma treatment the contact angle was 14°.

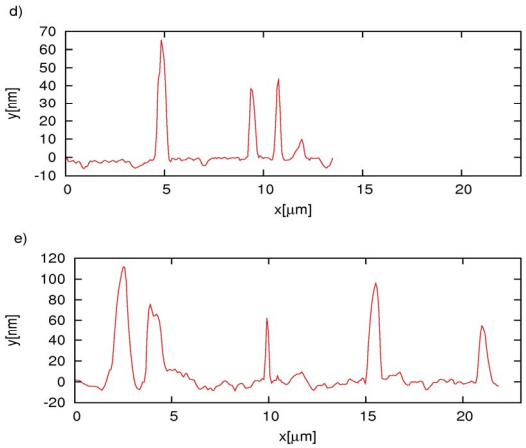

Fig. 9. **Surface profiles of plasma treated glass after long time plasma treatments: (d) 25s , (e) 60s**

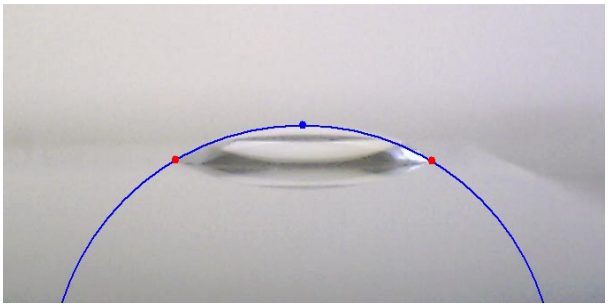

Fig. 10. **Photo of the contact angle of water on glass before plasma treatment** (the contact angle was 30°)

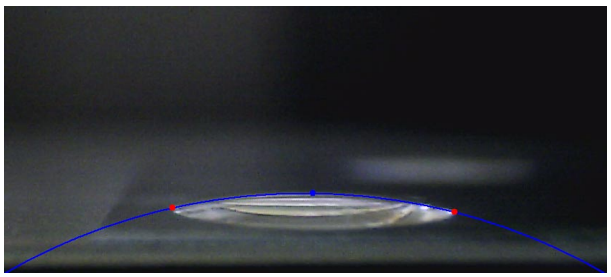

Fig. 11. **Photo of the contact angle of water on glass after 5 s of plasma treatment** (the contact angle was 14°)

5. Conclusion

On the basis of our present research we can conclude that plasma treatment, concretely DCSBD treatment, is a very powerful method to clean the surface of glass substrates. Short time plasma treatment (less then 10 s) using

DCSBD does not cause significant changes of roughness which is very useful finding for several industrial applications, especially for the utilization of DCSBD in the glass industry. During the short time of plasma treatment the substrate is roughened only slightly and evenly.

During the long time plasma treatment (more then 25 s) the substrate is roughened significantly and unevenly. The maximum roughness in this case reached several tens of nanometres, the changes in surface roughness increased almost of two orders of magnitudes.

The DCSBD plasma treatment exhibited substantial influence on the surface wettability of the glass. The wettability of the glass substrate significantly increased after plasma treatment comparing to the initial state of the glass surface. The next aim of our research is an investigation of the influence of aging on wettability and the study of the surface layer on glass substrates by means of MALDI-TOF and XPS analysis.

Support by European Regional Development Fund (project CZ.1.05/2.1.00/03.0086 'R&D center for low-cost plasma and nanotechnology surface modifications') and Czech Science Foundation (Project No.202/09/2064) are greatly acknowledged.

REFERENCES

1. Henke L., Nagy N., Krull U.: Biosens. Bioelectron. *17*, 547 (2002).
2. Cras L. L., Rowe-Taitt C. A., Nivens D. A., Ligler F. S.: Biosens. Bioelectron. *14*, 683 (1999).
3. Cernak M., Cernakova L., Hudec., Kovacik D., Zahoranova A.: Eur. Phys. J.: Appl. Phys. *47*, 22806 (2009).
4. Cernak M., Rahel J., Kovacik D., Simor M., Brablec A., Slavicek P.: Contrib. Plasma Phys. *44*, 492(2004).
5. Roth J. R.: *Industrial Plasma Engineering Vol II*, Inst. of Phys. Publish. Bristol and Philadelphia, 2001.
6. Schaefer J., Sigeneger F., Foest R., Loffhagen D., Weltmann K.-D.: Eur. Phys. J. D *60*, 531 (2010).
7. Barankova H., Bardos L.: Surf. Coat. Technol. *174 - 175*, 63 (2003).
8. http://gwyddion.net/(7.5.2012).
9. Foest R., Kindel E., Ohl A., Stieber M., Weltmann K.-D.: Plasma Phys. Controlled Fusion *47* B525 (2005).
10. Takeda S., Yamamoto K., Hayasaka Y., Matsumoto K.: J. Non-Cryst. Solids *249*, 41(1999).
11. Dobierzewska-Mozrzymas E., Rysiakiewicz-Pasek E., Bieganski P., Polanska J., Pieciul E.: J. Non-Cryst. Solids *354* , 3241 (2008).
12. Danzebrink H.-U., Koenders L., Wilkening G., Yacoot A., Kunzmann H.: Manuf. Technol. *55*, 841 (2006).

V. Štěpánová, D. Skácelová, P. Slavíček, and M. Černák *(Department of Physical Electronics, Faculty of Science, Masaryk University, Brno, Czech Republic):*
Diffuse Coplanar Surface Barrier Discharge for Cleaning and Activation of Glass Substrate

In this paper we present the results of plasma cleaning of glass substrates using the Diffuse Coplanar Surface Barrier Discharge (DCSBD) operated in air at atmospheric pressure. The results of AFM measurements indicate that short time of treatment of DCSBD did not increase the surface roughness substantially. The results of contact angle measurement show that the substrate after plasma treatment is more wettable than before plasma treatment.

Chem. Listy *106*, s1499–s1503 (2012) CEPLANT

PROPERTIES OF MODIFIED AMORPHOUS CARBON THIN FILMS DEPOSITED BY PECVD

ADRIAN STOICA[a,b]*, VALENTIN MOCANU[a], JAN ČUPERA[a], LUKÁŠ KELAR[a], VILMA BURŠÍKOVÁ[a,b]

[a] *Department of Physical Electronics, Faculty of Science, Masaryk University, Kotlářská 2, 611 37 Brno,* [b] *CEITEC, Central European Institute of Technology, Masaryk University, 601 77Brno, Czech Republic*
stoica@mail.muni.cz

Keywords: RF-PECVD, amorphous carbon, protective coatings, DLC, modification

1. Introduction

Diamond-like carbon (DLC) thin films are becoming increasingly important in many forms of industrial applications, including wear-resistant coatings for hard-disk drives and optical components, as well as in semiconductor devices. Due to their biocompatibility, chemical inertness and being impermeable to liquids, a-C:H coatings could protect biological implants against corrosion and serve as diffusion barriers[1–3]. However, the term DLC covers a range of materials with properties that can vary from those similar to graphite to those approaching those of natural diamond. Hydrogen-free DLC films (also known as amorphous carbon films, a-C, are believed to consist of a mainly graphitic sp^2 carbon matrix containing nm-sized clusters of sp^3 diamond-like carbon. Hydrogenated DLC films (also known as hydrogenated amorphous carbon films, a-C:H) add yet more degrees of complexity to the possible structure of the films. Various materials derived from a-C:H structure have been developed incorporating nitrogen, silicon, oxygen, fluorine or various metal atoms into its structure. Most modifications have been made to reduce their typically high internal compressive stresses, to increase the adhesion to the substrate (N, Si, metal incorporation), to modify surface free energy (N, F, O, Si), to increase their biocompatibility (F, Ti, Si, Ca) or to modify their electrical properties[3–7]. The nitrogen -doped DLC films have been proven to be very effective in magnetic storage technology as protective overcoats. Doping DLC with metals increases the wear resistance of the resultant coatings while maintaining the friction coefficients low. Deuterated amorphous carbon films (a-C:D) were also investigated for some specific applications, like storing ultra-cold neutron devices[8] or as neutron mirrors[9]. Diamond-like carbon (DLC) films have been deposited in a variety of ways. By choosing the deposition technique and the appropriate deposition parameters, the ratio between carbon atoms in sp^2 and sp^3 hybridization can be altered and the film properties can be controlled. The amorphous hydrogenated carbon films (a-C:H) can be deposited by PECVD technique, in a wide range of sp^2/sp^3 hybridized-carbon atoms ratio[10]. Radio frequency plasma-enhanced chemical vapour deposition (RF-PECVD) is a widely used technique. We have pursued doping of DLC films deposited using a RF-PECVD system as this method is suitable for the deposition of these films at low temperature. Added advantages lie in the fact that scaling up of the deposition system is possible. In this work, we will present a comparative study of the incorporation of D, N, Si and O into a-C:H films deposited by PECVD using CH_4 in mixture with H_2, D_2, N_2 and/or hexamethyldisiloxane (HMDSO) as precursor atmospheres. The effects on the film tribological and mechanical properties will be discussed, emphasizing the role of the doping species.

2. Experimental systems

A parallel-plate RF-PECVD reactor has been used for the deposition of a-C:H films. The reactor chamber consisted of a vertically mounted glass cylinder, inner diameter 285 mm and height 195 mm, closed by two stainless steel flanges. The bottom graphite electrode, diameter 148 mm and 8 mm thickness, was capacitively coupled to the RF generator operating at a frequency of 13.56 MHz. In this experimental arrangement the bottom electrode is used as the substrate holder. The grounded upper electrode made of graphite has a diameter of 100 mm.

For the deposition several types of substrates have been used. Single crystal silicon and glass are used for all depositions. Stainless steel substrates were used for the depositions of nitrogen containing films. Before the depositions the samples were cleaned in a mixture of cyclohexane and isopropyl alcohol. Then, in order to improve the film adhesion the samples were sputtered cleaned by argon ions for 15 minutes prior to film deposition.

In a last step, the deposition itself was performed after changing the operational parameters, without opening the reactor, but just by adding the precursor gases to the reaction chamber. The films were produced from different mixtures of the following precursor gases: CH_4, H_2, D_2, N_2, and HMDSO. The gases were simultaneously introduced into the chamber using separate valves and flow meters to control their individual flow rates. The experimental conditions are shown in Table I together with the mechanical properties of the deposited films on silicon substrates.

3. Characterization methods

Mechanical characteristics were investigated by the depth-sensing indentation (DSI) technique[12]. A Fischerscope H100 depth sensing indentation (DSI) tester equipped with Vickers indenter, microscope and CCD camera was used to study the indentation response of a-C:H and doped a-C:H deposited films. During the DSI test the load and the corresponding indentation depth were recorded as a function of time for both loading and unloading process. From the loading and unloading hysteresis it was possible to determine the hardness and the elastic modulus of studied samples. The universal hardness is the measure of resistance of the material against both elastic and plastic deformation. The loading period of 20 s was followed by a hold time of 5 s, an unloading period of 20 s and finished after holding the minimum load for 5 s. Several tests were made at different maximum loads (i.e. several different indentation depths) in order to study the load and/or depth dependence of the investigated mechanical characteristics. Each test was repeated from 9 to 16 times in order to minimize the experimental errors. All tests were performed in air at room temperature.

The interfacial fracture toughness K_{INT} was calculated on the basis of the indentation induced delamination of the thin films. There are several methods used to calculate this value. Most of them is based on the relationship between the applied load and the delaminated area created around the indentation print. Moreover, from the loading/ unloading characteristics it is also possible to calculate the indentation work, what is needed to create a delamination with a unit area (so called interfacial energy release rate) and using the known elastic modulus of the film and substrate the interfacial can be obtained[13,14].

The pin-on-disk wear test to measure of the lifetime of the coating is performed using a tribometer. The sample is mounted on a chuck which can be rotated at a predetermined speed. A ball or other static partner is mounted in contact with the rotating sample via an elastic arm which can move laterally and therefore measure the tangential forces (friction) between sample and ball with a sensor. The data acquisition system records the frictional force as a function of time or number of revolutions, although it is often recalculated so that the coefficient of friction (COF, μ) is displayed on the same axes. The advantage of a wear test is that it can give a measure of the lifetime of a particular coating-substrate system. In many applications of coatings, the resistance to wear can be more important than the critical load required to permanently damage the material. In our work the static partner was a 6 mm diameter Al_2O_3 ball applied with load 10 N and speed in the range from 5 to 20 cm s^{-1}. The testing radius r was in the range from 2,6 to 10 mm. The graph of COF versus distance shows a steady value of friction until the coating fails (i.e., is completely worn away). The onset of failure corresponds, in this case, to a distinct change in the friction signal, due to breakdown of the coating and formation of a tribological transfer film which is a mixture of the coating, substrate and static partner materials mixed together. The properties of the coating being tested and the substrate on which it has been deposited will influence the friction signal when the coating is worn through. In some

Table I
Summary of the deposition parameters (Q_x – flow rate of precursor gas x, t – deposition time, U_b – negative DC self bias voltage, p – total working pressure) together with the chracteristic properties (γ_{TOT} – total surface free energy, σ – internal stress, COF – coefficient of friction, K_{INT} – interfacial frature toughness, H_{IT} –hardness, Y – elastic modulus) of the obtained thin films. The applied power was 50 W

Sample	S01	S02	S03	S04	S05	S06	S07	S08	S09	S10
Q_{CH4} [sccm]	1.4	1.41	1.4	1.4	1.31	1.31	1.42	0.31	1.4	1
Q_{H2} [sccm]	0.4	5	–	5	5	5	–	–	5	1
Q_{D2} [sccm]	–	–	0.4	–	–	–	–	–	–	–
Q_{N2} [sccm]	–	–	–	5	7	1	1	–	–	–
Q_{HMDSO} [sccm]	–	–	–	–	0.4	0.4	1.31	1	0.2	0.23
t [min]	60	60	60	60	30	30	60	60	60	60
$-U_b$ [V]	260	355	260	127	105	265	191	294	270	227
p [Pa]	13	15	13	23	32	25	15	9	18	12
γ_{TOT} [mJ m^{-2}]	38	40	39	47	53	43	54	49	41	42
σ [GPa]	–2.3	–1.1	–1.9	–0.2	–0.4	–0.3	–0.5	–0.8	–0.3	–0.9
COF	0.04	0.1	0.05	0.18	0.23	0.1	0.07	0.13	0.08	0.06
K_{INT} [MPa $m^{0.5}$]	0.08	0.07	0.08	0.24	0.65	0.38	0.77	0.72	0.40	0.25
H_{IT} [GPa]	19.5	16.5	21.8	3.8	6.7	11	2.7	18.5	17.1	19
Y [GPa]	150	125	163	45	126	120	31	115	133	105
Deposition rate [nm min^{-1}]	5.7	4.58	5.5	4.75	2.26	9.8	15.8	13.4	10.1	12.5

cases this signal will rise dramatically, in others it may drop. However, the breakdown of the coating will nearly always manifest itself as a sharp change from the steady sliding state.

The surface free energy γ of the deposited films was determined from contact angle measuring method using SeeSystem[15].

The compressive stress in films was calculated from measurement of the radius of curvature on a 3 mm × 25 mm × 0.5 mm coated silicon strip and by analyzing the results with the well-known Stoney's equation[12].

4. Results and discussion

The DLC and modified DLC films obtained by RF-PECVD were characterized for their mechanical properties. The deposition conditions and mechanical properties of representative samples are summarized in Table I.

The mechanical properties of the hydrogenated films were found to be dependent on the flow ratio of methane in the gas mixture and on the self-bias voltage. Their values are listed in Table I for samples S01 and S02 in order to illustrate the effect. For a higher content of methane the internal compressive stress and hardness of the film decreased.

An improvement in mechanical properties was found for the deuterium containing films compared to the non-doped hydrogenated DLC films. In Fig. 1 it is presented the dependence of the hardness and elastic modulus on the relative indentation depth. Going deeper into the sample, the influence of the substrate becomes more visible, silicon having lower hardness and elastic modulus. Replacing H_2 by D_2 in the gas mixture during deposition proved advantageous, the modified DLC films exhibiting higher values of hardness and elastic modulus than the hydrogenated DLC films deposited in the same experimental conditions. The hardness value of 21.8 GPa was the highest among all other types of coatings that were prepared in this work. Moreover, the residual compressive stress, σ, is less pronounced in the deuterated DLC films, as listed in Table I.

The internal stress influences other important coating properties such the adhesive strength and wear resistance. The addition of HMDSO into the precursor atmosphere proved to decrease the internal compressive stress in the films (samples S09 and S10), increased their surface free energy and the interfacial fracture toughness (films were deposited on silicon substrates). Moreover, the silicon and oxygen containing DLC thin films prepared under optimum conditions reached a hardness value of 19 GPa (sample S10 in Table I). When increasing the H_2 flow to 5 sccm the hardness of the films decreased to a value of 17.1 GPa, however the internal stress in these films decreased too. In the absence of hydrogen from the precursor mixture the deposited films had comparable values of hardness and elastic modulus (sample S08), but still lower than the maximum achieved by the deuterated DLC layers.

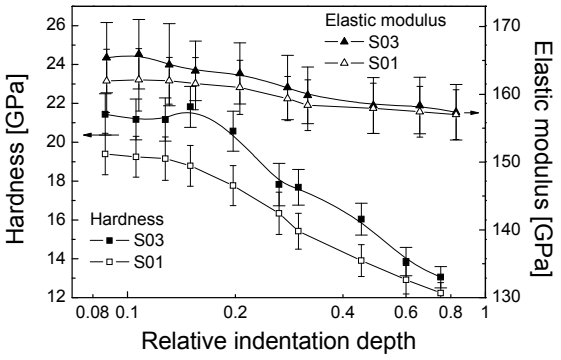

Fig. 1. **Dependence of the hardness and elastic modulus on the relative indentation depth for samples S01 (HDLC film) and S03 (DDLC film) on silicon substrates**

When nitrogen was added to the mixture, the hardness and elastic modulus values decreased dramatically (sample S07, H_{IT} = 2.7 GPa). The differences in the depth dependences of the hardness between films S07 and S08, both deposited on two different substrates (glass and single crystalline silicon) are demonstrated in Fig. 2. In this figure these differences are visible for the different substrates on which the films were deposited.

The coatings prepared from the mixture CH_4 + H_2 + N_2 + HMDSO performed better (samples S05 and S06) from the point of view of mechanical properties. The presence of hydrogen led to the deposition of less soft films, with hardness values ranging from 6.7 to 11 GPa. Hardness proves to be dependent on the nitrogen flow, harder films being obtained from gas mixtures with lower nitrogen flow rate ratios.

From the tribology point of view another effect of nitrogen incorporation is the increase of the coefficient of

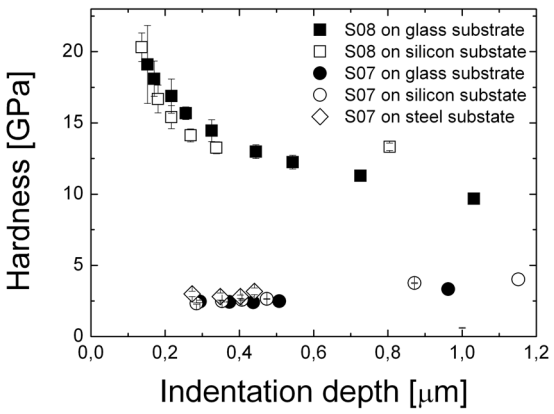

Fig. 2. **Dependence of the hardness on the indentation depth for samples S07 and S08 on glass, silicon and steel substrates**

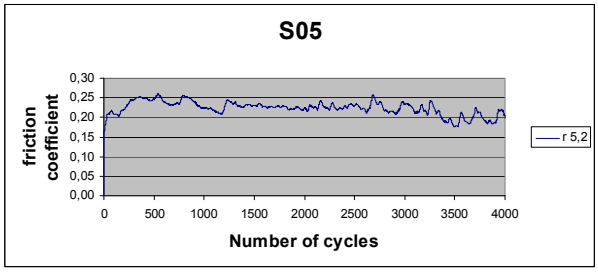

Fig. 3. **Dependence of the friction coefficient on the number of pin-on-disk cycles for sample S05**

friction compared to films prepared without nitrogen addition. In Fig. 3 it is presented the dependence of COF on the number of cycles in the pin-on-disk test performed on the sample S05. The graph shows the value of friction versus the number of pin-on-disk cycles.

In Fig. 4 there are presented the pin-on-disk test results for sample S06. Decrease of nitrogen content in the deposition mixture caused decrease in COF value. The graph of COF versus distance shows a steady value of friction until the coating fails (i.e., is completely worn away) after 15000 cycles. A confocal microscope image of the

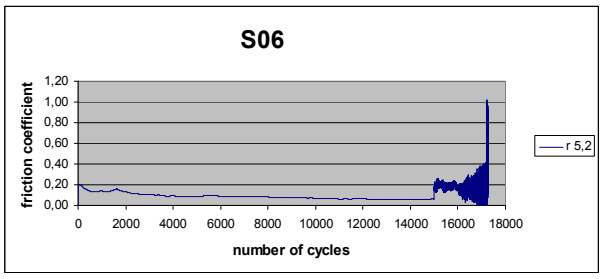

Fig. 4. **Dependence of the friction coefficient on the number of pin-on-disk cycles for sample S06**

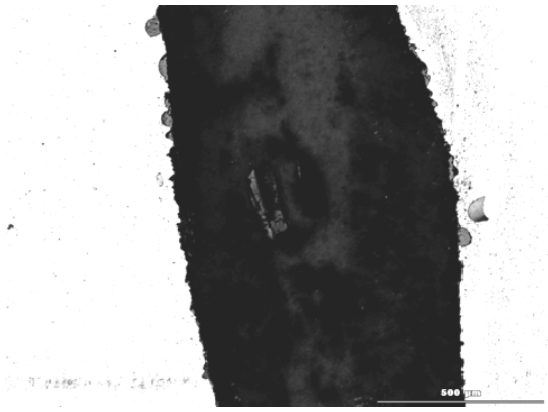

Fig. 5. **S06 after 15,000 cycles of pin-on-disk test**

wear scar on the tested sample S06 is presented in Fig. 5. There are no signs of delamination around the contact area.

5. Conclusions

Considering the mechanical results, we compared the effects of incorporating hydrogen, deuterium, and nitrogen into DLC films. The compressive stress, hardness and elastic modulus were found to have a dependence on the methane flow rate ratio and substrate bias voltage. With increasing content of methane, the compressive stress and hardness decreased. The incorporation of deuterium in the layer can enhance the hardness and the elastic modulus, taking into account the similar values of the bias voltage during the discharges. Deuterium doped a-C:H films present higher compressive stress than the a-C:H films. The incorporation of nitrogen in a-C:H films decreases the internal stress more efficiently, but in the same time the hardness and elastic modulus decrease also. Nitrogen incorporation increases the films coefficient of friction. On the other hand, silicon and oxygen incorporation led to decrease in coefficient of friction as well as in internal stress. Moreover, the interfacial fracture toughness and the surface free energy increased in case of HMDSO modified DLC films. When increasing the N content we observe a decrease in the deposition rate.

This research was supported by the Grant Agency of the Academy of Sciences of the Czech Republic under contract KAN311610701, by the project CZ.1.05/2.1.00/03.0086 'R&D centre for low-cost plasma and nanotechnology surface modifications' funded by European Regional Development Fund and by the Ministry of Industry and Trade, contract FTTA5114 and the Science Foundation of the Czech Republic, contract 202/07/1669. The authors thank for pin-on-disk results Assoc. Prof. O. Bláhová from West Bohemian University Pilsen, Czech Republic.

REFERENCES

1. Donnet C., Erdemir A.: *Tribology of Diamond-Like Carbon Films Fundamentals and Applications*, Springer Science + Business Media LLC, New York NY, 2008.
2. Robertson J.: Mater. Sci. Eng. R *37*, 129 (2002).
3. Grill A.: Thin Solid Films *355–356*, 189 (1999).
4. Grishke M., Hieke A., Morgenweck F., Dimigen H.: Diamond. Rel. Mater. *6*, 559 (1997).
5. De Martino C., Fusco G., Mina G., Tagliaferro A., Vanzetti L., Calliari L., Anderle M.: Diamond. Rel. Mater. *6*, 559 (1997).
6. Buršíková V., et.al.: Optoelectron. Adv. Mater., Rapid Commun. *1*, 491 (2007).
7. Marciano F. R., Lima-Oliveira D. A., Da-Silva N. S.,

Corat E. J., Trava-Airoldi V. J.: Surf. Coat. Technol. *204*, 2986 (2010).
8. Van der Grinten M. G. D., et al.: Nucl. Instrum. Methods Phys. Res. A *423*, 421 (1999).
9. Kawabata Y., Hino M., Horie T., Tasaki S., Yoshida K., Kanno I., Nakayama M.: Nucl. Instrum. Methods Phys. Res. A *9*, 84 (2004).
10. Robertson J.: Prog. Solid State Chem. *21*, 199 (1991).
11. Bolshakov A., Pharr G. M.: J. Mater. Res. *13*, 1049 (1998).
12. Janssen G. C. A. M., Abdalla M. M., Van Keulen F., Pujada B. R., Van Venrooy B.: Thin Solid Films *517*, 1858 (2009).
13. Malzbender J. et.al.: Mater. Sci. Eng. R *36*, 47 (2002).
14. Hutchinson J. W., Suo Z.: Adv. Appl. Mech. *29*, 63 (1992).
15. Buršíková V., Sťahel P., Navrátil Z., Buršík J., Janča J.: *Surface Energy Evaluation of Plasma Treated Materials by Contact Angle Measurement*, Masaryk University, Brno 2004.

A. Stoica[a,b], V. Mocanu[a], J. Čupera[a], L. Kelar[a], and V. Buršíková[a,b] *([a] Department of Physical Electronics, Faculty of Science, Masaryk University, Brno, [b] CEITEC, Central European Institute of Technology, Masaryk University, Brno, Czech Republic)*: **Properties of Modified Amorphous Carbon Thin Films Deposited by PECVD**

The aim of this work was to prepare a set of DLC films from different mixtures of precursor gases (methane, hydrogen, deuterium, nitrogen and/or HMDSO) using RF-PECVD on substrates such as crystalline silicon, glass, and steel. The prepared films were characterized by several diagnostic tools and the properties of hydrogenated amorphous carbon films and the modified diamond-like carbon thin films with different admixtures (N, Si, O, D) were compared. Mechanical tests were performed on the obtained films mainly using depth sensing indentation method. We focused our attention on the following coating properties: hardness, elastic modulus, fracture toughness, film-substrate adhesion. Additionally, the effect of the internal stress on the indentation response of the film-substrate systems was studied. The tribological properties of the films were also investigated. The surface free energy of the films was performed by contact angle measuring technique.

VIBRATIONAL AND ROTATIONAL ENERGY TRANSFER IN A $^2\Sigma^+$ STATE OF OH RADICALS MEASURED BY LASER INDUCED FLUORESCENCE

JAN VORÁČ[a,b], VOJTĚCH PROCHÁZKA[a], PAVEL DVOŘÁK*[a]

[a] *Dep. of Physical Electronics, Faculty of Science, Masaryk University, Kotlářská 2, 611 37 Brno, Czech Republic,* [b] *ZIK-Plasmatis, INP Greifswald e.V., Felix-Hausdorff-Str. 2, 17489 Greifswald, Germany*
pdvorak@physics.muni.cz

Keywords: LIF, OH, hydroxyl, plasma pencil

1. Introduction

OH radical has been in the scope of scientists and engineers for a long time, because it allows to track important chemical processes. It is also expected to play an important role in the plasma material processing and the interaction of plasma with living cells. Laser-induced fluorescence is very often employed in density measurements since it can access the ground state, but there are some experimental difficulties that need to be solved before a proper absolute measurement can be done.

A great deal of current knowledge about the spectroscopic constants of this molecule is nowadays compiled in LIFBASE, a program created by Luque and Crosley[1]. In addition to the database, it can also simulate the optical spectra and thus significantly facilitates the optical diagnostics. However, LIFBASE does not take into account the collisional energy redistribution processes – electronic quenching, rotational and vibrational energy transfer (RET, VET).

Another group, in Bielefeld, came with another simulation environment called LASKIN[2]. This allows us to take into account the electronic quenching, RET and VET[3,4]. Since these depend strongly on the concentration of collisional partners, one needs to specify their relative densities as an input into the simulation. Unfortunately, this information is at atmospheric discharges very often unknown.

The goal of this experiment was to investigate the RET and VET processes for different excitation schemes and recommend the most suitable scheme for absolute OH density measurement in the plasma pencil.

2. Experimental setup

Plasma pencil

Plasma pencil (see Fig. 1) is a type of RF plasma nozzle working at atmospheric pressure[5]. The powered electrode is driven by 13.56 MHz. It is separated from plasma by a dielectric tube (inner diameter 2 mm). The plasma is ignited in argon flowing through the dielectric tube. Plasma blows together with argon out from the noz-

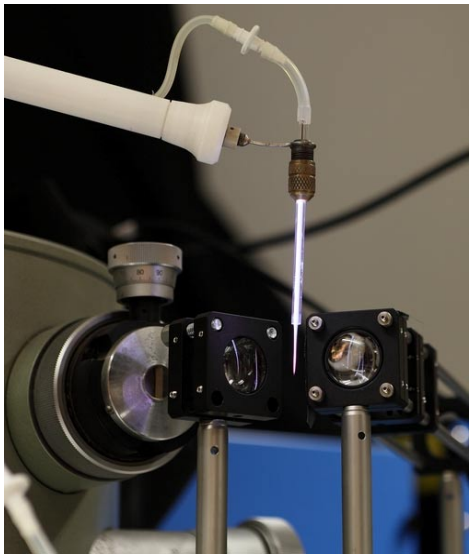

Fig. 1. **Image of the investigated plasma source.** The light-collecting lenses are also visible

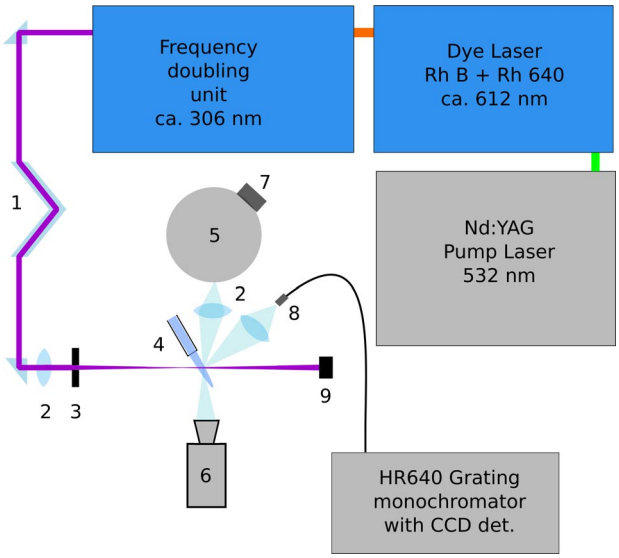

Fig. 2. **Experimental setup.** 1 – Fresnel Rhomb (turns polarization), 2 – positive UV lens, 3 – iris diaphragm, 4 – plasma pencil, 5 – prism monochromator (low resolution), 6 – ICCD camera with object-lens, 7 – photo-multiplier tube, 8 – optical fibre, 9 – laser power meter

zle, where it mixes with the ambient air and can be used for surface treatment.

Laser induced fluorescence

For excitation of OH radicals a laser setup was used consisting of pumping pulsed Nd:YAG laser (Quanta-Ray PRO-270-30), tunable dye laser (Sirah PRSC-D-24-EG) and a frequency doubling unit. The fluorescence was independently detected by an intensified CCD camera (PI-MAX 1024RB-25-FG43), a grating monochromator (HR 640) with CCD detection and a high-transition prism monochromator with photomultiplier detection (see Fig. 2). For time- and spectrally resolved measurements, the intensified CCD was coupled directly to the grating monochromator.

Two different vibrational transitions were used for the laser excitation. In both cases OH radicals were excited from the ground electronic and vibrational state to the electronic state A $^2\Sigma^+$. In the first case excitation to the first vibrationally excited state by 282.1 nm was used (see Fig. 3). In the second case OH radicals were excited to the ground vibrational state by wavelength 306.6 nm.

3. Results and discussion

In the first experiment, OH radicals were excited from ground electronic and vibrational state to the first excited vibrational state of A $^2\Sigma^+$ by the Q1(2) rotational transition at wavelength 282.1 nm. The fluorescence was measured in the range 305–320 nm where the vibrational bands (0,0) and (1,1) are located. By excitation to the first vibrational state the spectral overlap between the scattered laser radiation and the measured fluorescence was avoided. However, collisions of excited OH radicals lead to VET to the v'=0 state of A $^2\Sigma^+$. This fact is demonstrated in Fig. 4, where a part of the fluorescence spectrum is shown. Beside the transition from the v'=1 state, the fluorescence contains intensive radiation from the v'=0 state. At the beginning of the laser pulse, the radiation emitted directly from the v'=1 state (312–318 nm) dominates to the measured fluorescence spectra. However, VET induced by collisions quickly populates the v'=0 state of A $^2\Sigma^+$ and after the end of the laser pulse the radiative transitions from the v'=0 state (306–312 nm) is stronger than radiation from the originally excited v'=1 state.

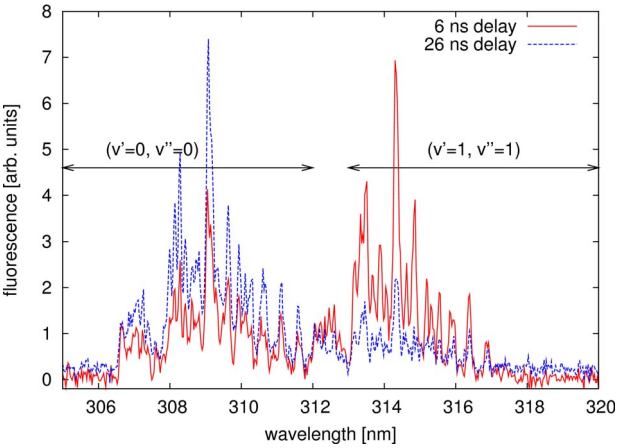

Fig. 4. **Fluorescence spectrum with 4ns time resolution in different delays with respect to start of the laser pulse.** The first vibrational state was excited

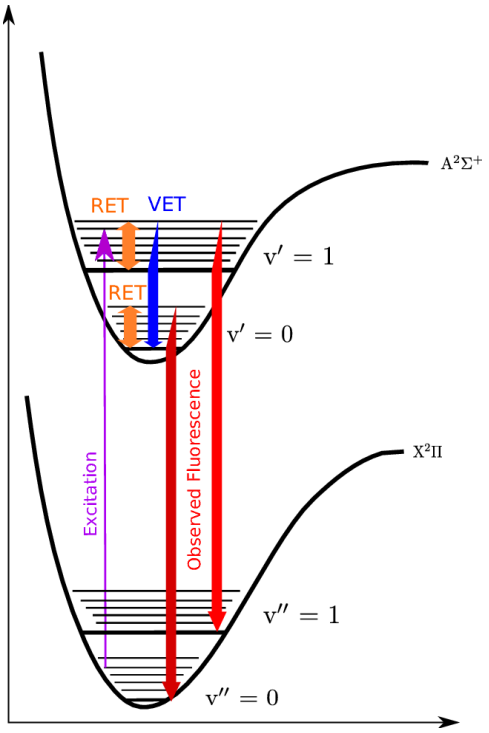

Fig. 3. **Diagram of the energy transfer processes in an OH molecule during the LIF measurement**

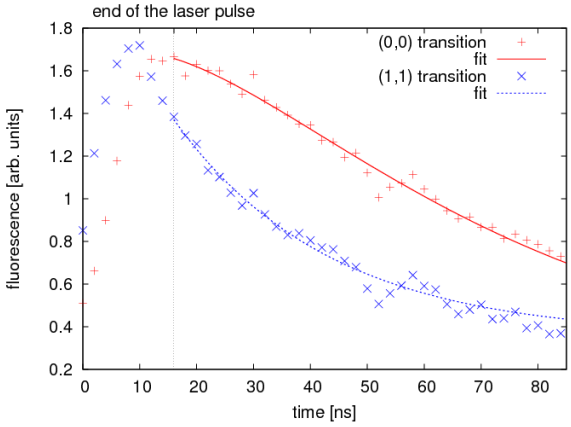

Fig. 5. **Time development of the (0,0) and (1,1) vibrational transition fitted with thegiven functions**

The different temporal development of the population of both v'=0 and v'=1 states of A $^2\Sigma^+$ is demonstrated in the Fig. 5. In this figure, time-resolved measurements of the (0,0) and (1,1) fluorescence radiation is presented. The v'=1 state is quickly populated at the laser pulse beginning, while the population of the v'=0 state falls behind. However, the relatively short life-time of the v'=1 state leads to its fast depopulation, partly to the v'=0 state. The v'=0 state, which is not depopulated by VET, has longer life-time, which is clearly visible in the Fig. 5.

The depopulation of the v'=1 state by VET does not lead to severe obstacles for evaluation of LIF necessarily. When the laser power is kept sufficiently low and saturation of LIF is avoided, the measured fluorescence radiation from the v'=1 state integrated over the whole fluorescence time ($F_{1\to1}$) is directly proportional to the ground state OH concentration (N_X):

$$F_{1\to1} \propto A_{1\to1}\,\tau_1\,N_X\,E_L$$

$$\frac{1}{\tau_1} = \sum_i A_{1\to i} + V + Q_{v=1}$$

where $A_{1\to i}$ are Einstein coefficients for the radiative transitions from the v'=1 state, τ_1 is life-time of this state, E_L energy of laser pulse, V the VET rate and $Q_{v=1}$ is quenching rate of the v'=1 state. $A_{1\to i}$ can be understood as a weighted average of the particular rotational Einstein coefficients, where the weight is given by population of each upper rotational state. Its dependence on rotational distribution will be discussed below. If the life-time τ_1 is sufficiently long, its value can be estimated from the exponential decay after the end of the laser pulse.

However, in some cases the VET complicates LIF experiments significantly. In discharges ignited at atmospheric pressure the collisional frequency is high and the VET rate can strongly decrease intensity of fluorescence from the v'=1 state. Moreover, the life-time of this state can be so reduced that the fluorescence decays simultaneously with the laser and it is not possible to estimate this life-time simply. Finally, some detection systems do not have sufficient blocking of the neighboring (0,0) transition. In these cases it is useful to know the VET rate and integral intensity of fluorescence from the v'=0 state ($F_{0,0}$), which follows the equation

$$\frac{F_{0\to0}}{F_{1\to1}} = \frac{A_{0\to0}}{A_{1\to1}}\,V\,\tau_0$$

$$\frac{1}{\tau_0} = \sum_i A_{0\to i} + Q_{v=0}$$

where $A_{0\to i}$ and $Q_{v=0}$ are Einstein coefficients and quenching rate for the v'=1 state. The simplest way to estimate the life-times τ_0 and τ_1 are time- and spectrally resolved LIF measurements. After the laser pulse end, the actual fluorescence intensities ($f_{0\to0}$, $f_{1\to1}$) follow the exponential decay

$$f_{1\to1} = C_A\,e^{-t/\tau_1}$$

$$f_{0\to0} = C_B\,e^{-t/\tau_1} + C_C\,e^{-t/\tau_0}$$

$$C_B = \frac{V\,C_A}{1/\tau_0 - 1/\tau_1}\,\frac{A_{0\to0}}{A_{1\to1}}$$

which can be fitted to the measured dependencies. Values of V, $Q_{v=1}$ and $Q_{v=0}$ can be estimated from a measurement set performed at various pressures, or, if partial pressures of colliding species are known, it can be advantageously calculated from known cross sections. Fit of the decay to data measured in plasma pencil is shown in the Fig. 5 with fitted values $\tau_0 = 41$ ns and $\tau_1 = 27$ ns demonstrating that the decay is relatively slow. This is caused by the fact that discharge in plasma pencil is ignited in argon, which is relatively inefficient quencher of excited OH states[2].

Since the life-time of excited state is relatively long, a second LIF experiment with excitation directly to the A $^2\Sigma^+$ (v'=0) state was tested. Such excitation avoids the VET but in this case the laser wavelength falls into the detected spectral interval. However, due to the long lifetime, the fluorescence can be measured after the laser pulse end without loosing significant amount of fluorescence signal. The measured fluorescence spectra are shown in the Fig. 6.

The laser populates only the 5th rotational level of the A $^2\Sigma^+$ (v'=0) state. However, collisions of excited states lead to RET and population of other rotational levels. Since rotational levels differ in transition probabilities, it is necessary to know the temporal changes of the rotational distribution of the excited state that occur during the fluorescence measurement. The Fig. 6 demonstrates, that the RET in plasma pencil is so fast that it leads to immediate thermalization of the rotational distribution, even during the laser pulse. Therefore, the Einstein coefficients $A_{0\to i}$ can be considered to be constant during the whole fluorescence pulse. Moreover, the population of the rotational level of the ground OH state which is depopulated by laser

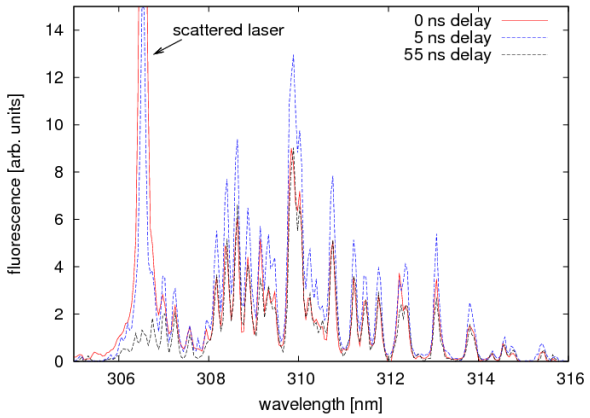

Fig. 6. **Fluorescence spectrum with 5ns time resolution in different delays with respect to start of the laser pulse.** The 0th vibrational state was excited

excitation can be considered to be approximately constant during the whole laser pulse since it is effectively repopulated by RET in the ground state.

4. Conclusion

Plasma pencil is an atmospheric pressure discharge with high collisional frequency of excited species, which lead to quenching of excited species and to vibrational and rotational energy transfer. Laser excitation to vibrationally excited states is therefore followed by fast VET to lower vibrational states and changes of fluorescence radiation described by formulas presented above. Since the discharge is operated in argon, which quenches excited states relatively slowly, the lifetimes of excited states are significantly longer than the laser pulse duration. RET in plasma pencil is so fast that the rotational energy distribution of OH radicals can be considered to be thermalized during the whole fluorescent measurement including the period of laser pulse excitation. Both the relatively long lifetime and fast RET are positive findings that simplify evaluation of measurements based on laser induced fluorescence.

This research has been supported by the project R&D center for low-cost plasma and nanotechnology surface modifications CZ.1.05/2.1.00/ 03.0086 funding by European Regional Development Fund.

REFERENCES

1. Luque J., Crosley D.R.: LIFBASE: Database and spectral Simulation Program (Version 1.5), SRI Internation-al Report MP 99-009 (1999).
2. Brockhinke A., Kohse-Hoeinghaus K.: Energy transfer in combustion diagnostics: Experiment and modeling, Faraday Discuss., *119*, 275 (2001).
3. Brockhinke A., Kreutner W., Rahmann U., Kohse-Höinghaus K., Settersten T. B., Linne M. A.: Appl. Phys. B, *69*, 477 (1999).
4. Kohse-Hoeinghaus K.: Prog. Energy Combus. Sci. *20*, 203 (1994).
5. Kapička V., Šícha M., Hubička Z., Touš J., Brablec A., Slavíček P., Behnke J. F., Tichý M., Vaculík R.: Plasma Sources Sci. Technol. *8*, 15 (1999).

J. Voráč[a,b], V. Procházka[a], and P. Dvořák[a] *([a] Dep. of Physical Electronics, Faculty of Science, Masaryk University, Brno, Czech Republic, [b] ZIK-Plasmatis, INP Greifswald e.V., Greifswald, Germany):* **Vibrational and Rotational Energy Transfer in A $^2\Sigma^+$ State of OH Radicals Measured by Laser Induced Fluorescence**

Laser induced fluorescence was used for detection of OH radicals in atmospheric pressure RF discharge ignited in argon in the so-called plasma pencil. Vibrational and rotational energy transfers in the excited states A $^2\Sigma^+$ (v=0,1) together with appropriate life-times were studied. Since argon is relatively uneffective quencher, lifetimes of the excited states in plasma pencil are in the order of tens of nanoseconds, which is appreciably longer than the laser pulse. It was shown that the RET rate in plasma pencil is very high. Therefore, the rotational energy distribution of the excited state can be considered to be well thermalized.

STUDY OF THE INDENTATION RESPONSE OF NANOCOMPOSITE n-TiC/a-C:H COATINGS

LUKÁŠ ZÁBRANSKÝ[a]*, VILMA BURŠÍKOVÁ[a,b], JIŘÍ BURŠÍK[c], PETR VAŠINA[a], PAVEL SOUČEK[a], ONDŘEJ CAHA[d], MOJMÍR JÍLEK[e], VRATISLAV PEŘINA[f]

[a] Department of Physical Electronics, Masaryk University, Brno, [b] CEITEC, Central European Institute of Technology, Masaryk University, 601 77 Brno, [c] Institute of Physics of Materials, Academy of Sciences of the Czech Republic, Brno, [d] Department of Condensed Matter Physics, Masaryk University, Brno, [e] SHM Šumperk, Průmyslová 3020/3, 787 01, Šumperk, [f] Nuclear Physics Institute, Academy of Sciences of the Czech Republic, Řež, Czech Republic
zerafel@mail.muni.cz

Keywords: nanocomposite coatings, PVD, mechanical properties, SEM, TEM, FIB

1. Introduction

Composites have often desirable combinations of properties that are not found in the individual components. Nanocrystalline titanium carbide embedded in an hydrogenated amorphous carbon matrix (nc-TiC/a-C:H) shows high hardness and Young's modulus together with low wear and low friction coefficient[1–8]. These coatings are usually deposited by the hybrid PVD-PECVD process using the unbalanced of even the close-field unbalanced magnetic field configuration in order to enhance the ion bombardment of the growing film[1,5,8]. The thickness of these coatings ranges typically from several hundreds of nm up to 3 μm.

The aim of the recent work was to compare the nc-TiC/a-C:H coatings mechanical properties and structure on various substrates, which were prepared using a well balanced and unbalanced magnetic field configuration. Acetylene flow was varied to obtain films with different chemical compositions. The structure and mechanical properties of these coatings were thoroughly analyzed to observe the dependencies of composition, structure and mechanical properties on the acetylene flow and on the pre-deposition cleaning time. And finally, the obtained results were used to optimize the preparation process and measuring methodology.

2. Deposition method

The depositions were carried out using industrial sputtering system Alcatel SCM 650. High speed steel and hardmetal samples were placed on a biasable (13.56 MHz RF) substrate holder. The deposition chamber was evacuated to the base pressure in the order of 10^{-4} Pa. Several mm thick nc-TiC/a-C:H coatings were prepared using sputtering of a pure titanium target in an acetylene-containing atmosphere. High speed steel and hardmetal substrates were used. A short pre-deposition cleaning was performed to ensure of removal any adsorbed contaminants from substrates and target. For all samples the deposition time was 45 minutes. Approximately 700 nm thick titanium layer was deposited prior the nc-TiC/a-C:H growth to promote the adhesion of the coating. Three sets of samples were prepared.

3. Diagnostic methods and results

The influence of the deposition conditions on the resulting mechanical properties was studied. For this purpose the new method combining nanoindentation test with the calotest was developed. This method enabled us to obtain the profile of mechanical properties depending on the depth. Fischerscope HC100 depth sensing indenter equipped with a Berkovich tip was used to study the indentation response of the samples. Additionally, several other methods were used to obtain more complex relationships between the chemical composition, inner structure and mechanical properties. Specifically, we used RBS, ERDA, X-ray diffraction, mechanical profilometry, Rockwell test for adhesion evaluation, SEM and TEM methods.

In the first set called as TiC55-59 the influence of pre-deposition cleaning time was measured. This cleaning time t_c was varied in the range from 5 minutes to 140 minutes (see Table I).

Table I
Mechanical properties of the set TiC55-59

t_c [min]	H_{IT}[a)] [GPa]	HU_{PL}[b)] [GPa]	E_{IT}[c)] [GPa]
5	31 ± 2	38 ± 3	330 ± 20
35	32 ± 3	41 ± 4	340 ± 30
70	26 ± 2	29 ± 3	330 ± 10
140	24 ± 3	29 ± 4	320 ± 20

[a)] Indentation hardness; [b)] plastic hardness; [c)] indentation modulus

For evaluation of mechanical properties we used nanoindentation method (at least 60 indents per sample) at applied load of 75 mN. It was proved that shorter cleaning times leads to higher plastic hardness HU_{PL}, indentation hardness H_{IT}, indentation modulus E_{IT}. The best results (plastic hardness 41 GPa and elastic modulus 340 GPa) were obtained for 35 minutes of cleaning. We used this option for preparation of the other two sets of samples.

In the next two sets (TiC70-79 and TiC127-135) of samples the effect of acetylene flow on the resulting mechanical properties was determined. The samples in the set TiC70-79 were prepared using well balanced magnetic field. Acetylene flow was varied to obtain films with different chemical compositions ranging from 30 at.% C to 68 at.% C. The chemical composition was measured using RBS and ERDA methods. Due to the titanium adhesive interlayer a very good adhesion corresponding to HF0-HF1 was reached according to the German DIN CEN/TS 1071-8 standard. XRD proves the presence of TiC grains of characteristic size ranging from several tens of nm to several nm depending of the carbon content in the coating. Macro-roughness of samples on hardmetal substrates was evaluated using a profilometer over length of 8 mm. For the acetylene flux ranging from 8 sccm to 10 sccm the roughness R_a was around 0.15 μm and from 11 sccm to 14 sccm the roughness decreased to values comparable with uncoated hardmetal substrates (R_a = 0.05 μm). Using nanoindentation tests at 75 mN load, the highest hardness and indentation modulus of 46 GPa and 415 GPa respectively was reached for 40 at.% Ti content.

The vertical structure of hardmetal samples was analyzed on fracture surfaces by a field-emission Scanning Electron Microscope LYRA 3 XMU FEG/SEM×FIB by Tescan.

Operating voltage of the SEM was 15 kV. The dense columnar structure was observed. All results for this set are summarized in the Table II.

In the last set TiC127-135 all samples were prepared using an unbalanced magnetic field configuration. The comparison of plastic hardness and indentation modulus of samples in these two sets is plotted in Fig. 1. The plastic hardness and indentation modulus were plotted as a functions of [C]/[Ti] in order to eliminate the shift in chemical composition between this two sets (see Fig. 2). The shift

Table II
Summary of all results for the set TiC70-79

C_2H_2 flow [sccm]	Thickness [μm]	Ti [at.%]	C [at.%]
8	7,5	62	30
9	7,2	53	39
10	7,4	56	39
11	5,7	39	55
11,5	5,7	-	-
12	**6,4**	**37**	**57**
13	5,9	28	63
14	5,6	22	38
Macro-roughness [μm]	Mean crystallite size [nm]	Plastic hardness [GPa]	Indentation modulus [GPa]
0,12	13	13	222
0,15	15	22	283
0,17	42	24	289
0,07	15	35	315
-	-	37	335
0,07	**19**	**46**	**414**
0,10	5	37	316
0,05	5	23	225

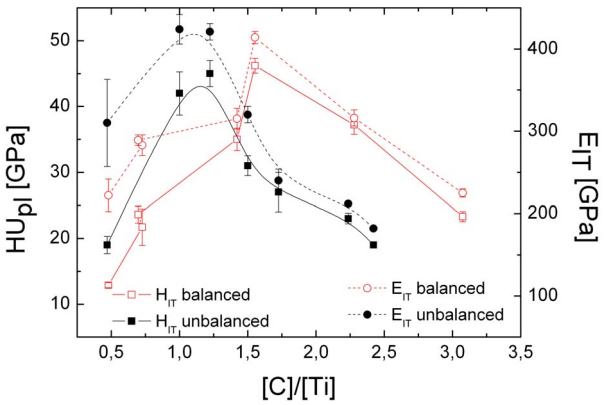

Fig. 1. **Comparison of plastic hardness and indentation modulus dependence on the carbon to titanium ratio**

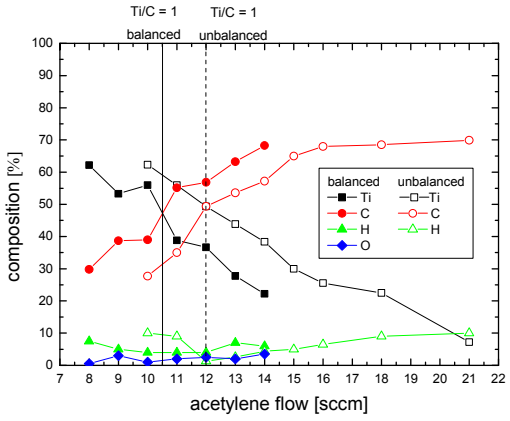

Fig. 2. **Dependence of the atomic composition on the acetylene flow**

was caused by different applied power on target during the deposition process. In case of the set made using an unbalanced magnetic field high values (i.e. HU_{PL} = 45 GPa and E_{IT} = 425 GPa) of both mechanical parameters are observable as well.

The observed shift between both dependencies shown in Fig. 1 can be explained by the presence of inner stress inside the samples within the set of TiC127-135.

4. Optimization of the preparation process

In both sets (Fig. 1) the maxima are sharp and exist only in a narrow range of acetylene flow. Therefore it is crucial to find a suitable method how to find them quickly without the necessity to prepare the whole set of samples. So a preparation of a thick gradient layer with a sequential change in the acetylene flow during its deposition has been performed. The resulting thick multilayer consisted of several thin layers, one for each acetylene flow. Each of them was about 1 μm thick. In this thick multilayered system there was an oblique cut performed at very low angle. The cut was used for nanoindentation test – a line of about 60 indents was led through the area of the cut. That allowed us to obtain the profile of mechanical properties depending on the location in the cut.

In Fig. 2 a graph of plastic hardness as the function of the test position d is shown, where a maximum in HU_{PL} is observable. Assuming that the growth-rate of layers is approximately the same, we can therefore attribute a proper flow to a proper range of locations in the cut.

Due to the influence of the lower located layers on the nanoindentation measurement, it is necessary to choose a suitable load. For this purpose and this type of coatings the load of 50 mN proved as usable.

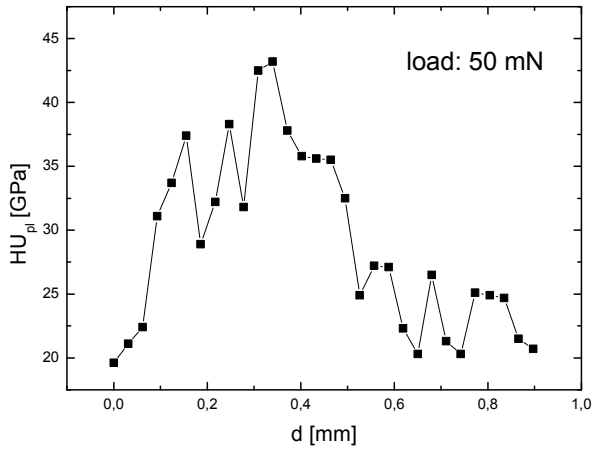

Fig. 3. **Plastic hardness dependence on the indentation print position obtained on the oblique cut**

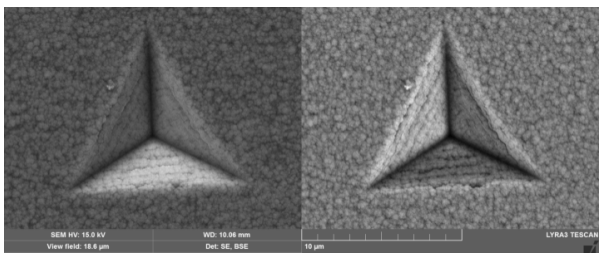

Fig. 4. **Scanning electron microscopy (SEM) images of an indentation print made with maximum load 1 N**

5. Electron microscopy

Thin lamella for TEM measurement was cut out from the sample TiC56 using a focused ion beam (FIB) gun integrated in the scanning electron microscope LYRA 3 XMU by Tescan. In Fig. 4 there is an image of an indent performed using a load of 1N in both secondary electrons and backscattered electrons signals. The lamella was cut close to this indent in order to determine the influence of this indent on the inner structure. For this purpose a transmission electron microscope CM12 STEM Philips was used.

In Fig. 5 there is a TEM image of prepared lamella with marked spots where diffraction patterns were taken. Analyzing this patterns it was proved that Ti interlayer contains small equiaxed grains and the nanocomposited layer grows in elongated grains. There were no cracks at the interfaces. The interlayer works as a transition between the substrate and the layer.

In Fig. 6 there are diffraction patterns from selected places shown in Fig. 5. Spot A is the closest to the indentation print while spots B and C are more distant.

The diffraction patterns revealed some indentation induced rearrangement of the crystallites within the a-C:H matrix. The crystallites showed high resistance against de-

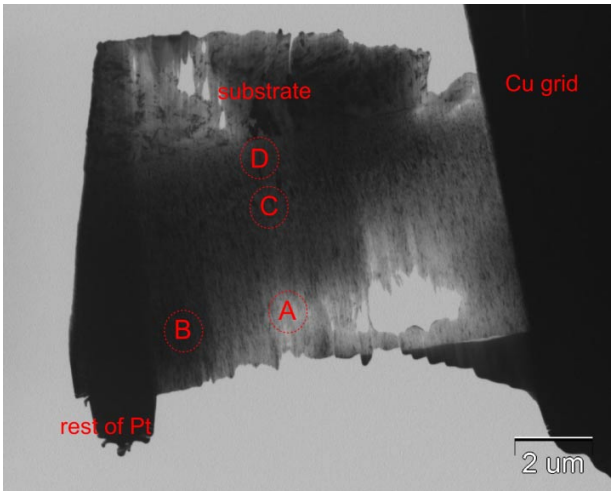

Fig. 5. **Transmission electron microscopy (TEM) image of a lamella**

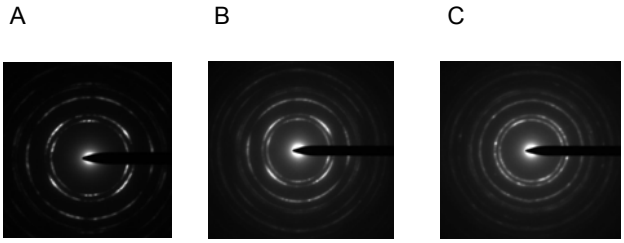

Fig. 6. **Diffraction patterns from places marked with A, B and C**

formation. Further SEM, FIB and TEM experiments are planned to explain the film deformation mechanism.

The work was supported by the Czech Science Foundation (Project No. P205/12/0407) and by the project CZ.1.05/2.1.00/03.0086 'R&D center for low-cost plasma and nanotechnology surface modifications' funded by European Regional Development Fund.

REFERENCES

1. Czyżniewski A., Prechtl W.: J. Mater. Proc. Technol. *157-158*, 274 (2004).
2. Sánchez-López J. C., et al. : Surf. Coat. Technol. *202*, 4011 (2008).
3. Cao D. M., et al. : Appl. Phys. Lett. *79/3*, 329 (2001).
4. Musil J., et al. : J. Vac. Sci. Technol. A *28*, 244 (2010).
5. Pei Y. T., et al. : Surf. Coat. Technol. *198*, 44 (2005).
6. Galvan D., et al.: Acta Mater. *53,* 3925 (2005).
7. Hu Y., et al.: Diamond Relat. Mater. *16*, 181 (2007).
8. Galvan D., et al. : J. Vac. Sci. Technol. A *24*, 1441 (2006).

L. Zábranský[a], V. Buršíková[a,b], J. Buršík[c], P. Vašina[a], P. Souček[a], O. Caha[d], M. Jílek[e], and V. Peřina[f] *([a] Department of Physical Electronics, Masaryk University, Brno, [b] CEITEC, Central European Institute of Technology, Masaryk University, Brno, [c] Institute of Physics of Materials, Academy of Sciences of the Czech Republic, Brno, [d] Department of Condensed Matter Physics, Masaryk University, Brno, [e] SHM Šumperk, [f] Nuclear Physics Institute, Academy of Sciences of the Czech Republic, Rež, Czech Republic):* **Complex Study of Mechanical Properties of Nanocomposite n-TiC/a-C:H Coatings**

This work is aimed on the study of relationship between mechanical properties, chemical composition and inner structure of nanocomposite n-TiC/a-C:H coatings. Furthermore the obtained results were used to optimize the preparation process and measuring methodology.

CONTENTS

AUTHOR INDEX

CHEMICKÉ LISTY • ročník/volume 106 (S), čís./no. Symposia • LISTY CHEMICKÉ roč./vol. 136, ČASOPIS PRO PRŮMYSL CHEMICKÝ, roč./vol. 122 • ISSN 0009-2770, ISSN 1213-7103 (e-verze), ISSN 1803-2389 (CD verze) • evidenční číslo MK ČR E 321 • Vydává Česká společnost chemická jako časopis Asociace českých chemických společností ve spolupráci s VŠCHT Praha, s ČSPCH a ÚOCHB AV ČR za finanční podpory Nadace Český literární fond a kolektivních členů ČSCH • IČO 444715 • Published by the Czech Chemical Society • VEDOUCÍ REDAKTOR/EDITOR-IN-CHIEF: P. Chuchvalec • REDAKTOŘI/ EDITORS: J. Barek, Z. Bělohlav, P. Drašar, J. Hetflejš, P. Holý, J. Horák, B. Kratochvíl, J. Podešva, P. Rauch; Bulletin: I. Valterová; Webové stránky: R. Liboska, P. Zámostný • ZAHRANIČNÍ A OBLASTNÍ REDAKTOŘI/FOREIGN AND REGIONAL EDITORS: F. Švec (USA), Z. Kolská (Ústí nad Labem) • KONZULTANT/CONSULTANT: J. Kahovec • TECHNICKÁ REDAKTORKA/EDITORIAL ASSISTANT: R. Řápková • REDAKČNÍ RADA/ADVISORY BOARD: K. Bláha, L. Červený, E. Dibuszová, J. Hanika, Z. Havlas, J. Káš, M. Koman, J. Koubek, T. Míšek, K. Melzoch, V. Pačes, O. Paleta, V. Růžička, I. Stibor, V. Šimánek, R. Zahradník • ADRESA PRO ZASÍLÁNÍ PŘÍSPĚVKŮ/MANUSCRIPTS IN CZECH, SLOVAK OR ENGLISH CAN BE SENT TO: Chemické listy, Novotného lávka 5, 116 68 Praha 1; tel./phone +420 221 082 370, +420 222 220 184, e-mail: chem.listy@csvts.cz • INFORMACE O PŘEDPLATNÉM, OBJEDNÁVKY, PRODEJ JEDNOTLIVÝCH ČÍSEL A INZERCE/ INFORMATION ADS: Sekretariát ČSCH, Novotného lávka 5, 116 68 Praha 1; tel. +420 222 220 184, e-mail: chem.spol@csvts.cz, chem.ekonom@csvts.cz • PLNÁ VERZE NA INTERNETU/FULL VERSION ON URL: http://www.chemicke-listy.cz • TISK: Rodomax s.r.o., Rezecká 1164, 549 01 Nové Město nad Metují • Redakce čísla Symposia (ISSUE EDITOR) V. Buršíková, M. Černák, K. Lepka • SAZBA, ZLOM: ČSCH, Chemické listy • Copyright © 2012 Chemické listy/Česká společnost chemická • Cena výtisku 170 Kč, roční plné předplatné 2012 (12 čísel) 1730 Kč, individuální členské předplatné pro členy ČSCH 865 Kč. Roční předplatné ve Slovenské republice 92 EUR (doručování via SCHS), individuální členské předplatné pro členy ČSCH 70 EUR (doručování via SCHS), 258 EUR (individuální doručování), ceny jsou uvedeny včetně DPH • DISTRIBUTION ABROAD: KUBON & SAGNER, POB 34 01 08, D-80328 Munich, FRG; Annual subscription for 2012 (12 issues) 225 EUR • This journal has been registered with the Copyright Clearance Center, 2322 Rosewood Drive, Danvers, MA 01923, USA, where the consent and conditions can be obtained for copying the articles for personal or internal use • Pokyny pro autory najdete na http://www.chemicke-listy.cz , zkratky časopisů podle Chemical Abstract Service Source Index (viz http://cassi.cas.org/search.jsp) • Chemické listy obsahující Bulletin jsou zasílány zdarma všem individuálním a kolektivním členům ČSCH a ČSPCH v ČR i zahraničí, do všech relevantních knihoven v ČR a významným představitelům české chemie a chemického průmyslu; v rámci dohod o spolupráci i členům dalších odborných společností • Molekulární námět na obálce: P. Drašar